EXPERIMENTAL STUDY ON ORDERING OF NEARLY IDEAL TWO-DIMENSIONAL-HEISENBERG ANTIFERROMAGNETS

Kuniyuki KOYAMA

1984

Abstract

Ordering of pure and nearly two-dimensional-Heisenberg antiferromagnets have been investigated experimentally by proton NMR, spontaneous magnetization and susceptibility measurements using a SQUID magnetometer, etc.

A compound $Cu(HCOO)_2 \cdot 2H_2O \cdot 2CO(NH_2)_2$ may present a closest system to the perfect two-dimensional (2d) Heisenberg one of all existing real materials. The critical index β of spontaneous magnetization is determined as 0.22 in the wide temperature range ($10^{-3} < \varepsilon < 8 \times 10^{-1}$). This wide range character can not be attributed to be so called crossover effect. This value of $\beta = 0.22$ are also measured in 2d Heisenberg antiferromagnets with canting interaction $Cu(HCOO)_2 \cdot 4H_2O$ and $Mn(HCOO)_2 \cdot 2H_2O$ as the critical exponents in temperature range a little far from the critical temperature. This critical exponent $\beta = 0.22$ is inconsistent with the exponents of any conventional universality class. This value is an intermediate value of 2d Ising and 3d systems, and may suggest the existence of a new universality class.

The magnetic ordering of a heterogeneous 2d Heisenberg system $Mn(HCOO)_2 \cdot 2H_2O$ is investigated. The inter-planer structure is composed of an alternate piling up of two in-equivalent magnetic planes i.e. a strongly coupled antiferromagnetic A plane and another almost paramagnetic B plane. The temperature dependence of subsystem susceptibilities are separately observed above T_N by proton NMR method. The susceptibility χ_A of A subsystem shows a broad maximum around $2T_N$, while χ_B of B subsystem follows the Curie law. Spontaneous magnetization of A subsystem follows two distinct

exponential laws. Outside of the crossover point ε^* ($= |1 - T^*/T_N|$) $\simeq 2 \times 10^{-2}$, $\beta = 0.23$ and the closer neighbourhood to T_N, $\beta = 0.30$ are obtained. The critical indices γ of susceptibility ($\gamma = 1.74$) and β are very close to the values for two different universality classes i.e. 2d Ising and 3d Ising ones. This fact is apparently inconsistent with the scaling law and the universality in the conventional sense.

The fully mapped temperature-magnetic field phase diagram of $Mn(HCOO)_2 \cdot 2H_2O$ is determined by the measurements of heat capacity and susceptibility. An anomalous increase of the Néel temperature with increasing field is found to be attributed to a crossover of spin symmetry from the Heisenberg-type to the XY-type induced by the field. The absolute values of magnetic heat capacity under the appropriate field is found to agree with the theoretical values for the 2d plane rotator model in the paramagnetic temperature region.

Three successive phase transitions are observed in the random diluted 2d Heisenberg antiferromagnet $Mn_{1-x}Zn_x(HCOO)_2 \cdot 2H_2O$ by the measurements of susceptibility, spontaneous magnetization and heat capacity. Neutron diffraction is investigated to get the information for spin correlations.

CONTENTS

Chapter I. Introduction

§I-1. General aspects of the study

There are many investigations of the critical phenomena in low-dimensional magnetic systems both theoretically and experimentally.[1)]

As for one-dimensional (1d) systems, behaviours of thermodynamic quantities can be more easily obtained theoretically than as for two-dimensional (2d) systems. It has been theoretically proved that there exists no long range ordered state at a finite temperature in one-dimensional systems of any spin symmetry (Ising, XY or Heisenberg).[2,3)] However, there have been observed the occurences of a long range order in a lot of real chain compounds, which are certainly brought by an inter-chain interaction. Exact expression for the heat capacity and magnetic susceptibility of one-dimensional Heisenberg and Ising spin systems have been given by Bonner and Fisher[4)] and many other authors.[5)] Experimental results of linear chain materials have been found in good agreement with the theory above their transition temperatures.[6)]

As for two-dimensional systems, it was rigorously proved by Onsager[7)] that a two-dimensional Ising spin system of $S = 1/2$ orders at a finite temperature with a symmetric and logarithmic divergence of heat capacity. Temperature dependence of spontaneous magnetization in this spin system has been given by Yang[8)] exactly. On the other hand, Mermin and Wagner[3)] gave the rigorous proof telling that one- and two-dimensional Heisenberg or XY spin systems do not have a spontaneous magnetization at a finite temperature.

As for three-dimensional (3d) spin system, we are convincing an existence of phase transition with a spontaneous magnetization at a finite temperature for any type of spin symmetry. There have been observed a lamda type anomaly of heat capacity and divergence of magnetic susceptibility.

For the so-called second order phase transition, the critical phenomena have been considered theoretically to be described by the "scaling law" and the "universality".[9] According to the concept of "universality", the critical phenomena of any system should be described by a set of exponents for the corresponding universality class. The phase transition is determined by a few fundamental factors i.e. (1) lattice dimensionality, (2) symmetry of spin interaction and (3) force range, and is independent of any other details of the system i.e. connectivity, lattice structure, spin quantum number and so on. The critical exponents follow to the well-known scaling relations among the critical indices, e.g. $\alpha' + 2\beta + \gamma' = 2$. The concept of "weak universality" has been recently proposed, which claims that reduced critical index λ/ν (λ: α, β, etc.) is universal, where ν is the critical index of correlation length.[10] The former universality is called "strong universality".

The hypothesis of universality requires the observation of the "crossover" phenomena to the three-dimensional class in real quasi-two-dimensional system. Stanley[11] gave the following expression for the thermodynamic quantity.

$$f(R,a) = A(R,a)\left|1 - T/T_C\right|^{\lambda}. \qquad \text{(I-1)}$$

In the region of very vicinity of the critical point T_C, λ is the

critical index for three-dimensional Ising spin system. a (= H_A/H_E) is the degree of anisotropy of interaction J in two-dimensional lattice, and H_A and H_E are the anisotropy and exchange field, respectively. R (= J'/J) is the ratio of inter-layer interaction J' to the intra-layer interaction J, which is a measure of two-dimensionality of the system. Outside of the crossover region the quantity f(R,a) is identified to that of the two-dimensional system.

Now, "scaling law" and "universality" are taken to be valid experimentally for some examples, but there are lots of examples which seem not to realize these laws. Accordingly there are problems as follows, (i) Whether the previous criteria (1), (2) and (3) are proper or not, and (ii) Whether a new universality class which is not known so far exists or not. In this thesis, we will examine these problems experimentally.

These laws are taken to be valid experimentally as well for some simple magnetic systems like e.g. Rb_2CoF_4, a quasi-two-dimensional Ising system. In this salt, spin correlation function[28] and magnetic heat capacity[29] and so on in the vicinity of T_N can be well described by the Onsager's rigorous solution, although this salt is not perfect Ising-type magnet.

Systematic investigations by neutron diffaction on 2d Heisenberg like antiferromagnets K_2NiF_4 and K_2MnF_4 have been done,[12] which show that the critical exponents of spontaneous magnetization in these salts are well described as the exponent for 2d Ising class below T_N although the 3d long range order is observed below T_N. It may suggest that the dominant purturbation is the Ising-type anisotropy within each plane in these salts. While, the investi-

gation by neutron diffraction on K_2CuF_4[13] shows that the critical exponent β of spontaneous magnetization is in good agreement with that for 3d XY universality class. It may suggest that the dominant purturbation is the three-dimensionality in this salt.

As mentioned before, we will examine the criteria of universality and search a new universality class if any. For this purpose, we have planed to investigate some systems in the neighbourhoods of 2d Heisenberg one which is in the openest situation for the new problem. Because, perfect 2d Heisenberg system is known not to order at any finite temperature[3] and could order with weak purturbation like Ising anisotropy,[27] three-dimensionality or an antisymmetric interaction, for example. If 2d Heisenberg system with antisymmetric interaction orders at a finite temperature, this system might reveal a new feature of phase transition unexpected so far.

As for 2d Heisenberg antiferromagnets, we examine especially so called the canted antiferromagnets i.e. $Cu(HCOO)_2 \cdot 2H_2O \cdot 2CO(NH_2)_2$ (CuFUH), $Cu(HCOO)_2 \cdot 4H_2O$ (CuF4H) and $Mn(HCOO)_2 \cdot 2H_2O$ (MnF2H) with small anisotropy and the three-dimensionality. Further, as the case that purturbation is the external field, the phase transition under the external field is investigated for MnF2H. Moreover, as the case that purturbation is the random dilution of magnetic ions, the critical phenomena of $Mn_{1-x}Zn_xF2H$ is investigated.

The magnetic property of CuFUH may be a most close to the perfect 2d Heisenberg system of all existing real materials.[14] There is the canting of the moment caused by in-equivalent $\tilde{g}$-tensor. The log-log plot of spontaneous magnetization versus ε ($\equiv 1 - T/T_N$)

is found to be extremely straight in the wide temperature range ($10^{-3} < \varepsilon < 8 \times 10^{-1}$) and β is determined as 0.22 ± 0.02. This fact can not be attributed to be so-called crossover effect, because the straight region is wide enough. This value of $\beta = 0.22$ are also measured in 2d Heisenberg antiferromagnets with canting interaction CuF4H and MnF2H as the critical exponents in temperature range a little far from the critical temperature.

In Chapter II, the critical phenomena and the quantum effects of the 2d Heisenberg antiferromagnet CuFUH are investigated. The compound CuF4H, the inter-layer interaction of which is twenty times as large as that of CuFUH, is also investigated. The critical indices β of other 2d Heisenberg-like systems are surveyed on the diagram of Ising anisotropy versus three-dimensionality. In the several salts, the value of critical indices β is about 0.22, although the range of reduced temperature ε are rather narrow except for CuFUH and MnF2H. In the case of CuFUH and MnF2H, the straight line regions are wide enough to asign the coefficients as the critical indices.

This critical exponent $\beta = 0.22$ is inconsistent with the exponents of any conventional universality class i.e. 2d Ising, 3d Ising, 3d XY or 3d Heisenberg. This value is an intermediate value of 2d Ising and 3d system, and may indicate the existence of a new universality class. The origin of this anomalous index is discussed there.

In Chapter III, the magnetic ordering of a heterogeneous 2d Heisenberg system $Mn(HCOO)_2 \cdot 2H_2O$ (MnF2H) is investigated. The interplaner structure of this compound is composed of a alternate

piling up of two in-equivalent magnetic planes i.e. a strongly coupled antiferromagnetic A plane and another almost paramagnetic B plane. Each paramagnetic B ion lies on a inter-plane interaction path between the adjacent two A planes. It is interesting to examine the influence of the heterogeneity or such a modification of inter-plane interaction on the ordering of an especially Heisenberg-like system. Spontaneous subsystem magnetization L_A of A subsystem follows two distinct exponential laws. Outside of the crossover point $\varepsilon^* \simeq 2 \times 10^{-2}$, $\beta = 0.23 \pm 0.02$. In the closer neighbourhood to T_N, $\beta = 0.30 \pm 0.02$ indicates apparently a three-dimensional nature of ordering below T_N.[15] While, the spontaneous magnetization L_B of B subsystem is found to grow up under a local field from the ordered A subsystem. The value of $\beta = 0.23 \pm 0.02$ may suggest that the present salt belongs to the same universality class as that in CuFUH.

The spontaneous magnetization and the susceptibility are measured simultaneously under negligibly small residual DC field and exciting AC field using a SQUID magnetometer. The critical indices γ and β are very close to the values for two different universality classes i.e. 2d Ising and 3d Ising ones, respectively. This fact is inconsistent with the scaling law and the universality in the conventional sense.

The temperature dependences of subsystem susceptibilities are separately observed above T_N by proton NMR in the external fields along the special directions determined by the dipole sum tensors.[16] The susceptibility χ_A of A subsystem shows a broad maximum around 7 K ($\simeq 2T_N$). While χ_B of B subsystem follows the Curie's law for $S = 5/2$ and $g = 2.0$.

In Capter IV, the magnetic ordering of 2d Heisenberg antiferromagnet under the field is investigated.[17] It is expected a crossover phenomena of spin symmetry from the Heisenberg-type to the XY-type induced by the field. The fully mapped T-H (temperature= magnetic field) phase diagram of MnF2H has been determined by the measurements of magnetic heat capacity and susceptibility.[18] The critical field which is the transition field from spin flopped to paramagnetic state has been estimated to be 105 $\pm$ 5 kOe at T = 0 K, which gives the intra-layer exchange constant $|J|/k_B$ = 0.35 $\pm$ 0.02 K. The magnetic structure in various phases and the mechanisms of transitions under the field are examined by the measurement of proton NMR. An anomalous increase of the Néel temperature $T_N(H)$ which is nearly linear with increasing field has been found in this 2d compound as in the case of quasi-1d compounds.[19] The anomalous increase of $T_N(H)$ in the field has been found to be attributed to a crossover of spin symmetry from the Heisenberg= type to the XY-type induced by the field. The absolute values of magnetic heat capacity of this 2d XY system induced by the field of H = 20 kOe have been compared with the theoretical values expected for the 2d plane rotator model.[19] A quantitative agreement has been found between them in the paramagnetic temperature region.

In Chapter V, the phase transition of random diluted 2d Heisenberg system $Mn_{1-x}Zn_x(HCOO)_2 \cdot 2D_2O$ (MnZnF2D) is investigated. The random dilution of magnetic ion may be taken a kind of symmetry breaking purturbation. Three successive phase transitions are observed in this quasi-2d random magnetic system by the measurements of susceptibility and spontaneous magnetization using a

SQUID magnetometer[15,20] and of heat capacity. There are three transition temperatures T_0, T_{p1} and T_{p2} ($T_0 > T_{p1} > T_{p2}$). Combining with the experimental results of neutron diffraction, the second transition point T_{p1} is sure to be the 3d long range order temperature.[15,21,22] The first transition point T_0 is that from the paramagnetic into a kind of 2d ordered state. The third transition point T_{p2} is that from the intermediate 3d into the final unified long range ordered state.

In Appendix, the phase diagram for $Cu(HCOO)_2 \cdot 2H_2O \cdot 2CO(NH_2)_2$ (CuFUH) under the external field is investigated by the measurement of differential susceptibility. This is a supplement of chapter II.

§I-2. Experimental procedure

Nuclear magnetic resonance of proton was measured by the conventional steady method. As for the experiments under the zero field or small external field, the second- and first-derivatives of NMR spectra, respectively were detected by field modulation and frequency sweep. And as for those under the high external field, the first derivative were detected by field modulation and field sweep. The NMR experiments at higher frequency from 1 to 40 MHz were performed by the Robinson type spectrometer,[24] and those at lower frequency from 500 kHz to 1.5 MHz were by another Robinson type spectrometer[25] which is sensitive in low frequency oscillation. The experiments at higher frequency than 40 MHz up to 250 MHz were performed using Hewlett Packard vector voltmeter 8405-A. The block diagrams are given in Fig.I-1 and Fig.I-2, respectively.

The NMR measurements at the temperatures above 4.2 K were made

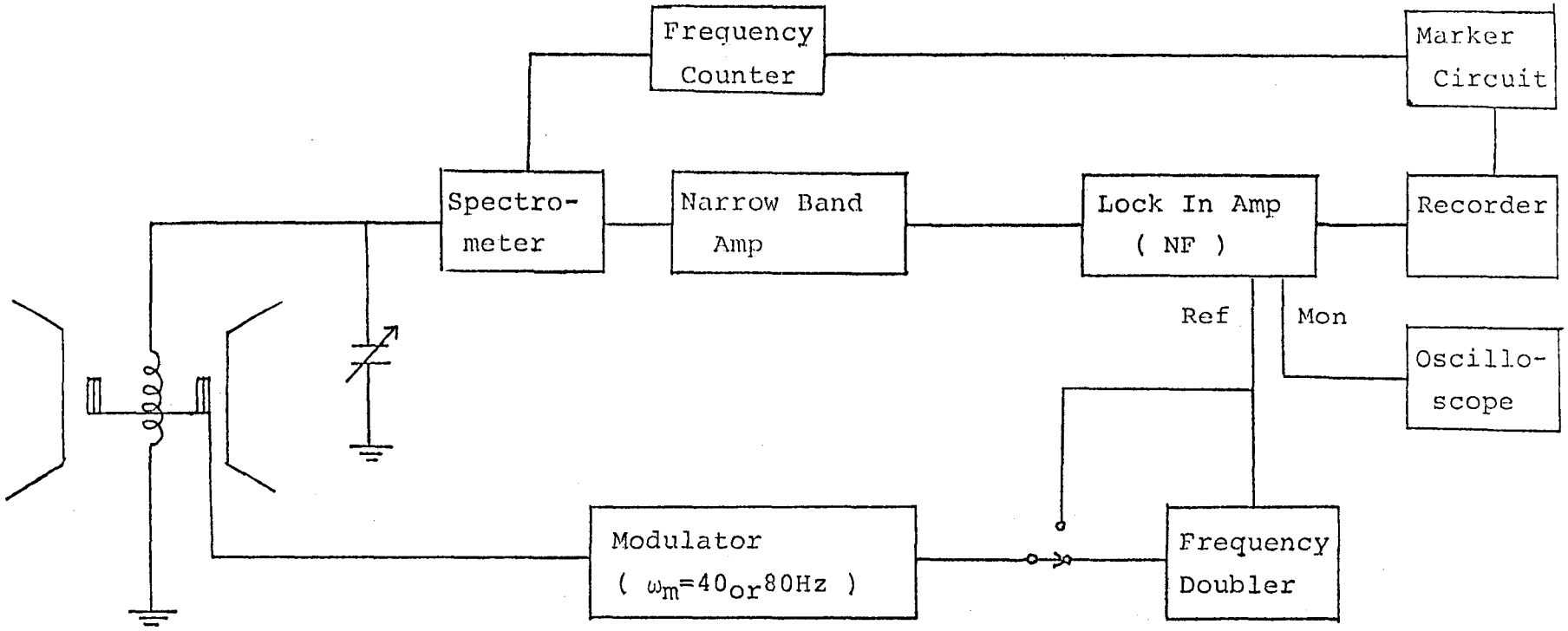

Fig.I-1. The block diagram of neuclear magnetic resonance measurement, for $\nu \lesssim$ 40 MHz.

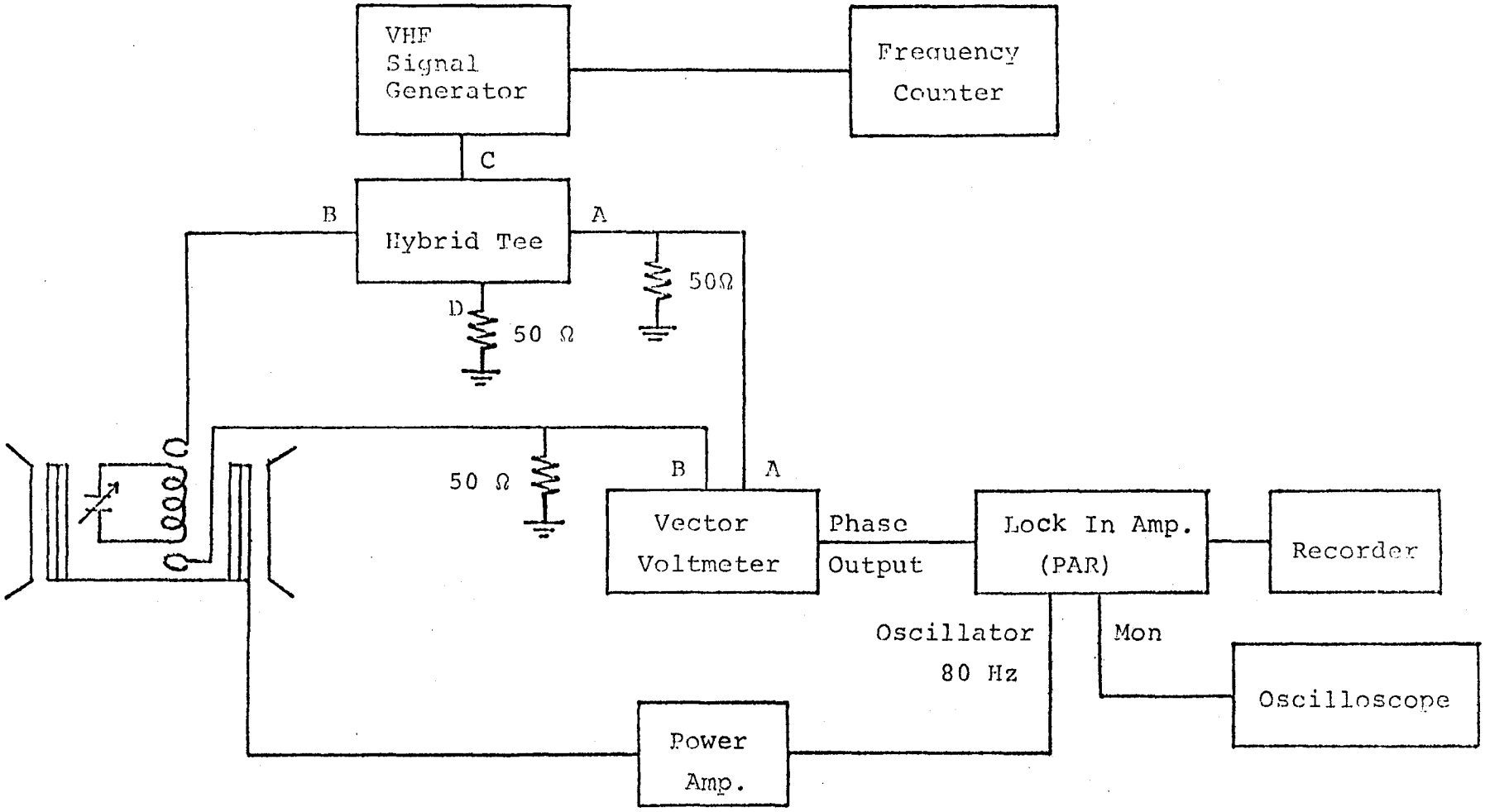

Fig.I-2. The block diagram of NMR measurement for 40 MHz $\lesssim \nu \lesssim$ 250 MHz.

in adiabatic cell. In order to avoid the heat up caused by eddy current losses, the thermal block consists of quartz plates. Quartz has an excellent heat conductivity below 50 K which is almost comparable with that of Cu metal. The temperature control is $\Delta T/T \lesssim 10^{-4}$ at the temperature below 20 K.

The direction of external field is corrected precisely by additional field which is perpendicular to the main field and is generated by the small-sized handmade superconducting magnet. Accordingly, the field direction is able to be setted spatially with the error less than 0.2°. It will be described in detail in §II-2.3.

The experimental method for measuring the heat capacity was essentially the same as ever reported.[25,26] The ac susceptibility was usually measured by Hartshorn bridge method operated at the frequency of 100 Hz with the amplitude of about 1 Oe.

The temperature dependences of the spontaneous magnetization and ac susceptibility at zero field in the immediate neighbourhood of T_N was measured simultaneously by using a SQUID magnetometer. The zero field measurements are made at negligibly small residual dc field including earth field and a suppression of exciting ac field intensity. Both fields are less than 5 mOe. In order to obtain the spontaneous magnetization, so-called "field cooling" method is applied.

Neutron diffraction experiment was performed by using the double axis spectrometer of Institute for Solid State Physics (ISSP), the University of Tokyo in JRR-3 of JAERI, Tokai. For the quasi elastic scattering, the triple axis spectrometer of ISSP in JRR-2 is used without doing energy analysis, to improve the S/N ratio of

the Bragg ridge, and also used to detect the Bragg points.

§I-3. Sample preparation

Samples of CuFUH and CuFUD of which protons are deuterated except for the protons of formic radicals were used for the experiments in Chap.II. The single crystals of CuFUH (CuFUD) were grown from saturated aqueous solution of CuF4H [CuF4D] and $(NH_2)_2CO$ [$(ND_2)_2CO$] by recrystallization using the temperature dependence of solubility in the temperature range between 20°c and 30°c. The single crystals were grown from seed crystals hung by nyron fibers in the solution. Single crystals of CuF4H and CuF4D were obtained in the same way. Colors of CuFUH [CuFUD] and CuF4H [CuF4D] are blue and light blue, respectively. There are not change of colors and lattice structure by deuteration.

Single crystals of MnF2H and MnF2D were grown by a slow evaporation of saturated aqueous solution at the constant temperature about 50°c. Colors of MnF2H and MnF2D are light pinc. These samples were used for the experiments in Chap.III and IV.

Single crystals of $Mn_{1-x}Zn_xF2D$ are grown by the following procedure.[20] First, the deuterated powdered specimen is prepared by usual slow evaporation method from the saturated heavy water solution of the mixture of the hydrated salts MnF2H and ZnF2H of reagent grade. Second, in a saturated heavy water solution of the powdered specimen mentioned above, single crystals are grown by suspending small seed crystals which are quite transparent and of good outer shape, by fine nylon fibers. In the whole recrystallization process, the saturated aqueous solution is kept at constant

temperature of about 50°c and at a constant and homogeneous concentration by a steady stiring of the solution at a constant speed in thermostat. In this way, transparent crystals of light pinc color and of nearly hexagonal block with linear dimension of about 5 mm are grown in several weeks. On the single crystals such prepared, the ac susceptibility measurement is made in order to check the randomness of dilution.

The substitution ratio from proton to deuterium is about 90 % after twice deuteration for CuFUH. These ratios are larger than 90 % for MnF2H and $Mn_{1-x}Zn_xF2H$. The deuteration is very important for the experiment of neutron diffraction because of incoherent diffraction of protons.

References (I)

1) See, e.g. L. J. de Jongh and A. R. Miedema: Advances in Phys. 23(1974) 1.

2) E. Ising: Z. Phys. 31 (1925) 253.

3) N. D. Mermin and H. Wagner: Phys. Rev. Lett. 17 (1966) 1133.

4) J. C. Bonner and M. E. Fisher: Phys. Rev. A 135 (1964) 640.

5) See, e.g. C. Domb: Phase Transitions and Critical Phenomena ed. Domb and Green Vol.3 P.357.

6) See, e.g. M. Steiner, J. Villain and C. G. Windsor: Advances in Phys. 25 (1976) 87.

7) L. Onsager: Phys. Rev. 5 (1944) 117.

8) C. N. Yang: Phys. Rev. 85 (1952) 809.

9) R. B. Griffiths: Phys. Rev. Lett. 24 (1970) 1479,
L. P. Kadanoff: Proceedings of the Enrico Fermi Summer School, edited by M. S. Green (Academic Press, 1972)

10) M. Suzuki: Progr. Theor. Phys. 51 (1974) 1992.

11) L. L. Liu and H. E. Stanley: Phys. Rev. B 8 (1973) 2279.

12) R. J. Birgeneau, J. Als-Nielsen and G. Shirane: Phys. Rev. 16 (1977) 280.

13) K. Hirakawa and H. Ikeda: J. Phys. Soc. Jpn. 35 (1973) 1328.

14) K. Yamagata, Y. Kozuka and T. Morita: J. Phys. Soc. Jpn. 50 (1981) 421.

15) M. Matsuura, K. Koyama and Y. Murakami: J. Phys. Soc. Jpn. 52 (1983) Suppl. 37.

16) K. Koyama, N. Terata and M. Matsuura: J. Phys. Soc. Jpn. 51 (1982) 2697.

17) K. Koyama, K. Amaya and K. Takeda: J. Mag. Mag. Materials 31-34 (1983) 1196.

18) K. Takeda and K. Koyama: J. Phys. Soc. Jpn. 52 (1983) 648.

19) K. Takeda and K. Koyama: J. Phys. Soc. Jpn. 52 (1983) 656.

20) M. Matsuura, Y. Yamamoto, S. Ohtake, K. Koyama an T. Haseda: J. Mag. Mag. Materials 15-18 (1980) 235.

21) M. Matsuura, K. Koyama, Y. Murakami, Y. Ajiro and N. Terata: Physica 120 B (1983) 206.

22) M. Matsuura, Y. Ajiro, K. Adachi, N. Terata and K. Koyama: J. Mag. Mag. Materials 14 (1979) 157.

23) F. N. H. Robinson and H. A. D. Phil: J. Sci. Instrum. 36 (1959) 481.

24) D. T. Edmond and F. N. H. Robinson: J. Sci. Instrum. 44 (1967) 475.

25) W. J. M. de Jonge, J. P. A. M. Hij ans, F. Boersma, J. C. Shouten and K. Kopinga: Phys. Rev. B 17 (1978) 2922.

26) K. Takeda, T. Koike, T. Tonegawa and I. Harada: J. Phys. Soc. Jpn. 48 (1980) 1115.

27) J. Fröhlich and E. H. Lieb: Phys. Rev. Lett. 38 (1977) 440.

28) H. Ikeda, M. Suzuki and M. T. Hutchings: J. Phys. Soc. Jpn. 46 (1979) 1153.

29) H. Ikeda, I. Hatta and M. Tanaka: J. Phys. Soc. Jpn. 40 (1976) 334.

Chapter II. Ordering of $Cu(HCOO)_2 \cdot 2H_2O \cdot 2CO(NH_2)_2$ and $Cu(HCOO)_2 \cdot 2D_2O \cdot 2CO(ND_2)_2$

§II-1. Characteristic of $Cu(HCOO)_2 \cdot 2H_2O \cdot 2CO(NH_2)_2$

The crystal and the magnetic structure of $Cu(HCOO)_2 \cdot 2H_2O \cdot 2CO(NH_2)_2$ (CuFUH) are essentially the same as those of a well-known quasi-two-dimensional antiferromagnet $Cu(HCOO)_2 \cdot 4H_2O$ (CuF4H).[1] The crystal of CuFUH has a distinct layer structure with copper formate sheets parallel to the (100) plane as seen in Fig.II-1. All Cu^{2+} ions are in the (100) plane and form a slightly distorted square lattice which is almost the same as in CuF4H. The bridging formate groups provide a superexchange pathway in the plane. The adjacent planes of Cu^{2+} ions are separated by water and urea molecules, while those in CuF4H only by water molecules. Consequently the inter-layer interaction J' of CuFUH is much weaker than that of CuF4H. The compound CuFUH approximates a 2d Heisenberg antiferromagnet of S = 1/2 with the intra-layer interaction J/k = -33 K [2] It is an interesting system in which a quantum effect like e.g. spin reduction may be observed experimentally. It goes into the 3d antiferromagnetic ordered state at T_N = 15.5 K.

The compound CuFUH is a crystallographic two sublattice (C_2) system, magnetic basic properties of which are rigorously studied on the basis of the linear responce theory.[3] For C_2 system in which the $\tilde{g}$-tensors of magnetic ions at the two sublattice points are not equivalent, the basic Hamiltonian is expressed as

$$\mathcal{H} = \mathcal{H}_0 + \mathcal{H}_z \qquad (2.1)$$

where $\mathcal{H}_0$ is the Hamiltonian without external field and $\mathcal{H}_z$ is the

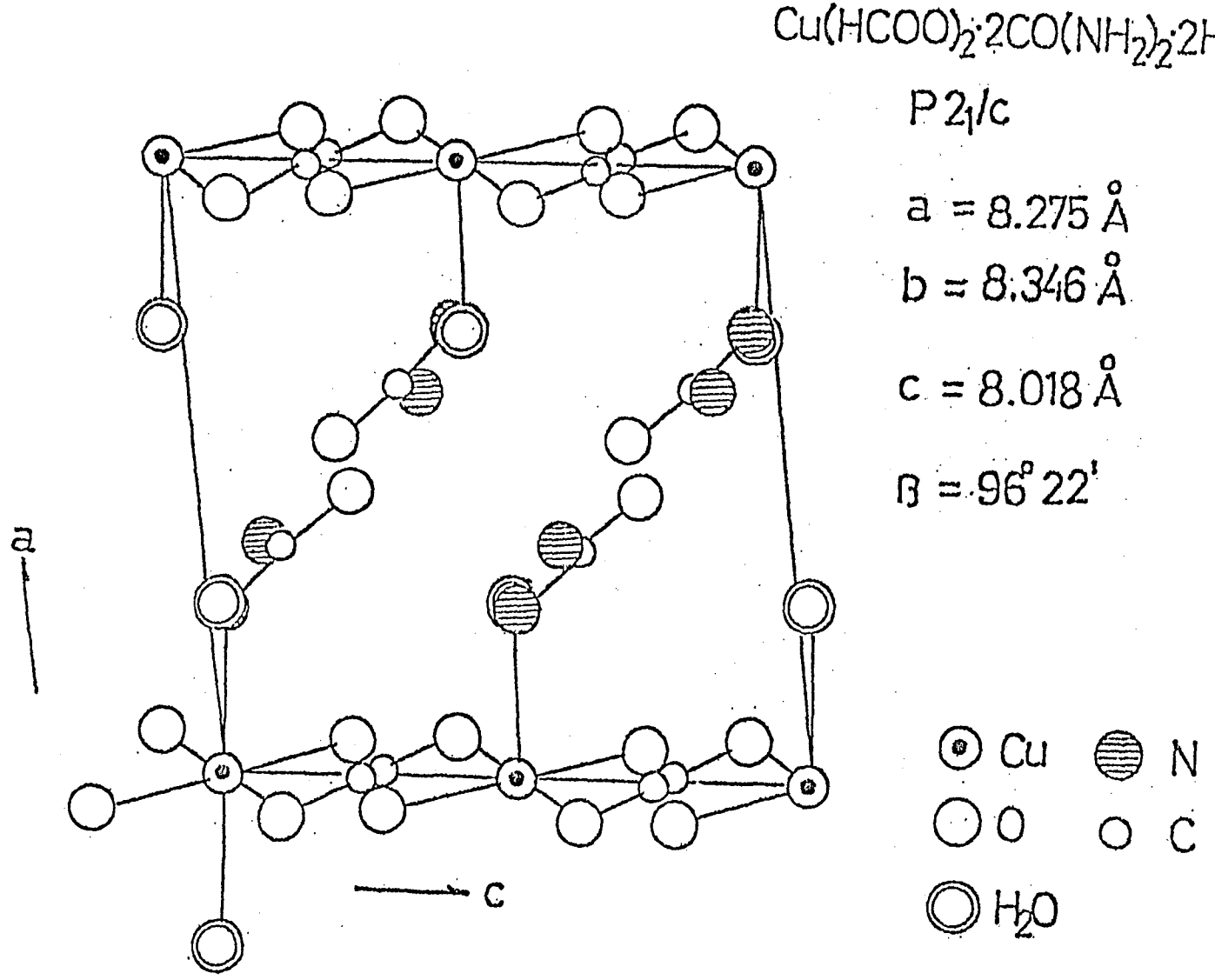

Fig.II-1. Crystal structure of $Cu(HCOO)_2 \cdot 2CO(NH_2)_2 \cdot 2H_2O$.

Hamiltonian of Zeeman interaction and expressed as

$$\mathcal{H}_z = -\mu_B \cdot \Sigma_{ij} (S_1^i \tilde{g}_1 + S_2^j \tilde{g}_2) \vec{H} \tag{2.2}$$

where $\tilde{g}_1$ and $\tilde{g}_2$ are the $\tilde{g}$- tensors of magnetic ions at 1 and 2 sublattice points, respectively. This Zeeman term is expressed in another form as

$$\mathcal{H}_z = -\mu_B \Sigma_{ij} (S_1^i + S_2^j) \cdot \tilde{g} \cdot \vec{H} - \mu_B \Sigma_{ij} (S_1^i - S_2^j) \cdot \tilde{g} \cdot \vec{H}_s \tag{2.3}$$

where $$\vec{H}_s = \tilde{g}^{-1} \cdot \tilde{d} \cdot \vec{H} \tag{2.4}$$

$\tilde{g}$ and $\tilde{d}$ are the average and the difference tensors of $\tilde{g}_1$ and $\tilde{g}_2$ defined by

$$\tilde{g} = \frac{1}{2}(\tilde{g}_1 + \tilde{g}_2) \tag{2.5}$$

$$\tilde{d} = \frac{1}{2}(\tilde{g}_1 - \tilde{g}_2) \tag{2.6}$$

and $\tilde{g}^{-1}$ is the inverse tensor of $\tilde{g}$. From a physical view point, it means the fact that a C_2 system under a uniform field is quite equivalent to a crystallographically single lattice system (C_1 system) in which the $\tilde{g}$-tensor of magnetic ions at all lattice points are equal to $\tilde{g}$ under both a uniform field $\vec{H}$ and a staggered field $\vec{H}_s$. The staggered field is generally defined as a wavy excitation field whose wave length is a half of the lattice spacing. As the staggered field is the conjugate field of order parameter of antiferromagnets, it is just the staggered susceptibility that characterizes the critical phenomena of antiferromagnet. In order to distinguish this fictious C_1 system, let us add a suffix "f" to the physical quantity of C_1 system.

The uniform and the staggered magnetization operator for the C_2 and C_1 system are defined by

$$\vec{m} = \mu_B \sum_{ij} (\tilde{g}_1 S_1^i + \tilde{g}_2 S_2^j) \tag{2.7}$$

$$\vec{\ell} = \mu_B \sum_{ij} (\tilde{g}_1 S_1^i - \tilde{g}_2 S_2^j) \tag{2.8}$$

and

$$\vec{m}_f = \mu_B \sum_{ij} \tilde{g} (S_1^i + S_2^j) \tag{2.9}$$

$$\vec{\ell}_f = \mu_B \sum_{ij} \tilde{g} (S_1^i - S_2^j) \ , \tag{2.10}$$

respectively. The uniform and staggered magnetizations of the C_2 system $\vec{M}$ and $\vec{L}$, which are the canonical average of $\langle\vec{m}\rangle$ and $\langle\vec{\ell}\rangle$, are related to those of the C_1 system $\vec{M}_f$ and $\vec{L}_f$ by the equations

$$\vec{M} = \vec{M}_f + \tilde{a} \cdot \tilde{g}^{-1} \cdot \vec{L}_f, \tag{2.11}$$

and

$$\vec{L} = \vec{L}_f + \tilde{a} \cdot \tilde{g}^{-1} \cdot \vec{M}_f. \tag{2.12}$$

Owing to this one to one correspondence between the C_1 and C_2 systems all the magnetic properties of the C_2 system can be derived from those of the C_1 system and vice versa.[3,4,5)]

In the following, the basic properties of a C_1 system is examined when both an external uniform and a staggered fields are applied. If the external fields are weak enough and the system is in the paramagnetic state, the uniform and the staggered magnetizations $\vec{M}_f$ and $\vec{L}_f$ are expressed by the linear combination of $\vec{H}$ and $\vec{H}_s$ as follows.

$$\vec{M}_f = \tilde{\chi}_u^f \vec{H} + \tilde{\chi}_{us}^f \vec{H}_s \tag{2.13}$$

$$\vec{L}_f = \tilde{\chi}_{su}^f \vec{H} + \tilde{\chi}_s^f \vec{H}_s. \tag{2.14}$$

The coefficients $\tilde{\chi}_{us}^f$ and $\tilde{\chi}_{su}^f$ are the uniform and staggered

magnetizations induced by a unit staggered and a unit uniform fields, respectively. The coefficients χ_u^f and χ_s^f are the uniform and the staggered susceptibility tensors, respectively.

Putting eqs. (2.13) and (2.14) into eqs. (2.11) and (2.12), the uniform susceptibility of C_2 system, which is defined by $\vec{M} = \tilde{\chi}_u \cdot \vec{H}$, is written as

$$\tilde{\chi}_u = \tilde{\chi}_u^f + \tilde{\chi}_{us}^f \cdot \tilde{g}^{-1} \cdot \tilde{d} + \tilde{d} \cdot \tilde{g}^{-1} \cdot \tilde{\chi}_{su}^f + \tilde{d} \cdot \tilde{g}^{-1} \cdot \tilde{\chi}_s^f \cdot \tilde{g}^{-1} \cdot \tilde{d}. \quad (2.15)$$

The effective staggered susceptibility of C_2 system is defined by $\vec{L} = \tilde{\chi}_s^{ef} \cdot \vec{H}$, then

$$\tilde{\chi}_s^{ef} = \tilde{\chi}_{su}^f + \tilde{\chi}_s^f \cdot \tilde{g}^{-1} \cdot \tilde{d} + \tilde{d} \cdot \tilde{g}^{-1} \cdot \tilde{\chi}_u^f + \tilde{d} \cdot \tilde{g}^{-1} \cdot \tilde{\chi}_{us}^f \cdot \tilde{g}^{-1} \cdot \tilde{d}. \quad (2.16)$$

Thus in the real C_2 system not only the uniform magnetization but also the staggered magnetization are induced by applying a uniform field $\vec{H}$. The corresponding susceptibilities $\tilde{\chi}_u$ and $\tilde{\chi}_s^{ef}$ are expressed by the linear combination of the uniform, the staggered and the cross susceptibilities of the C_1 system.

The uniform susceptibility is obtained directly by measuring the ac susceptibility by taking the limiting of zero frequency and amplitude of the excitation field. The effective staggered susceptibility is related to the internal field of nucleus and thus to the NMR frequency. The shift of NMR frequency from that of free nucleus is expressed as

$$\Delta\omega = \frac{2}{N} \cdot \gamma \cdot \hat{H} \cdot (\tilde{A}^+ \cdot \tilde{\chi}_u + \tilde{A}^- \cdot \tilde{\chi}_s^{ef}) \cdot \vec{H} \quad (2.17)$$

where $\tilde{A}^{\pm} = \tilde{A}_1 \pm \tilde{A}_2$ and $\tilde{A}_1$ and $\tilde{A}_2$ are the interaction sum tensors of the nucleus with the neighbouring magnetic ions at 1 and 2

sublattice points, respectively. $\hat{H}$ is the unit vector along the external field direction. Once we know $\tilde{\chi}_u$ and $\tilde{\chi}_s^{ef}$, using eqs. (2.15) and (2.16) we can get the information on the uniform, the staggered and the cross susceptibilities of the C_1 system. In the special case in which the zero field Hamiltonian $\mathcal{H}_0$ does not include any antisymmetric term for the interchange of sublattices, the cross susceptibilities $\tilde{\chi}_{us}^f$ and $\tilde{\chi}_{su}^f$ are exactly zero since these quantities are antisymmetric for the interchange of sublattices. $\tilde{\chi}_u$ and $\tilde{\chi}_s^{ef}$ are shorted as

$$\tilde{\chi}_u = \tilde{\chi}_u^f + \tilde{d}\cdot\tilde{g}^{-1}\cdot\tilde{\chi}_s^f\cdot\tilde{g}^{-1}\cdot\tilde{d} \qquad (2.15')$$

$$\tilde{\chi}_s^{ef} = \tilde{\chi}_s^f\cdot\tilde{g}^{-1}\cdot\tilde{d} + \tilde{d}\cdot\tilde{g}^{-1}\cdot\tilde{\chi}_u^f. \qquad (2.16')$$

In antiferromagnet the staggered susceptibility grows much larger than the uniform susceptibility with decreasing temperature towards T_N ($\tilde{\chi}_s^f >> \tilde{\chi}_u^f$). So if $\tilde{\chi}_s^f$ diverges at T_N, the temperature dependence of $\tilde{\chi}_u$ is in proportional to $\tilde{\chi}_s^f$ near T_N ($\tilde{\chi}_u \simeq |\frac{\tilde{d}}{\tilde{g}}|^2\cdot\tilde{\chi}_s^f$), although $\tilde{\chi}_u$ is almost expressed as $\tilde{\chi}_u^f$ at high temperature. There are two contributions of $\tilde{\chi}_u$ and $\tilde{\chi}_s^{ef}$ in the line shift of NMR. Near T_N $\Delta\omega$ is in proportion to $\tilde{\chi}_s^{ef}$ ($\Delta\omega \simeq |\frac{\tilde{d}}{\tilde{g}}|\cdot\tilde{\chi}_s^f$) and the proportional coefficient of $\Delta\omega$ is as about $|\tilde{g}/\tilde{d}|$ times large as that of $\tilde{\chi}_u$ (susceptibility measurement). $|\tilde{d}/\tilde{g}|$ is about 1/25 in this salt as shown later in §II-2.2 experimentally.

Using above staggered field effect, the anisotropy field (H_A) and the inter-layer exchange field (H_E') are estimated. Magnetization curves at 4.2 K[6] are shown in Fig.II-2. Below T_N, sublattice moment is aligned along nearly c-axis (or L_3-axis). The relation between the crystalline axes and the principal axes of the magnetic susceptibility is shown in Fig.II-3. The L_1- and L_3-axis, and the

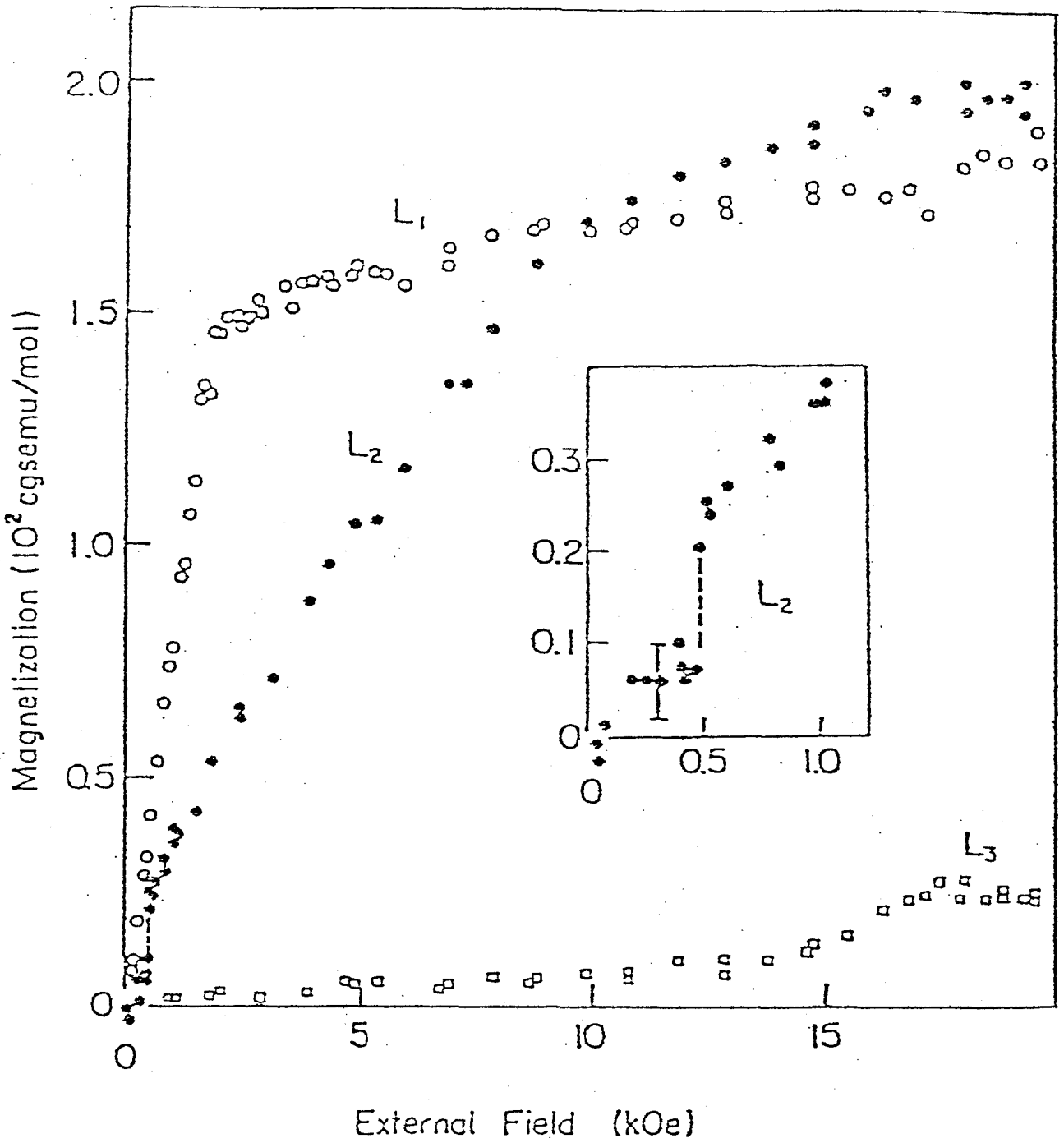

Fig.II-2. Magnetization curves for a single crystal of CuFUH at 4.2 K. The insert is the magnetization curvesaround the jump for H // L_2.[6)]

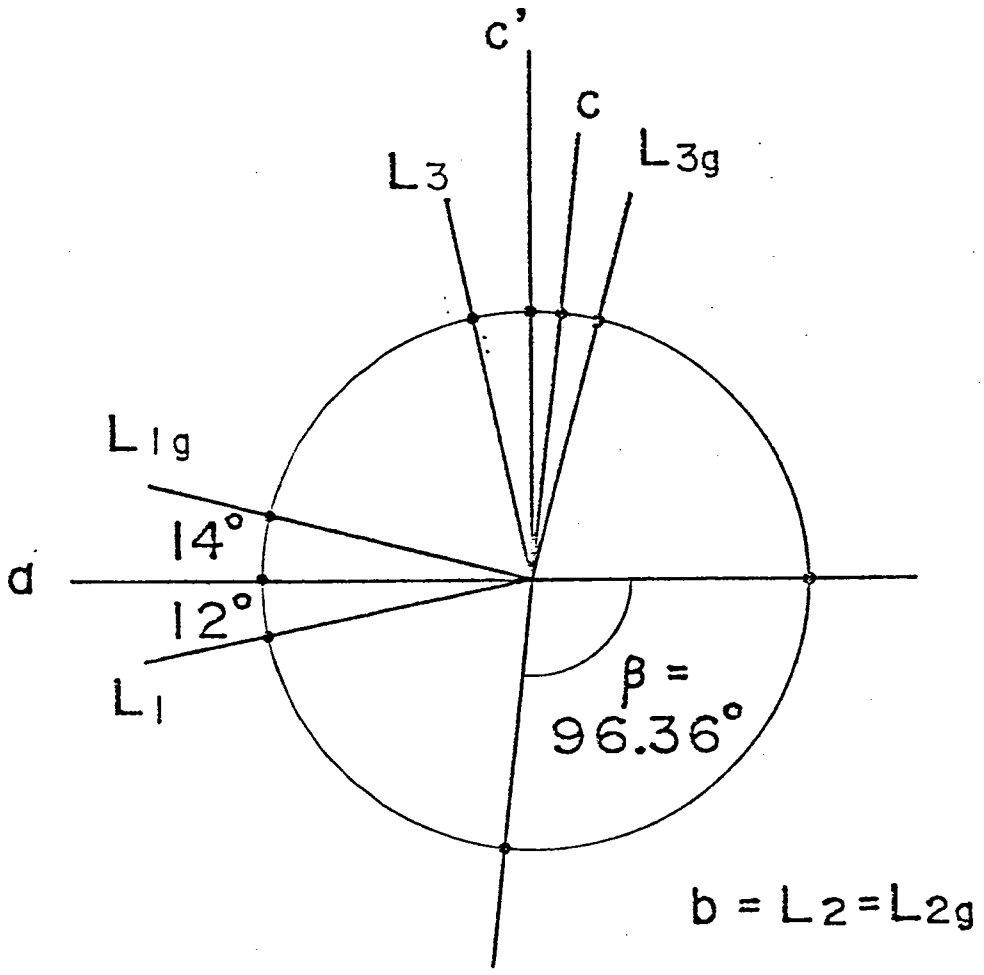

a, b, c : crystalline axis

L_1, L_2, L_3 : the principal axis of the magnetic susceptibility

L_{1g}, L_{2g}, L_{3g} : the principal axis of the g-tensor

Fig.II-3. Relation between the crystalline axes, the principal axes of the susceptibility and the principal axes of the $\tilde{g}$-tensor.

L_{1g}- and L_{3g}-axis were determined from the magnetic susceptibility and the ESR measurement, respectively. When the external field is applied along the L_1- (L_2-)axis, the staggered field is induced along the L_2- (L_1-)axis. And the bendings of magnetization were observed at $H \simeq 2$ kOe and 10 kOe for the field applied parallel to the L_1- and L_2-axis, respectively. This situation is analogous to the case that the external field is applied perpendicular to the easy axis in ferromagnet. So it is possible to estimate the anisotropy field using the staggered field effect. Using that the value of d/g equals to about 1/25 in this salt, we can get two kinds of anisotropy field as $H_A^1 = 80$ Oe and $H_A^2 = 400$ Oe. The exchange field H_E which is known from the intra-layer interaction J (J/k = -33 K) is 1.7×10^6 Oe. Consequently we can evaluate the degree of anisotropy $a \equiv H_A/H_E$ as $5 \sim 24 \times 10^{-5}$, which is excellently small.

While, when the external field was applied along only L_2-axis, the jump of magnetization was observed at $H \simeq 500$ Oe in Fig.II-2. The field of this jump is a good measurement of the inter-layer coupling J', because this jump is occured owing to the phenomenon like the metamagnetic transition concerning inter-layer antiferromagnetic interaction. Inter-layer exchange field H_E' is estimated as 3.5 Oe using the staggered field effect and the discrepancy between the direction of spontaneous magnetization and that of staggered field, and the ratio of inter- to intra-layer interaction $R \equiv |J'/J| \simeq H_E'/H_E$ is given as 2×10^{-6}. After all, CuFUH may present a closest system to the ideal 2d Heisenberg antiferromagnet of all existing real materials.

For CiF4H similar estimations of a and R can be achieved, a is almost the same and R is as about twenty times large as that of

CuFUH, respectively.[7,8]

The phase transition of CuFUH at T_N = 15.5 K is very characteristic. The temperature dependence of susceptibility and heat capacity for this salt is shown in Fig.II-4.[2] A remarkable peak of susceptibility at T_N certainly shows an onset of the phase transition at the temperature. A very small peak of heat capacity is found at T_N. The extra entropy associated with it was about 0.006 % of the total magnetic entropy Rln2 (where R is the gas constant).

§II-2. Experimental results and analysis.

II-2.1 Spin reduction

The result of angular dependence of NMR frequency (pattern) of CuFUD in the ac-plane at T = 17 K > T_N (= 15.5 K) is shown in Fig.II-5. This pattern was examined under the external field of 7.57 kOe. The solid curve is calculated using the induced staggered moment along the b-axis which is induced by the L_1-axis component of the external field. The magnitude of induced staggered moment at this temperature and under the field is 4.1×10^{-21} emu/ion, which is about 42 % of the full moment. The fitting of the data to the calculating internal field with the use of point dipole model or dipole tensor is roughly good. And the value of the induced staggered moment (42 %) is consistent with the result in CuF4D.[4]

The positional parameters of seven crystallographically non-equivalent protons in the unit cell are listed in Table II-1. Using these positional parameters, the dipole sum tensors in 4 sub-lattice structure and in 2 sub-lattice structure are calculated

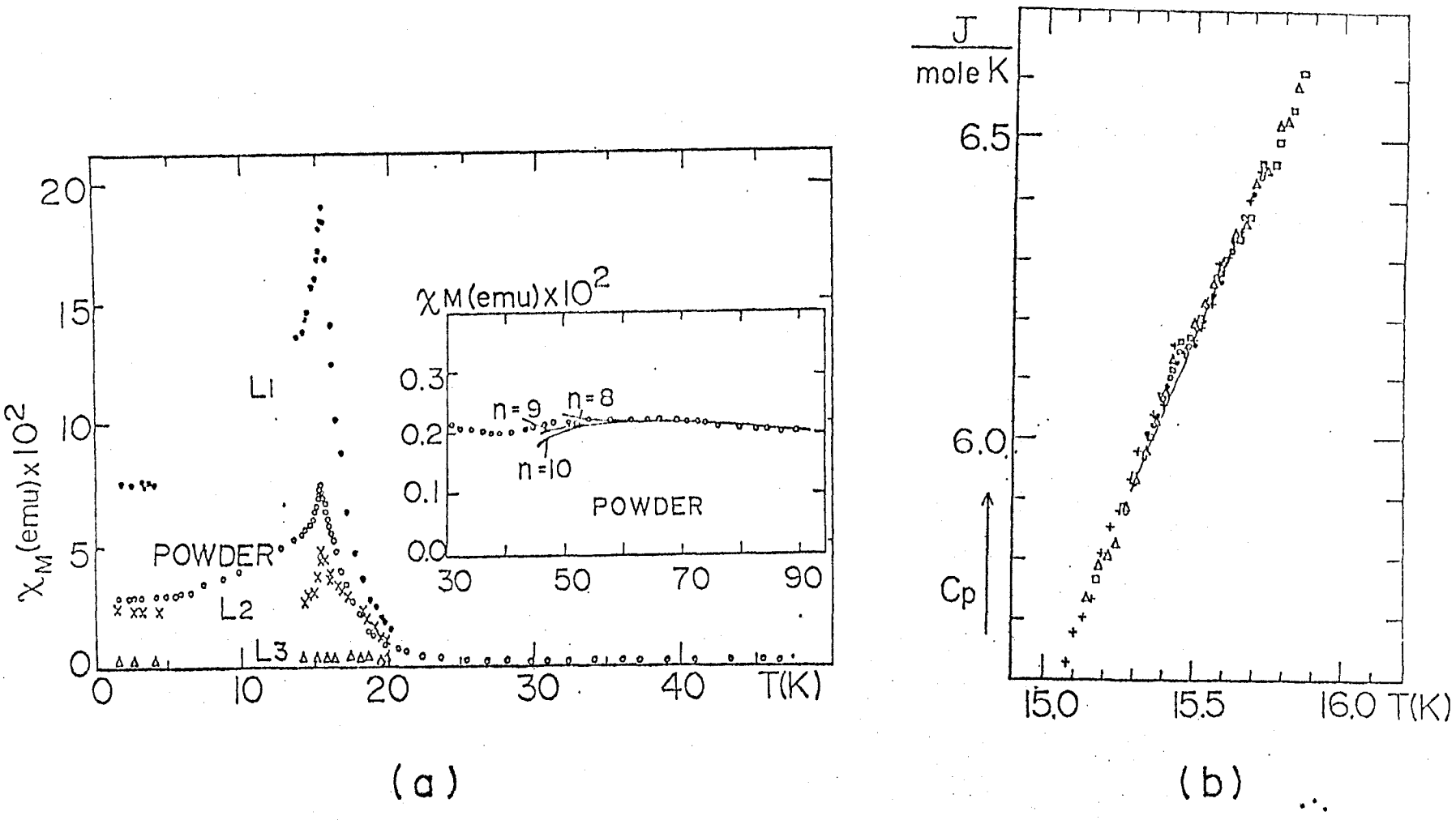

Fig.II-4. Temperature dependences of (a) magnetic susceptibility and (b) heat capacity in CuFUH.[2)]

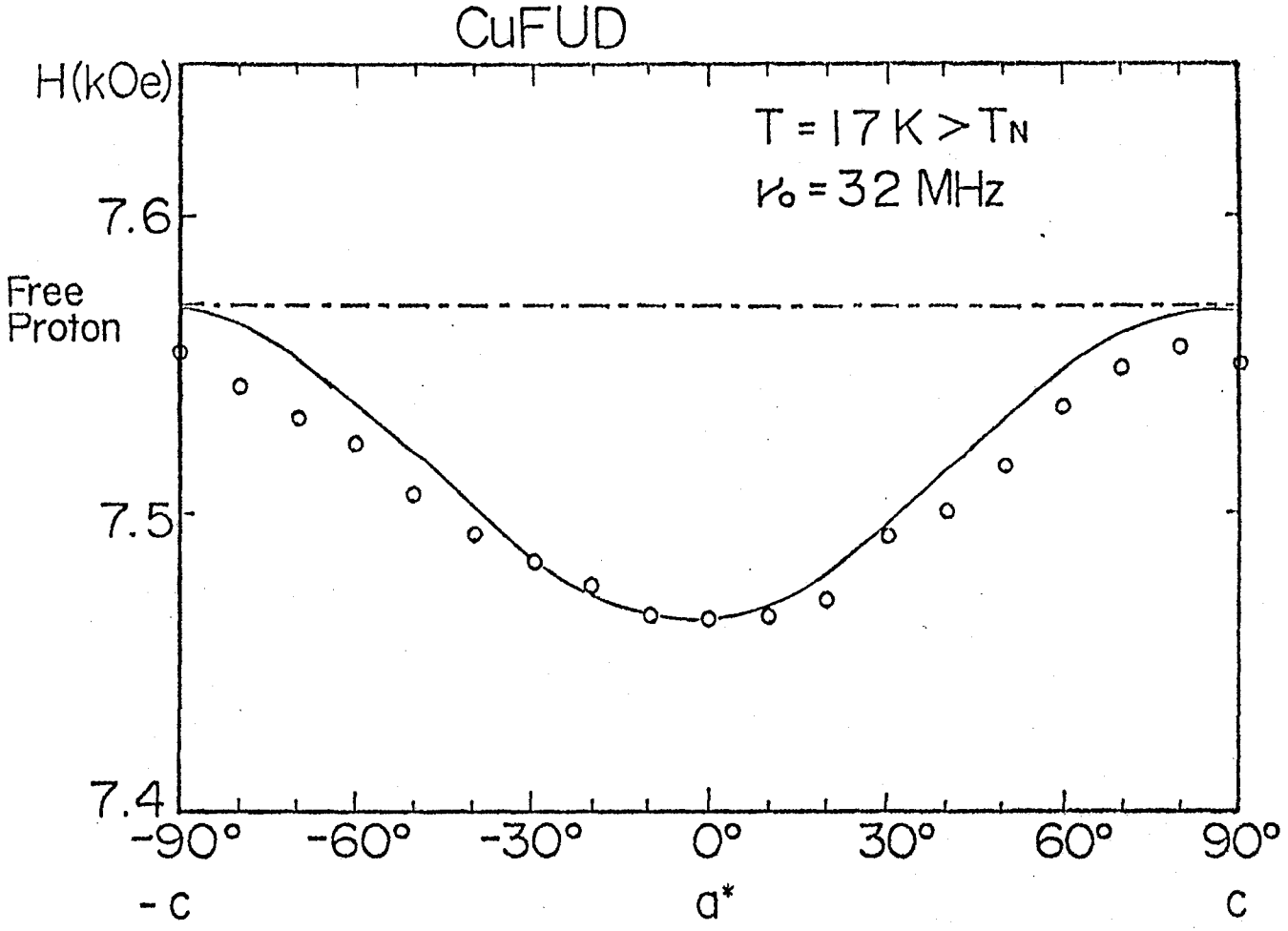

Fig.II-5. Angular dependence pattern under the field (H = 7.57 kOe) in ac-plane above T_N (T = 17 K).

Table II-1.

positional parameters of CuFUH :

proton		positional parameters		
		a	b	c
H_F	F	0.0635	0.2041	0.3165
H_1	N11	0.7097	0.2413	0.4605
H_2	N12	0.5869	0.2572	0.3235
H_3	N21	0.7801	0.0082	0.5435
H_4	N22	0.7266	-0.1338	0.4598
H_5	1W	0.3486	0.0692	0.1019
H_6	2W	0.3280	0.0769	-0.0534

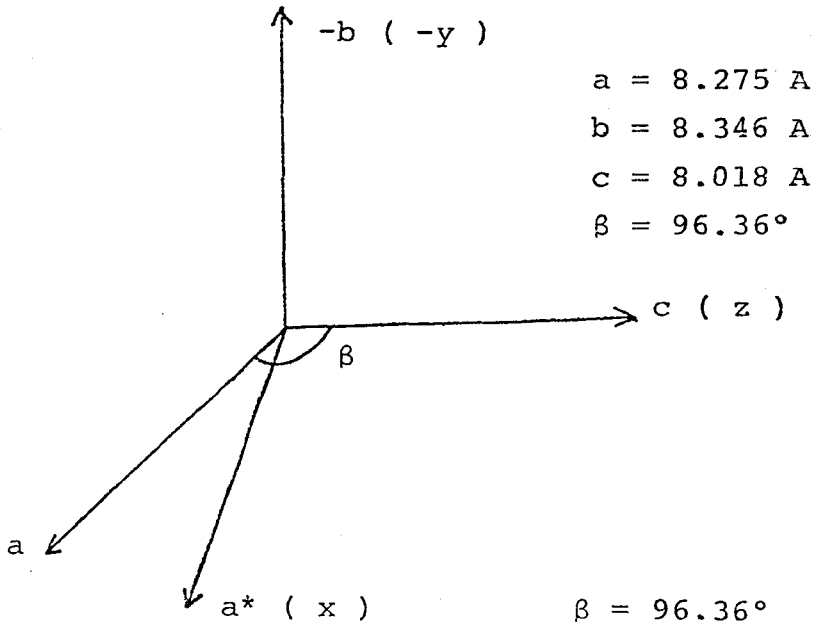

Table II-2.

The dipole sum tensor of CuFUH

4 sub lattice spin structure

($\times 10^{22}$) (cm^{-3})

	x	y	z	
H_F	-0.30	-2.66 4.91	-2.38 0.36 -4.61	x y z
H_1	-2.08	-5.15 -1.85	-0.38 -0.05 3.92	
H_2	-1.16	-2.92 -1.82	-2.04 -0.15 1.35	
H_3	-0.01	-0.17 -4.85	1.38 -0.01 4.86	
H_4	-0.45	2.83 -3.38	-0.39 0.02 3.83	
H_5	-6.45	-2.54 3.11	-2.38 -0.27 3.34	
H_6	-6.49	-3.11 3.47	3.12 0.56 3.02	

Table II-3.

The dipole sum tensor of CuFUH
2 sub lattice spin structure
($\times 10^{22}$) (cm^{-3})

	x	y	z	
H_F	-0.25	-2.59 4.97	-2.37 0.36 -4.72	x y z
H_1	2.49	4.46 1.88	-0.38 0.03 -4.37	
H_2	1.30	1.44 0.07	0.71 0.15 -1.37	
H_3	-0.03	0.16 5.27	-1.52 0.01 -5.23	
H_4	0.41	-2.39 3.78	-0.03 -0.01 -4.19	
H_5	-7.75	-2.12 4.00	-1.56 -0.28 3.75	
H_6	-8.08	-2.69 4.24	3.30 0.55 3.84	

and listed in Table II-2 and Table II-3, respectively. The spin structure formed by the induced staggered moment is 2 sub-lattice structure in which arrangements of inter-later spins are parallel and intra-layer are antiparallel. While, in 4 sub-lattice structure the arrangements of both intra- and inter-layer spins are antiparallel.

For the purpose of determination of the spin structure and the spin reduction in ordered phase at zero field, proton NMR experiments were performed for both CuFUH and CuFUD at 4.2 K. The angular dependence of resonance frequencies was investigated in the bc'- and the ac-planes. Figure II-6(a) and (b) are the patterns in the bc'- and ac-plane under the field of about 50 Oe, respectively. From the figures, it is found that there is no b-(y-)axis component of internal fields at all proton sites. This situation is understood that there is no y-(b-)axis component of sublattice magnetization considering the symmetry. The internal fields at the proton sites are calculated using the dipole-dipole interaction as follows,

$$H_i^{(4)} = \sum_j \tilde{D}_{ij}^{(4)} \cdot L_j^{(4)} = \tilde{D}_i^{(4)} \cdot L^{(4)} \qquad (2.18)$$

where $H_i^{(4)}$ is the internal field at the i-th proton site, $L_j^{(4)}$ is the spontaneous sub-lattice staggered magnetization of j-th sub-lattice and $\tilde{D}_i^{(4)}$ is the dipole sum tensor at the i-th proton site, which is already shown in Table II-2. The line of proton in formic radical is determined from the experiment of CuFUD. Using this result, the spontaneous sub-lattice magnetization was determined by least square fitting as follows,

$$\begin{cases} L_x^{(4)} = 0.78 \times 10^{-21} \text{ emu /ion} \\ L_y^{(4)} = 0 \\ L_z^{(4)} = 5.23 \times 10^{-21} \text{ emu/ion} \end{cases} \qquad \left|L^{(4)}\right| = 5.28 \times 10^{-21} \text{ emu/ion}$$

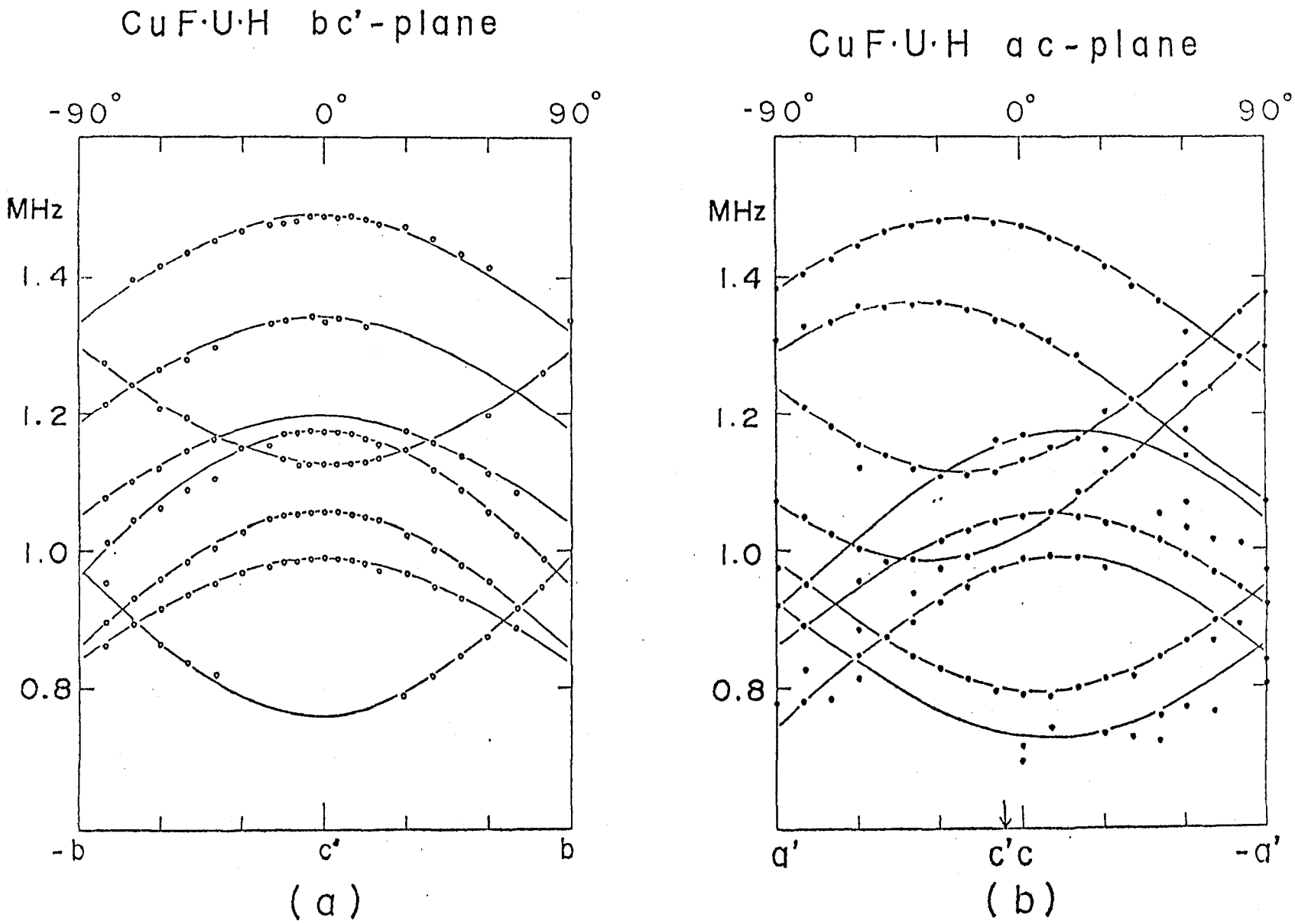

Fig.II-6. Angular dependence patterns under 50 Oe in (a) bc'- and ac-plane.

The amplitude of the canting moment could not determined by proton NMR measurement. Schematic spin structure is shown in Fig.II-7. Using three principal g-values which are $g_{L_{1g}} = 2.37$, $g_{L_{2g}} = 2.11$ and $g_{L_{3g}} = 2.08$[6], the magnitude of spin S is determined as S = 0.276 and the spin reduction is determined as $\Delta S = 45$ %. The calculated internal fields from these sub-lattice magnetizations are listed in Table II-4 and compared with the experimental results. Agreement between them is rather good. An important thing is that this experimental results are explicable with only the unusual magnitude of spontaneous moment.

The spin reduction under the external field was also investigated by proton NMR. When the external field is applied along a*-axis (or ac-plane), the staggered moment is induced along b-axis. Above the field of 2 kOe at which the bending of magnetization was observed,[6] 2 sub-lattice structure is realized. The internal field of i-th proton $H_i^{(2)}$ is expressed as follows, using dipole sum tensor in 2 sub-lattice structure,

$$H_i^{(2)} = \sum_j \tilde{D}_{ij}^{(2)} \cdot L_j^{(2)} = \tilde{D}_i^{(2)} \cdot L^{(2)} \qquad (2.19)$$

where $L^{(2)}$ is the staggered sub-lattice magnetization and has only y-component. As the external field H_{ex} is along a*- (x-)axis, the resonance condition is expressed as

$$|H_{ex} + H_i^{(2)}| = |H_0| \qquad (2.20)$$

where $|H_0|$ is the resonance field of free proton ($|H_0| = \nu_0/\gamma$: ν_0 is the resonance frequency and γ is the gyromagnetic ratio). Equation (2.20) is that of the second degree with respect to the

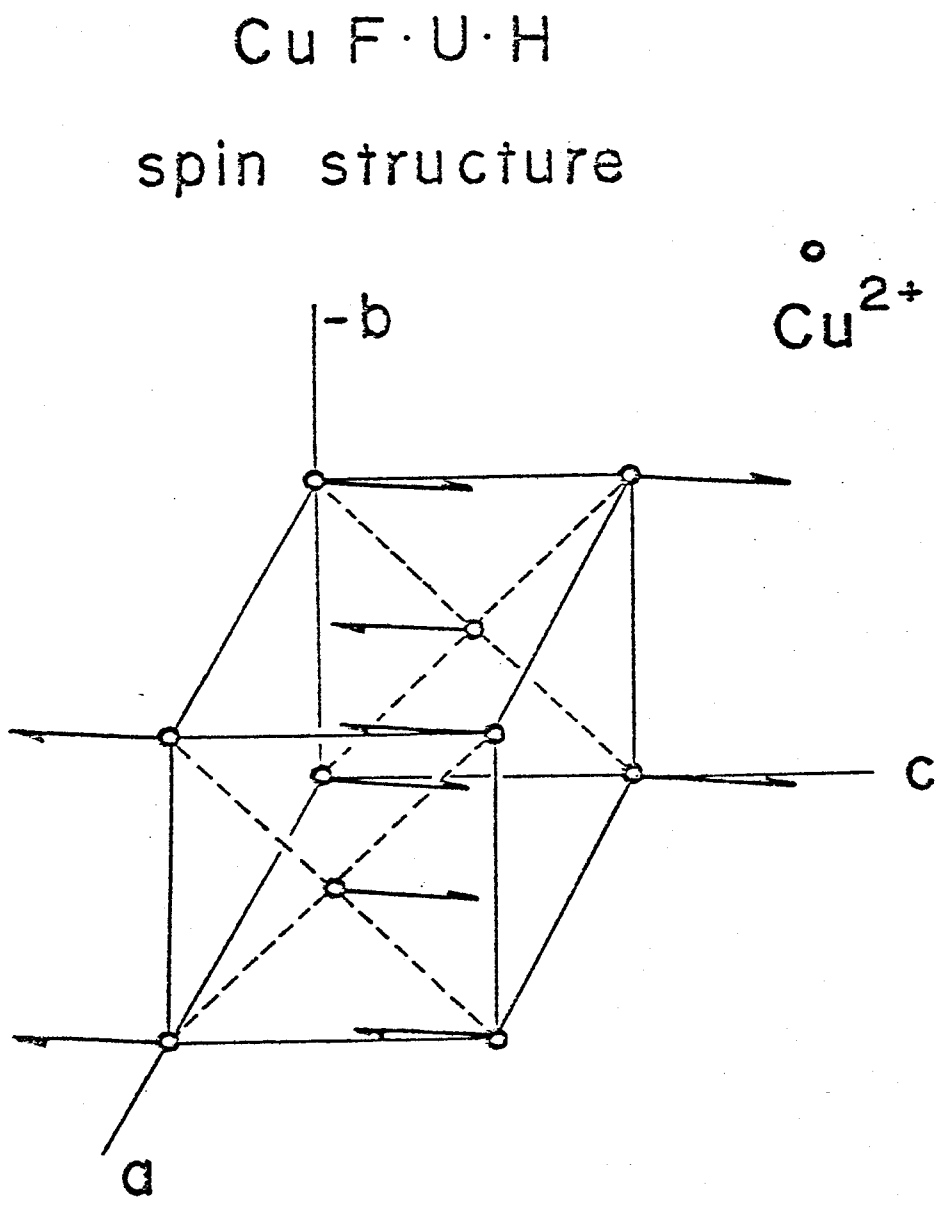

Fig.II-7. Schematic spin structure in 4 sub-lattice state at zero field.

Table II-4. The internal field at proton sites at 4.2 K.

	Experiment			Calculation			
	H (Oe)	α (deg)	β (deg)	H	α	β	Proton
H_F	274	36	0	287	26	0	H(F)
H_3	304	21	0	274	15	0	H(N21)
H_5	241	-	0	235	-48	8	H(1W)
H_6	229	- 6	0	216	32	1	H(2W)
H_1	201	-11	0	209	-10	-12	H(N11)
H_4	189	-16	0	198	- 7	6	H(N22)
H_2	128	-	0	125	-66	-14	H(N12)

$$\begin{cases} L_x = 0.74 \times 10^{-21} \text{ emu/ion} \\ Ly = 0. \\ L_z = 5.23 \times 10^{-21} \text{ emu/ion} \end{cases}$$

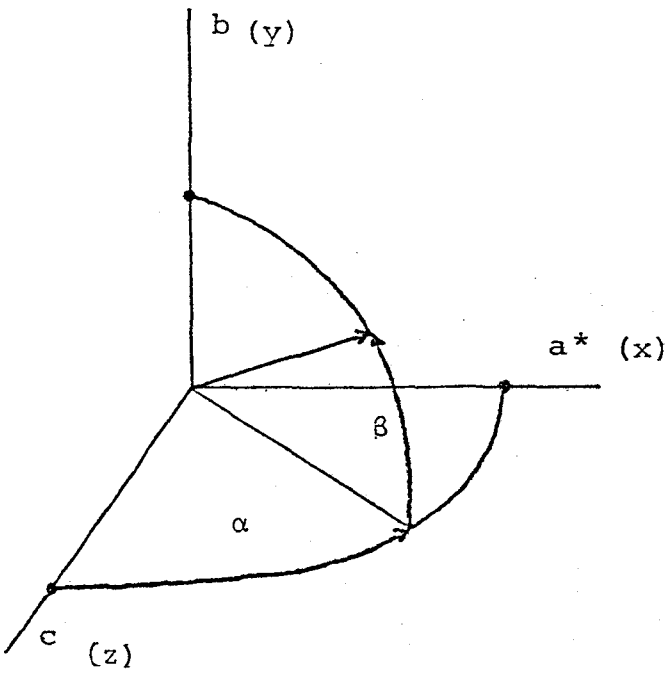

staggered sub-lattice magnetization $L^{(2)}$. As $L^{(2)}$ is along y-(b- or L_{2g}-)axis, using $g_{L_{2g}} = 2.11$ the magnitude of full moment of Cu^{2+} ion (S = 1/2) are calculated as $L_f = 9.78 \times 10^{-21}$ emu/ion. The change of L_y with increasing field was investigated experimentally and shown in Fig.II-8 comparing with L_f. The spin reduction ΔS is 30 ± 3 % and almost constant between 2 kOe and 54 kOe. This value ΔS = 30 % is good agreement with the theoretical value of 28.2 %[9] by the spin wave theory taking into account kinetic interaction (due to finite magnitude of spin). This fact suggest the accuracy of dipole sum tensor again.

The anomalous large spin reduction ΔS = 45 % at H = 0 (in 4 sub-lattice structure) is obtained using the same dipole sum tensor which is used to get ΔS = 30 % at $H > H_{bend}$ (in 2 sub-lattice structure). So the value of ΔS = 45 % at H = 0 must be sure experimentally and anomalous value. This reduction value is almost the same as that of CuF4H (ΔS = 47 %) at H = 0.[10]

II-2.2 Observation of staggered susceptibility

Magnetic susceptibility of CuFUH was measured between 1.2 K and 90 K by Yamamoto et.al[2] (cf. Fig.II-4). A broad maximum of the uniform susceptibility of antiferromagnet associated with the development of short range order was observed near 60 K. A remarkable peak was also found at 15.5 K, which certainly shows an onset of a phase transition. This peak is caused by the staggered susceptibility according to the description in §II-1. Magnetic susceptibility in high temperature region agreed with the calculated one by high temperature series expansion with J/k = -33 K down to about 60 K.

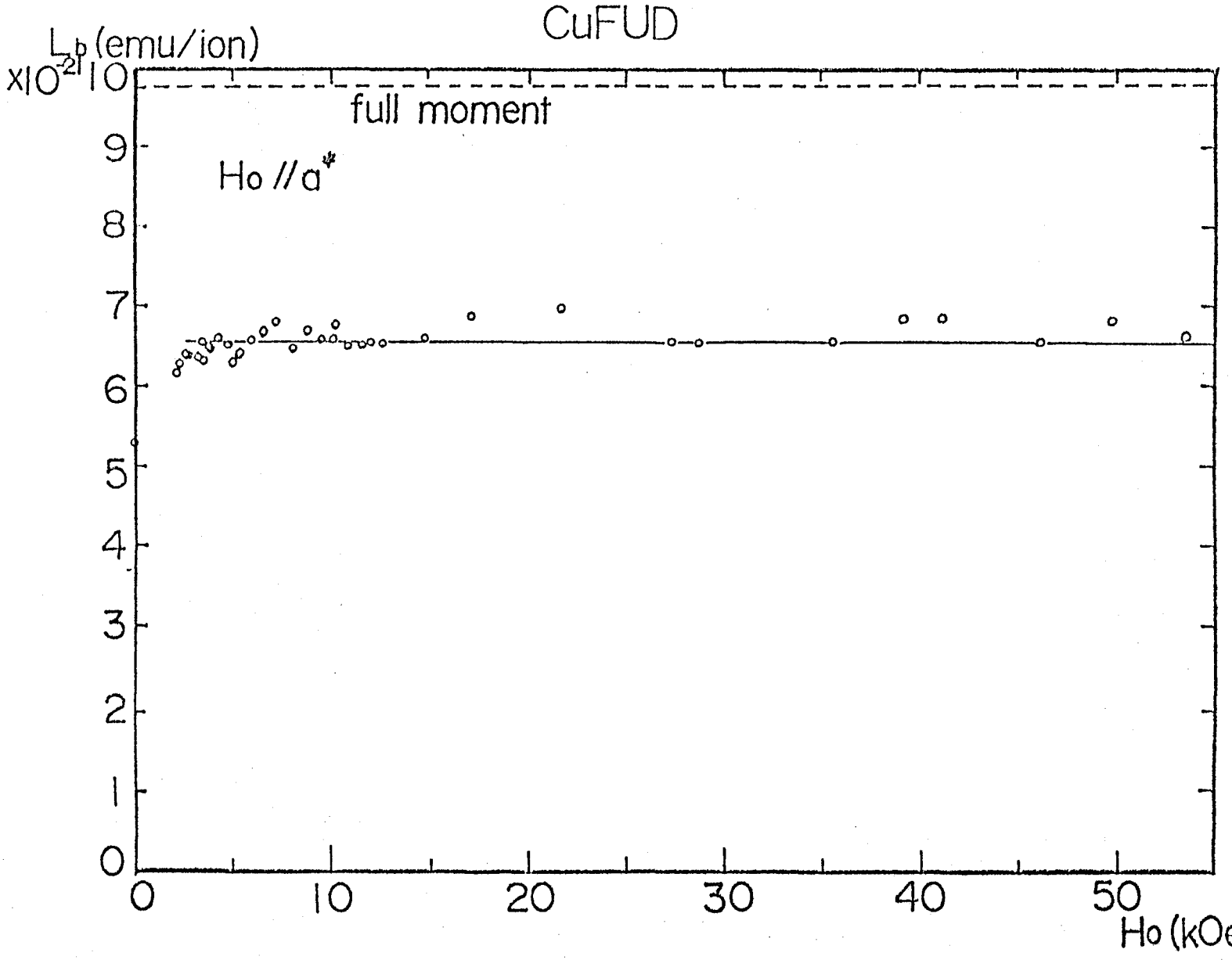

Fig.II-8. Field dependence of staggered moment in 2 sub-lattice state at 4.2 K.

It is possible to measure the staggered susceptibility directly by proton NMR method according to the discription in §II-1. Figure II-9 shows the line shift of a proton in formate radical, which is caused by the staggered moment versus the external field, which is proportional to the staggered field. The initial slope is proportional to the staggered susceptibility. Therefore we can get the temperature dependence of the staggered susceptibility above T_N up to 28 K by the measurement of proton NMR and the uniform susceptibility. Log-log plot of this staggered susceptibility χ_s and the reduced temperature $\varepsilon = (T - T_N)/T_N$ is shown in Fig.II-10. It looks strange that the rounding begins to occur far from the critical point ($\varepsilon \simeq 2 \times 10^{-1}$). According to §II-1, the magnitude of $\xi^2\chi_s^f$ is determined by the direct measurement of susceptibility and $\xi\chi_s^f$ is also determined by the measurement of internal field of proton using NMR method, where ξ is estimated $|\tilde{d}/\tilde{g}|$. As to this salt, the next relation is practically realized.

$$\xi^2\chi_s^f = \frac{1}{1.23}(\chi_{L1} - \chi_{L3}) \simeq \frac{1}{1.23}\cdot\chi_{L1} \qquad (2.21)$$

because $\chi_{L3} \ll \chi_{L1}$ for the low temperature. So, the value of ξ and absolute χ_s^f is calculated from the experimental results, and $\xi \simeq 1/25$.

The theoretical prediction for the susceptibility (χ) of the classical two-dimensional Heisenberg ferromagnet, as calculated directly from the ten-term high-temperature series expansion becomes unreliable for $t \equiv kT/J \simeq 1.5$.[11] The blending of block-spin RG ideas with Monte Carlo techniques has greatly increased the versatility of these methods.[12,13] Monte Carlo data calculated using one-coupling Hamiltonian is extended down to $t \equiv kT/J \simeq 1$.[14]

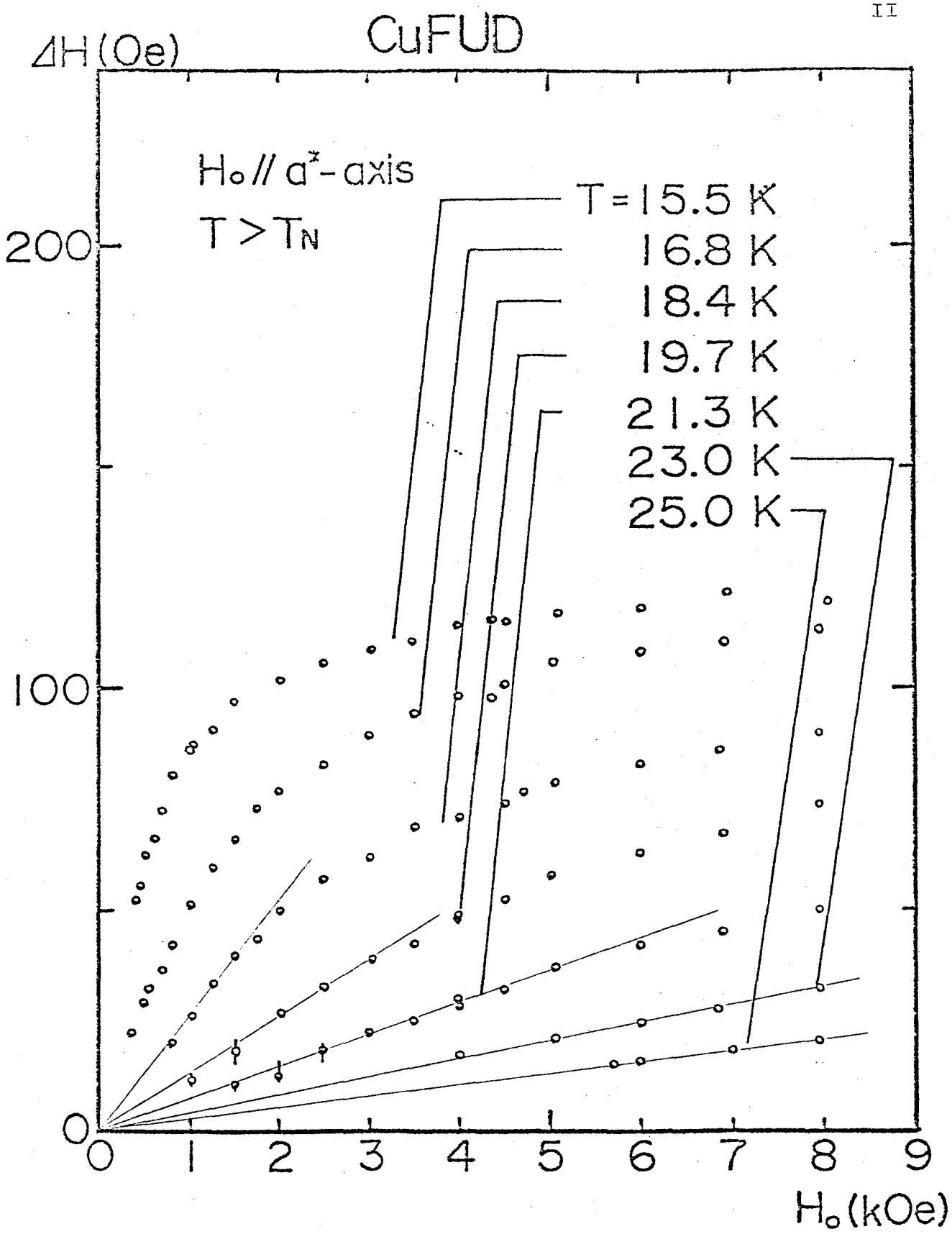

Fig.II-9. Field dependence of NMR line shift above T_N.

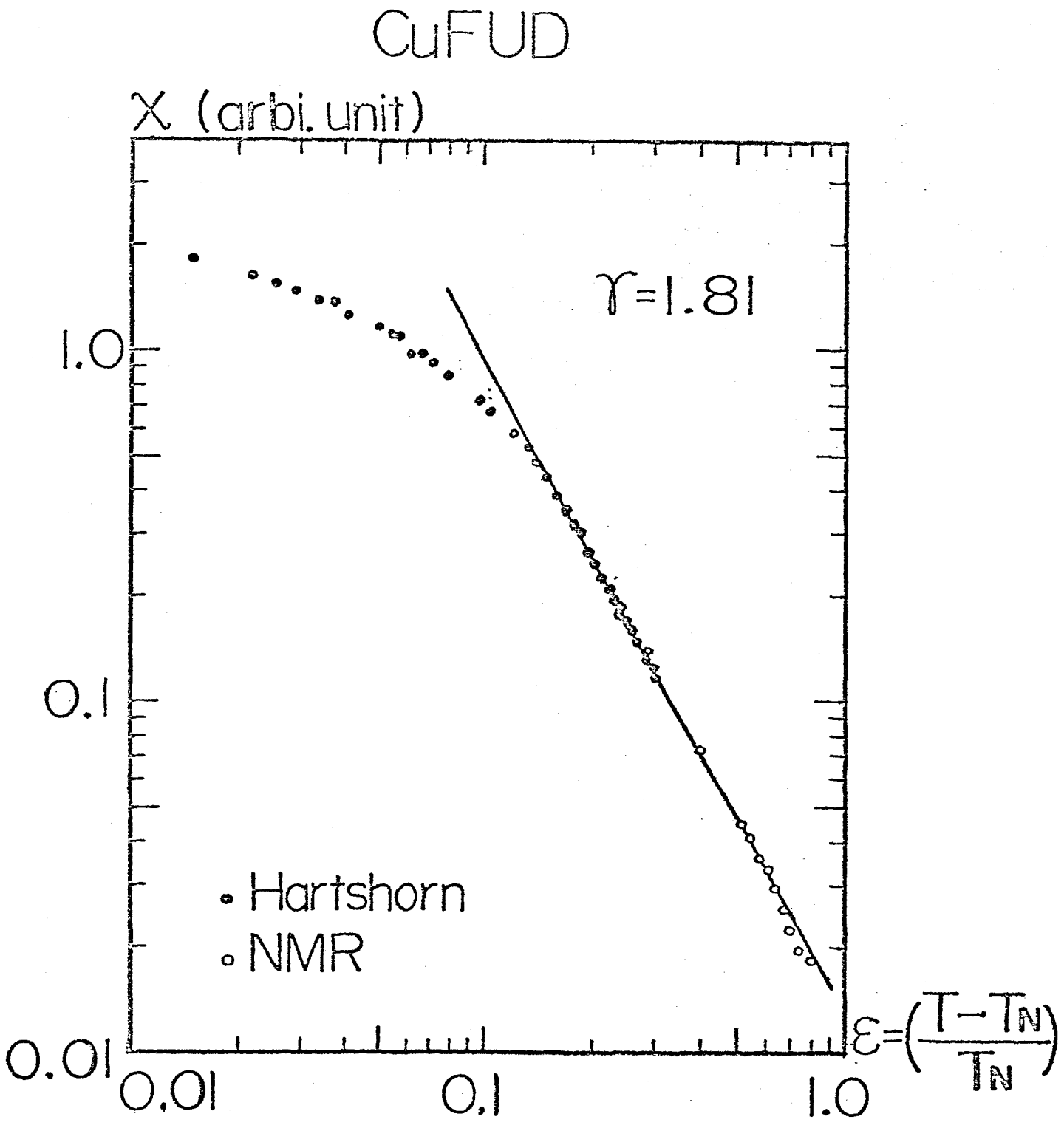

Fig.II-10. Log-log plot of the staggered susceptibility and the reduced temperature $\varepsilon = (T - T_N)/T_N$.

Our experimental data for the staggered susceptibility χ_s^f, which is normalized to Curie's susceptibility C/T, are plotted with the theoretical ones (i.e. M. C. data and the data by high-temperature series expansion and by low-temperature renormalization group method) in Fig.II-11. With decreasing temperature, the experimental data becomes extremely small comparing with the data by the low-temperature renormalization group method. The cause of this discrepancy may be regarded as the quantum effect on susceptibility. Because the staggered magnetization or the order parameter of antiferromagnet does not commute with the exchange Hamiltonian.

II-2.3 Critical index of spontaneous staggered moment

The antiferromagnetic axis in 4 sub-lattice structure below T_N is nearly c-(z-)axis at zero field. Under the external field, the rotation of spins is known to be caused by the staggered field effect as described in §II-2.1 and 2.2. When the external field reachs a certain value H_t, 2 sub-lattice structure that inter-layer spins are arranged parallel is realized. The resultant phase diagram in the ac-plane is shown in Fig.II-12 for the various temperatures below T_N. There exists the L_3-axis where H_t turns to be infinitely large. The phase diagram is symmetric around the L_3-axis. This phase boundary can be explained as the curve on which the magnitude of the staggered field is constant or the L_1-axis component of the external field is constant. (L_1-axis is perpendicular to L_3-axis.) In other expression, $H_t(\theta)\cdot\sin\theta$ is constant for any θ, where θ is the angle from L_3-axis and $H_t(\theta)$ is the transition field from 4 sub- to 2 sub-lattice structure at the angle. When the external field is applied along the L_3-axis, there is not

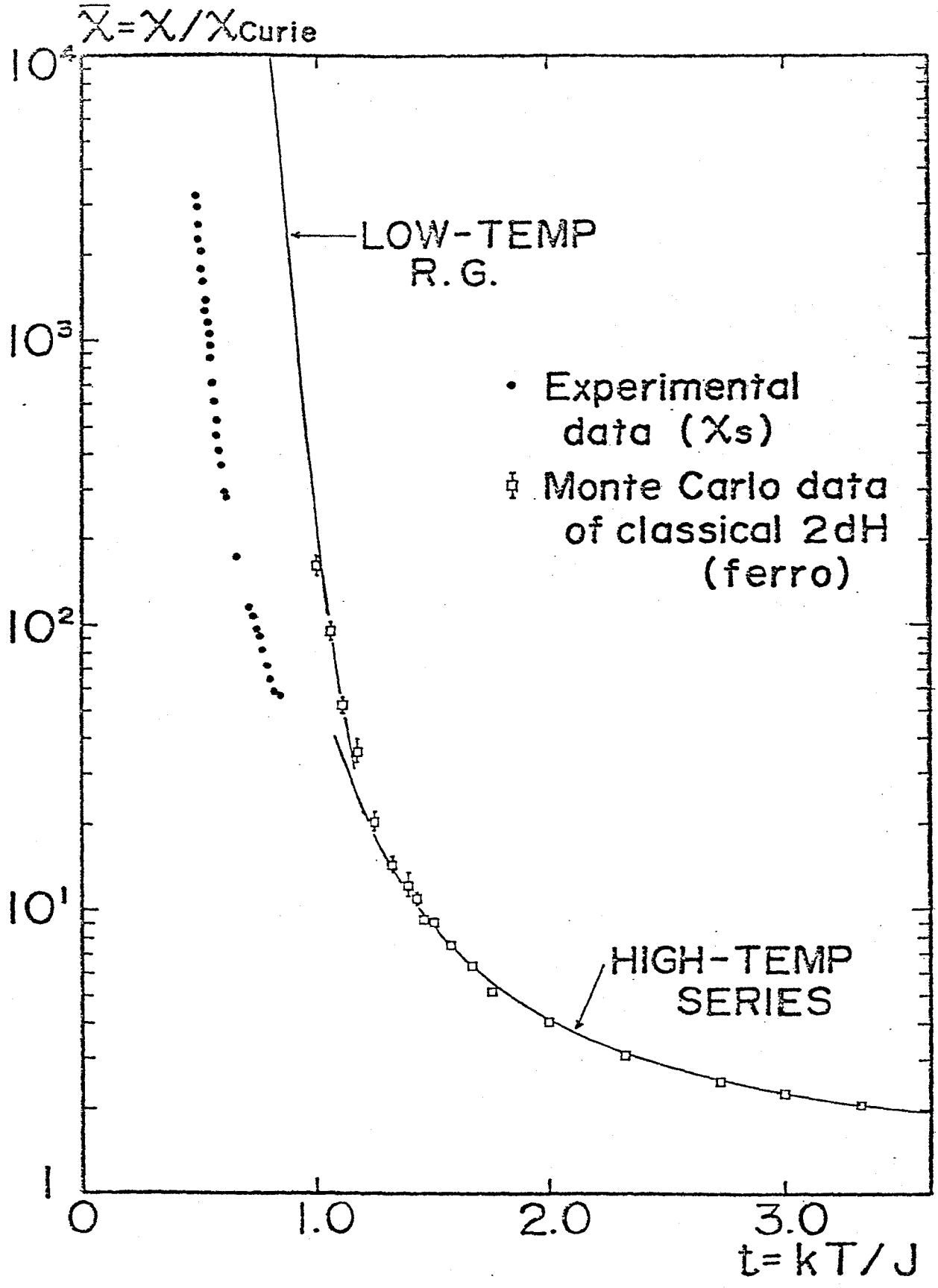

Fig.II-11. Comparison of the experimental data for the staggered susceptibility χ_s^f with the theoretical ones in absolute values.

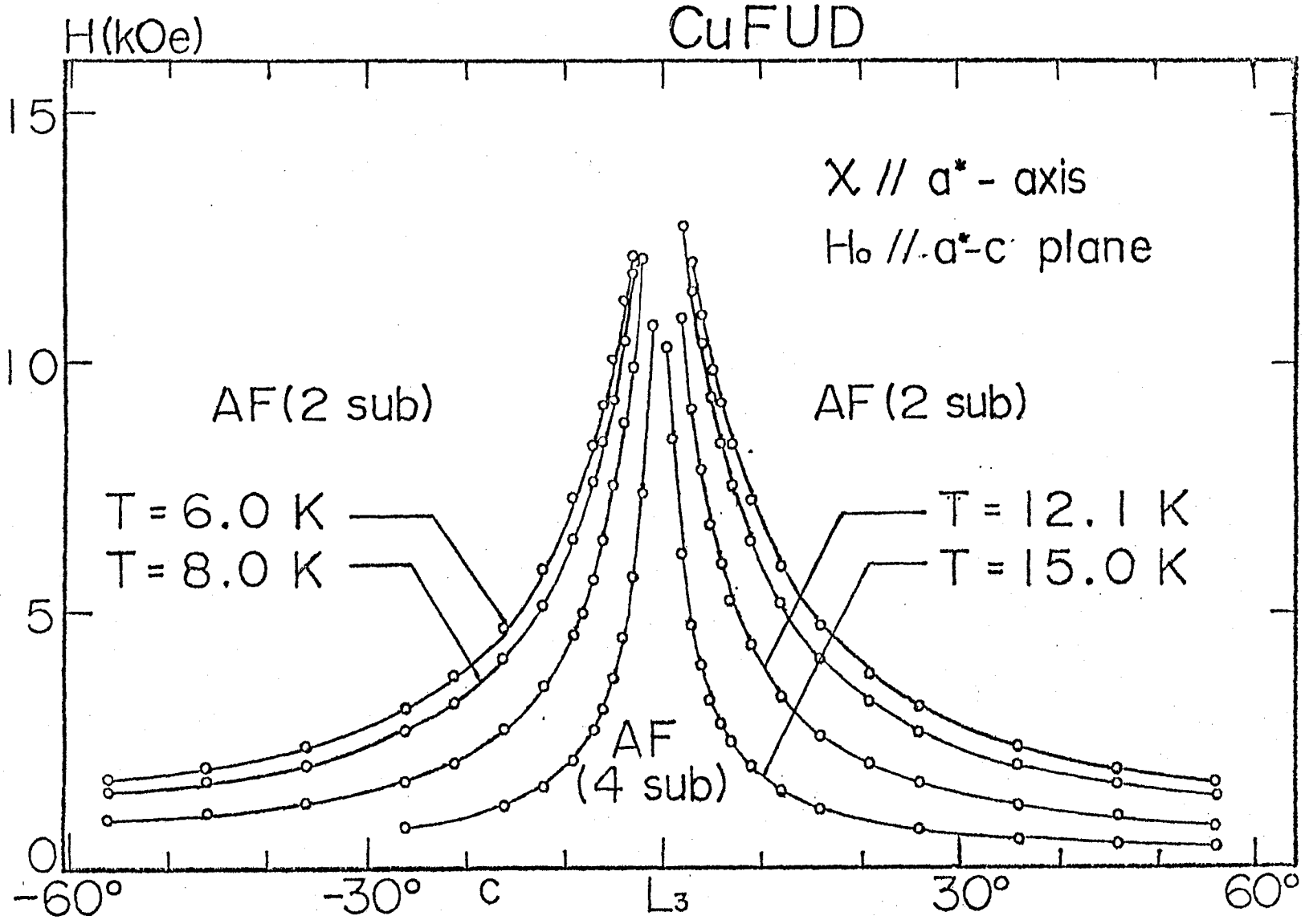

Fig.II-12. Field-angle from L_3-axis phase diagram in ac-plane for various temperatures below T_N.

any staggered field effect at all. In the sense, this ordering is essentially the same as the ordering under the zero external field. However, in the case the observation of spontaneous magnetization by NMR is possible to be made under the external field or in high frequency region. Therefore the observation is more sensitive in the vicinity of the critical temperature under the external field than the zero field. For such an observation, it is necessary to set the direction of external field along the L_3-axis precisely. It is possible to set the external field along the L_3-axis within 0.2° in the ac-plane, but difficult to set the field exactly perpendicular to the b-(y-)axis. This difficulty was overcomed by setting an additional field $H_\perp$ which is perpendicular to the main external field. The discrepancy of sample setting in this case was kept less than 0.8° from the ac-plane as shown in Fig.II-13.

The temperature dependence of the line shift of proton NMR under the external field applied along the L_3-axis is independent upon the magnitude of the field. The Néel temperatures in the fields decrease slightly by the effect of the uniform field ($T_N(H=0)$ = 15.5 K, $T_N(H_{L_3}$=10 kOe) ≃ 15.1 K). The temperature dependence of the line shift down to 1.4 K was examined and the part of the vicinity of T_N is shown in Fig.II-14. The symmetric lines which appear both above and below the free proton show that 4 sub-lattice structure is realized below T_N. The derived spin reduction value extrapolated to T = 0 K is in agreement with the result in §II-2.1 (ΔS = 45 %). The temperature dependence and the magnitude of the line shift does not depend upon the magnitude of external field at all within the measured field range. This fact means that this

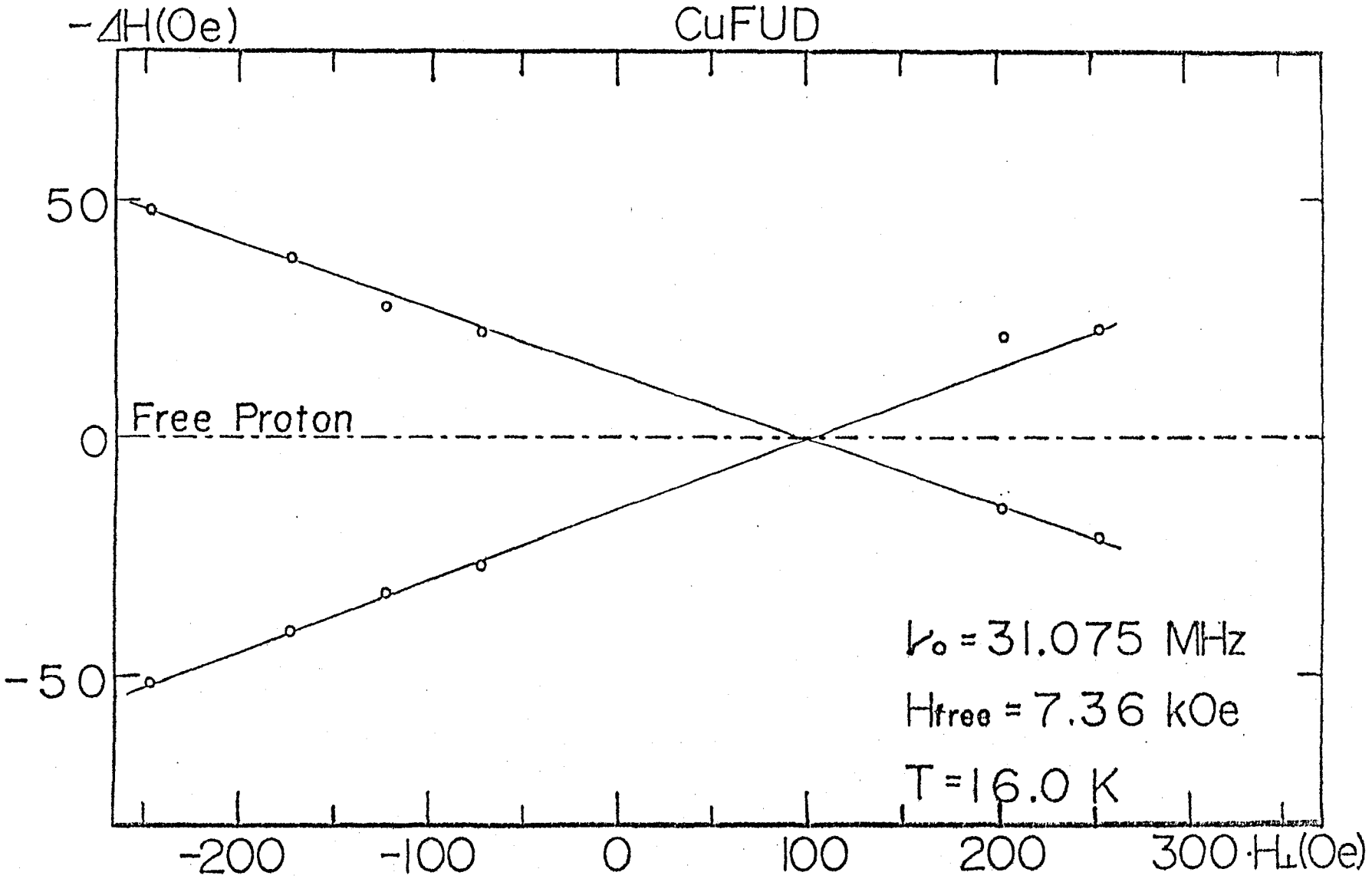

Fig.II-13. Correction of the external field direction by applying the additional field $H_{\perp}$.

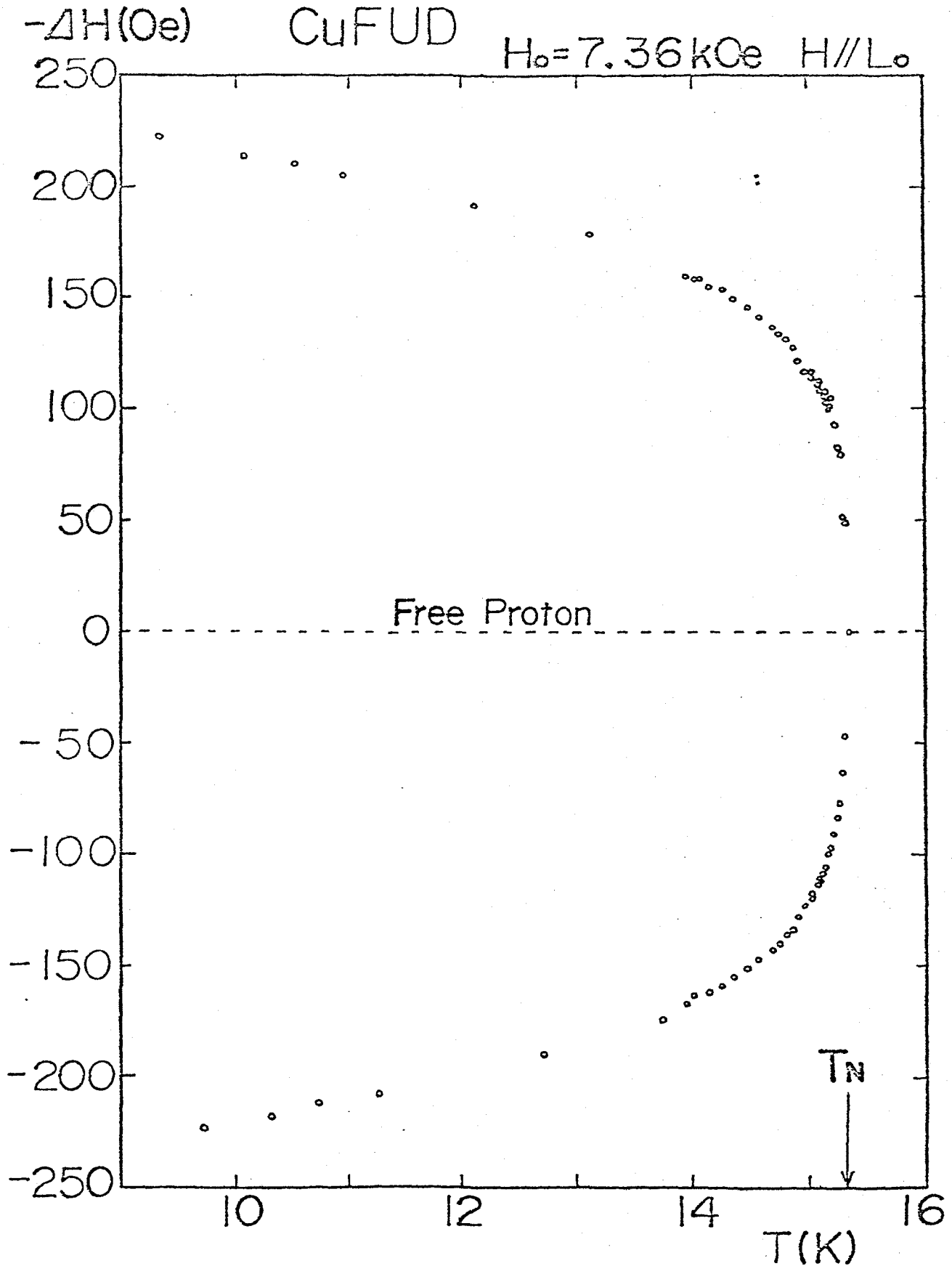

Fig.II-14. Temperature dependence of the line shift of the formate proton under the field along L_3-axis.

line shift is mostly determined by only the spontaneous magnetization. Log-log plot for line shift versus reduced temperature $\varepsilon = |T - T_N|/T_N$ is shown in Fig.II-15. Line shift or spontaneous magnetization follows a power law at very wide ε range, $10^{-3} < \varepsilon < 8 \times 10^{-1}$ as seen in the figure. The critical exponent β is 0.22 ± 0.02.

In the compound CuF4H, Ising anisotropy is almost the same as and inter-layer interaction is about twenty times larger than that of CuFUH, respectively. By the similar experiment, the critical exponent β is obtained as follows, $\beta = 0.22 \pm 0.01$ for $10^{-1} < \varepsilon < 4 \times 10^{-1}$ and $\beta = 0.30 \pm 0.02$ for $10^{-3} < \varepsilon < 10^{-1}$ shown in Fig. II-15. The latter value $\beta = 0.30$ is in good agreement with the result of proton NMR under the zero field by Dupas and Renard.[10]

§II-3. Discussion

According to the hypothesis of universality, the following phenomena would be expected to occur. If the Ising-type anisotropy is added to the 2d Heisenberg system, the value of critical exponent β must be that of 2d Ising universality class ($\beta_{2dI} = 0.125$). While, if inter-layer coupling (J') is added to 2d Heisenberg system, β must be the value of 3d universality class ($\beta_{3dI} = 0.31 \sim \beta_{3dH} = 0.35$). For examples, K_2NiF_4 and K_2MnF_4 are known to show the 2d Ising like index.[15] While, K_2CuF_4[16] and $Mn(HCOO)_2 \cdot 2H_2O$,[17] etc. are known to show the 3d system's indices.

As mentioned in §II-2, the value of $\beta = 0.22$ is obtained for CuFUD. This salt is quasi 2d Heisenberg system, Ising anisotropy and inter-layer interaction are both extremely small. The exponents

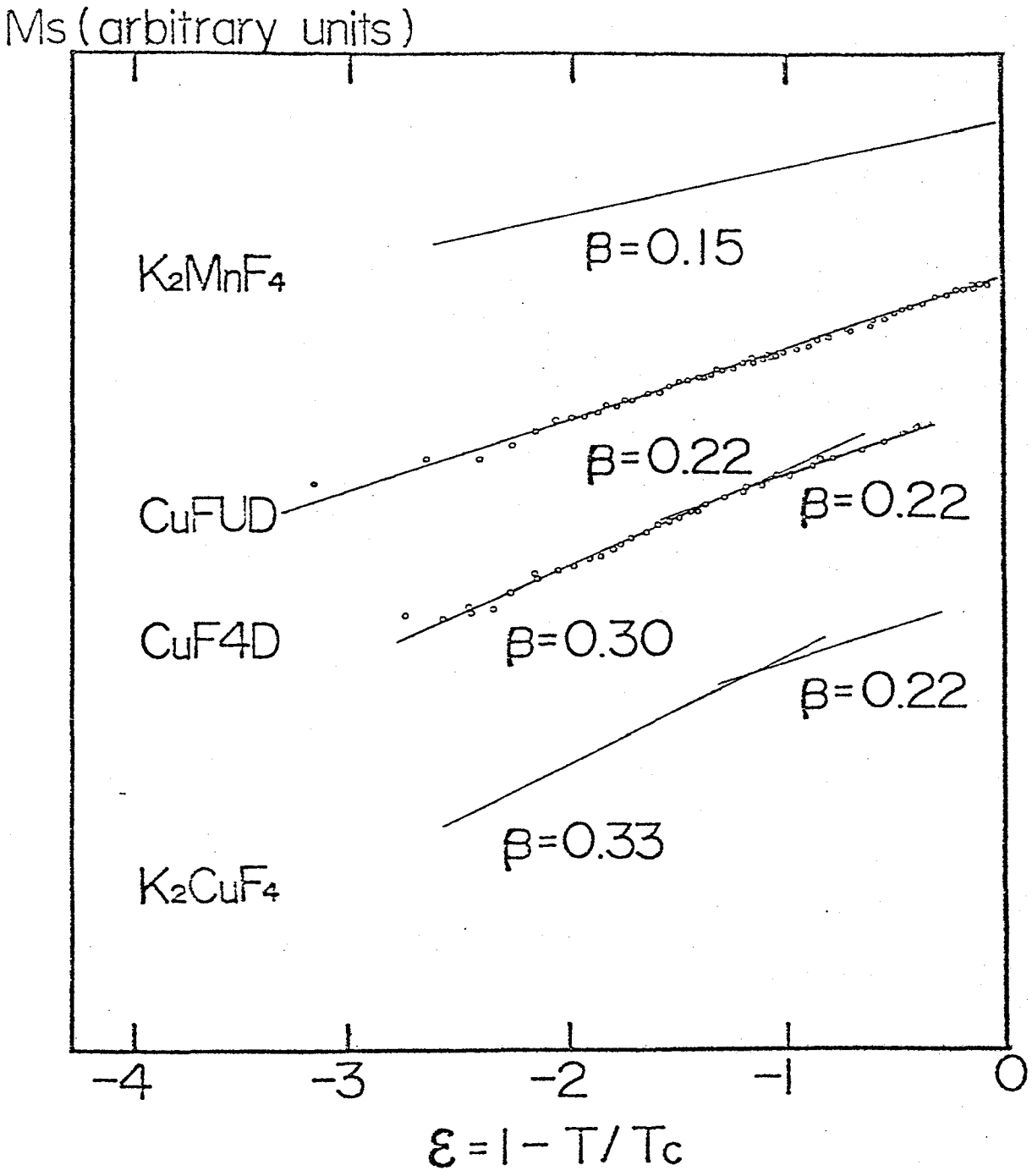

Fig.II-15. Log-log plot of the spontaneous magnetization and the reduced temperature $\varepsilon = 1 - T/T_c$ for CuFUD and CuF4D compared with K_2MnF_4 and K_2CuF_4.

close to $\beta = 0.22$ have been also observed in a certain ε range of some materials, e.g. MnF2H, CuF4H, K_2CuF_4 and so on (cf. Table II-5). The result of log-log plot for CuF4H is also shown in Fig.II-15 and that for MnF2H in Fig.III-6 in Chap.III. The ε range which indicates $\beta = 0.22$ is comparatively wide for MnF2H ($2 \times 10^{-2} < \varepsilon < 5 \times 10^{-1}$). The index $\beta = 0.22$ for wide ε ranges in these two examples i.e. CuFUH and MnF2H may indicate that the value is not the intermediate one in the crossover regions. The value of $R = J'/J$ and $a = H_A/H_E$ on various materials are summarized with the observed values of β and indicated in Fig.II-16. The dotted line of $J'/J = 1$ indicates the pure 3d system. Turnig to the left in the figure, two-dimensionality of the system becomes increasingly good. While, turning to the right, one-dimensionality becomes increasingly good. Turning to the upper side, the system becomes growingly Ising like. While, turning to the lower side, it becomes growingly Heisenberg like. The ideal 2d Heisenberg system is located at the limit of left and lower side. It is well shown how ideal CuFUH is in comparison with other materials. 2d Ising system which is solved exactly is located at the limit of left and upper side. The materials, the value β of which indicate about 0.22 for the temperature range far from the critical temperature, are located at the position of neither 2d Ising like nor 3d system.

The perfect 2d Heisenberg system has not any spontaneous magnetization at a finite temperature at all. But with a certain small perturbation, the system may go into a new kind of universality class. For CuFUH, MnF2H and CuF4H, antisymmetric interaction might be the small perturbation. For the other compounds, the

Table II-5. Exsamples of which the critical index β indicates nearly 0.22.

Materials	β	$\varepsilon = \lvert T - T_C \rvert / T_C$	Reference
$Cu(HCOO)_2 \cdot 2H_2O \cdot 2CO(NH_2)_2$	0.22	$10^{-3} < \varepsilon < 8 \times 10^{-1}$	present work
$Cu(HCOO)_2 \cdot 4H_2O$	0.22	$10^{-1} < \varepsilon < 4 \times 10^{-1}$	present work
	0.30	$10^{-3} < \varepsilon < 10^{-1}$	
$Mn(HCOO)_2 \cdot 2H_2O$	0.23	$2 \times 10^{-2} < \varepsilon < 5 \times 10^{-1}$	present work (Chap.III)
	0.31	$3 \times 10^{-3} < \varepsilon < 2 \times 10^{-2}$	
$KFeF_4$	0.209	$2 \times 10^{-3} < \varepsilon < 4 \times 10^{-2}$	23)
$RbFeF_4$	0.249	$10^{-2} < \varepsilon < 6 \times 10^{-1}$	25)
	0.316	$5 \times 10^{-4} < \varepsilon < 10^{-2}$	
Rb_2FeF_4	0.20	$3 \times 10^{-2} < \varepsilon < 3 \times 10^{-1}$	22)
	0.30	$5 \times 10^{-3} < \varepsilon < 3 \times 10^{-2}$	
K_2CuF_4	0.22	$7 \times 10^{-2} < \varepsilon < 5 \times 10^{-1}$	16)
	0.33	$4 \times 10^{-3} < \varepsilon < 7 \times 10^{-2}$	

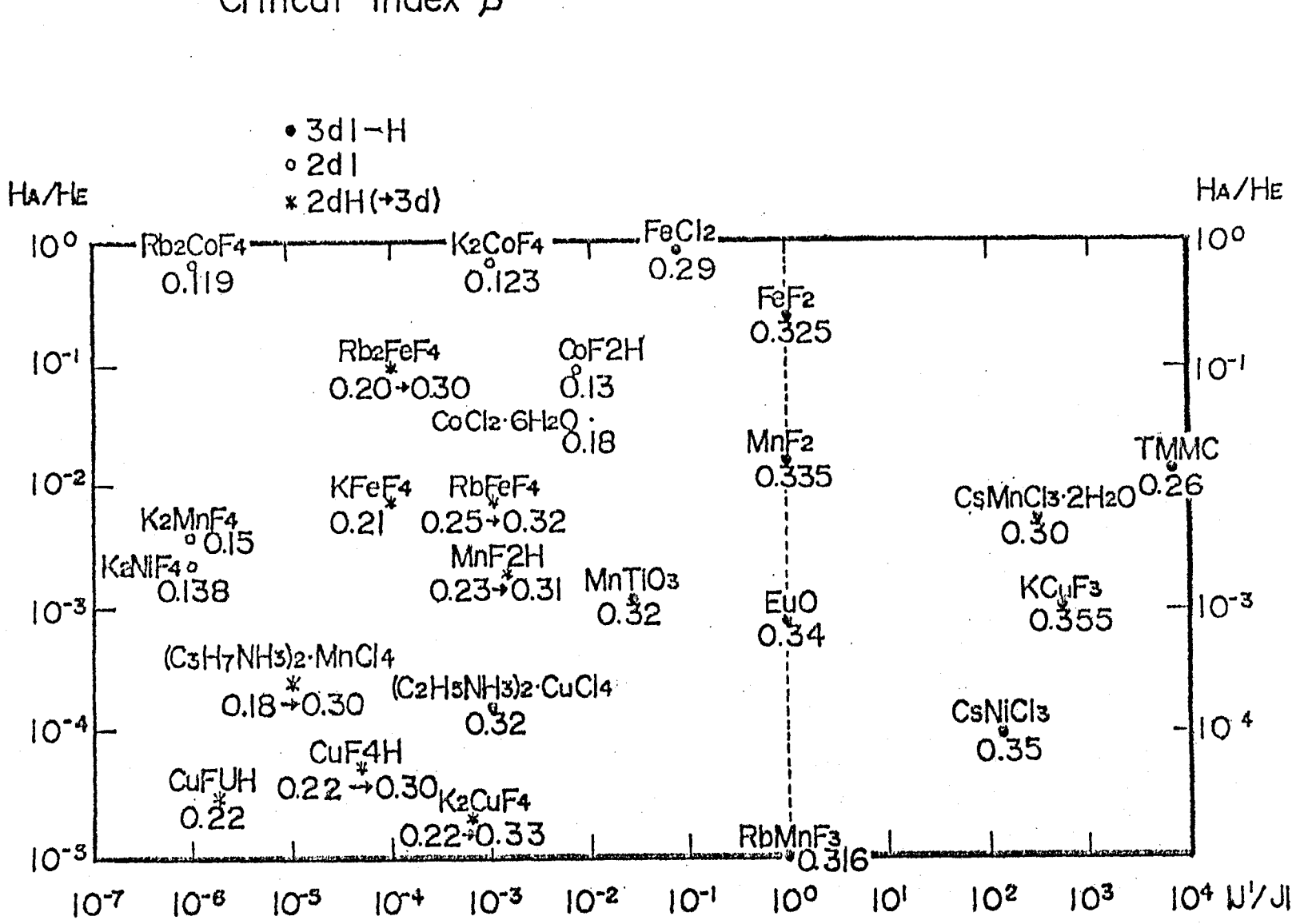

Fig.II-16. Summary of R = J'/J and a = H_A/H_E on various materials with the observed values of β.

value β of which indicate about 0.22, the origin have not been discussed in detail. It is expected to seek some possible perturbations if any, which introduce such a new universality class.

The value of spin reduction in 2 sub-lattice phase is in good agreement with the theoretical value for S = 1/2 ΔS = 28 % by the spin wave theory. The comparison with the other quasi 2d Heisenberg antiferromagnets with large spin reduction is shown in Table II-6. There are no example for S ≒ 1/2 except CuFUH and CuF4H. The question is the cause of large spin reduction in 4 sub-lattice phase at zero field. This anomalous large reduction should be attributed to the inter-layer antiferromagnetic interaction. Because, the intra-layer antiferromagnetic interaction in 2 sub-lattice phase is just the same as that in 4 sub-lattice phase. The values of spin reduction have been calculated by the spin wave theory for the case of 2d and 3d Heisenberg antiferromagnets. However, it is unknown for the case of intermediate of 2d and 3d Heisenberg antiferromagnets. It may be suggested by this experiments that the model of 2d Heisenberg antiferromagnet with the very small purturbation for symmetry breaking which expresses β = 0.22 is possible to indicate the larger reduction than the pure 2d Heisenberg antiferromagnet. There is other possibility except for the quantum effect. For instance, a similar situation to the so-called chirality order for triangular antiferromagnet may be considered to happen in this quadratic lattice concerned with the probable 4 sub-lattice interaction if any.

Table II-6.

Quasi-two-dimensional nearly Heisenberg antiferromagnets with large spin reduction ΔS.

	S	J'/J	a	exp ΔS	s.w.	ref.
$Mn(HCOO)_2 \cdot 2H_2O$	5/2	10^{-3}	10^{-3}	10 %	8 %	40)
$MnTiO_3$*	5/2		10^{-3}	∿25 %		29)
Ca_2MnO_4	3/2	10^{-6}		33 %	13 %	41)
$Cu(HCOO)_2 \cdot 4H_2O$	1/2	10^{-5}	10^{-5}	47 %	28 %	10)
$Cu(HCOO)_2 \cdot 2H_2O \cdot 2CO(NH_2)_2$	1/2	10^{-6}	10^{-5}	45 %	28 %	present work

J'/J : The ratio of inter-planer to intra-planer interaction.

a : The anisotropy in inter-planer interaction.

s.w. : The spin wave theory for 2-dim. Heisenberg Magnet.

ref.9) I. Ishikawa. & T. Oguchi.: Prog. Theor. Phys. 54 (1975) 1282.

* : The honeycomb lattice.

References (II)

1) H. Kiriyama and K. Kitahara: Acta Cryst. B32 (1976) 330.

2) Y. Yamamoto, M. Matsuura and T. Haseda: J. Phys. Soc. Jpn. 40 (1976) 1300.

3) M. Matsuura and Y. Ajiro: J. Phys. Soc. Jpn. 41 (1976) 44.

4) Y. Ajiro, K. Enomoto, N. Terata and M. Matsuura: Solid State Commn. 20 (1976) 1151.

5) M. Matsuura: J. Phys. Soc. Jpn. 43 (1977) 1805.

6) K. Yamagata, Y. Kozuka, E. Masai, M. Taniguchi, T. Sakai and I. Takata: J. Phys. Soc. Jpn. 44 (1978) 139.

7) K. Yamagata and T. Sakai: J. Phys. Soc. Jpn. 49 (1980) 2165.

8) K. Yamagata, Y. Kozuka and T. Morita: J. Phys. Soc. Jpn. 50 (1981) 421.

9) I. Ishikawa and T. Oguchi: Prog. Theor. Phys. 54 (1975) 1282.

10) A. Dupas and J. P. Renard: Phys. Lett. 33A (1970) 470.

11) W. J. Camp and J. P. Van Dyke: J. Phys. C8 (1975) 336.

12) S. K. Ma: Phys. Rev. Lett. 37 (1976) 461.

13) R. Swendson: Phys. Rev. Lett. 42 (1979) 859.

14) S. H. Shenker and J. Tobochnik: Phys. Rev. B22 (1980) 4462.

15) R. J. Birgeneau, J. Als-Nielsen and G. Shirane: Phys. Rev. 16 (1977) 280.

16) K. Hirakawa and H. Ikeda: J. Phys. Soc. Jpn. 35 (1973) 1328.

17) See Chap.III or
M. Matsuura, K. Koyama and Y. Murakami: J. Phys. Soc. Jpn. 52 (1983) Suppl.37.

References in Fig.II-15.

Two-dimensionality and degree of anisotropy are mainly examined from ref. 18) and 19).

18) K. Hirakawa: Solid State Physics 16 (1981) 522. (Japanese)

19) L. J. de Jongh and A. R. Miedema: Adv. in Phys. 23 (1974) 1.

*Rb_2CoF_4 → 20) H. Ikeda, M. Suzuki and M. T. Hutchings: J. Phys. Soc. Jpn. 46 (1979) 1153.

*K_2MnF_4 → 21) R. J. Birgeneau, H. J. Guggenheim and G. Shirane: Phys. Rev. B8 (1973) 304.

*K_2NiF_4 → 22) R. J. Birgeneau, H. J. Guggenheim and G. Shirane: Phys. Rev. B1 (1970) 2211.

*Rb_2FeF_4 → 22)

*$KFeF_4$ → 23) G. Heger and R. Geller: Phys. Stat. Sol. 53 (1972) 227.

*K_2CoF_4 → 24) H. Ikeda and K. Hirakawa: Solid State Commn. 14 (1974) 529.

*$RbFeF_4$ → 25) I. M. Savic, H. Keller, W. Kündig and P. F. Meier: Phys. Lett. 83A (1981) 471.

*$(C_2H_5NH_3)_2 \cdot CuCl_4$ → 26) L. J. de Jongh, W. D. van Amstel and A. R. Miedema: Physica 58 (1972) 277.

*K_2CuF_4 → 16)

*CoF2H → 27) H. Yamakawa and M. Matsuura: J. Phys. Soc. Jpn. 41 (1976) 798.

*$CoCl_2 \cdot 6H_2O$ → 28) W. Van der Lugt and N. J. Poulis: Physica 26 (1960) 917.

*$MnTiO_3$ → 29) J. Akimitsu, Y. Ishikawa and Y. Endoh: Solid State Commn. 8 (1970) 87.

*$FeCl_2$ → 30) W. B. Yelon and R. J. Birgeneau: Phys. Rev. B5 (1972) 2615.

*FeF_2 → 31) G. K. Wertheim and D. N. E. Buchanan: Phys. Rev. 161

(1967) 478.

*MnF_2 → 32) P. Heller and G. B. Benedek: Phys. Rev. Lett. 14 (1965) 71.

*EuO → 33) J. Als Nielsen, O. W. Dietrich, W. Kunnmann and L. Passell: Phys. Rev. Lett. 27 (1971) 741.

*$RbMnF_3$ → 34) H. Y. Lau, J. W. Stout, W. C. Koehler and H. R. Child: J. Appl. Phys. 40 (1969) 1136.

*$CsMnCl_3 \cdot 2H_2O$ → 35) J. Skalyo, Jr., G. Shirane, S. A. Friedberg and H. Kobayashi: Phys. Rev. B2 (1970) 1310 and 4632.

*$KCuF_3$ → 36) H. Ikeda and K. Hirakawa: J. Phys. Soc. Jpn. 35 (1973) 727.

*$CsNiCl_3$ → 37) M. Mekata, K. Adachi, H. Takagi and N. Achiwa: Proc. 12th Int. Conf. Low Temp. Phys., 1970 Kyoto.

*TMMC [$(CH_3)_4NMnCl_3$] → 38) R. J. Birgeneau, G. Shirane and T. A. Kitchens: Proc. 14th Low Temp. Conf. Boulder, Colorado (1972)

References in Table II-6.

*MnF2H → 39) H. Yamakawa: thesis, Osaka University (1977)

*$MnTiO_3$ → 29)

*Ca_2MnO_4 → 40) D. E. Cox, G. Shirane, R. J. Birgeneau and J. B. MacChesney: Phys. Rev. 188 (1969) 930.

Chapter III. Ordering of $Mn(HCOO)_2 \cdot 2H_2O$ and $Mn(HCOO)_2 \cdot 2D_2O$ at nearly zero field

§III-1. Characteristic of $Mn(HCOO)_2 \cdot 2H_2O$

The compound $Mn(HCOO)_2 \cdot 2H_2O$ (hereafter MnF2H) is a layer structure antiferromagnet and approximated to a quadratic Heisenberg system of $S = 5/2$.[1-3] The inter-planer structure of this compound, however, is heterogeneous or composed of a alternate piling up of two inequivalent magnetic planes i.e. a strongly coupled antiferromagnetic A (100) plane and another almost ideally paramagnetic B (200) plane consisting of non-interacting ions. Each paramagnetic B ion lies on a inter-plane interaction path -O(CH)O-Mn-O(CH)O- between the adjacent two A planes and say decorates the interaction. Such a inter-planer structure is qualitatively different from any other quasi two-dimensional (2d) systems so far investigated like e.g. K_2MnF_4.[4] The crystal structure of MnF2H is shown in Fig.III-1. The lattice parameters and proton positions in this hydrated salt are listed in Table III-1.[5] Six independent protons are in the unit cell, two of which, denoted as No.5 and No.6, belong to the formate radicals forming the intra-plane (in A plane) and the inter-plane (between A and B plane) interaction paths, respectively and remain unchanged after deuteration as mentioned in next section (§III-2).

This compound is an antiferromagnet with some very weak but non-zero moment canting interactions i.e. antisymmetric exchange interaction, inequivalence of $\tilde{g}$-tensors and so on. Through the canting mechanism, the applied uniform field is coupled to the staggered moment in the system and the staggered one is recoupled

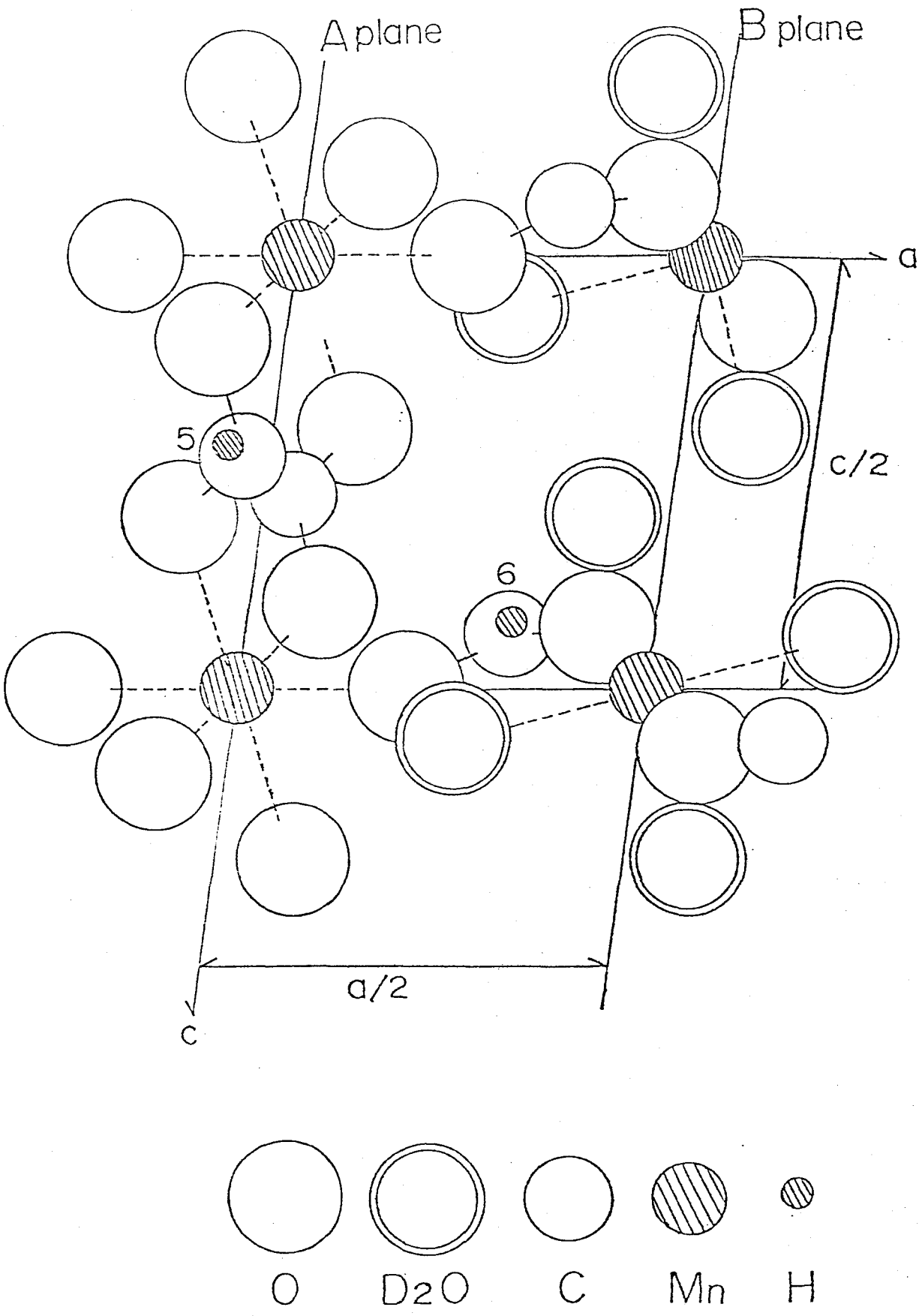

Fig.III-1. Crystal structure of $Mn(HCOO)_2 \cdot 2D_2O$.

Table III-1.

Proton Positional Parameters of $Mn(HCOO)_2 \cdot 2H_2O$

	Positional Parameters		
Proton	x	y	z
$H_1(D)$	0.307	0.099	0.261
$H_2(D)$	0.460	0.146	0.224
$H_3(D)$	0.203	0.106	0.509
$H_4(D)$	0.227	0.891	0.551
H_5	-0.065	0.283	0.227
H_6	0.335	0.482	0.395

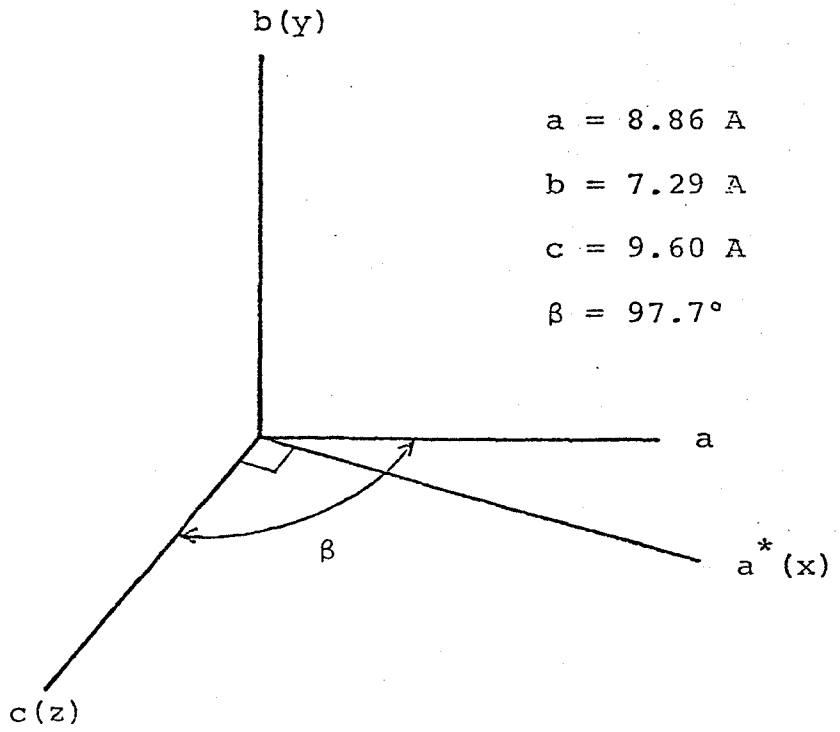

to the uniform one.[1,6] Insuch a way, the following relations are found to be satisfied in the same way as those in §II-1.

$$M^{\perp} = \eta L^{/\!/} \tag{3.1}$$

and

$$\chi^{\perp} = \chi_u^{\perp} + \eta^2 \chi_s^{/\!/} \tag{3.2}$$

where L and χ_s are the staggered magnetization and the staggered susceptibility of the system without the moment canting mechanism and the suffix // and $\perp$ means the easy (b-) and the perpendicular (nearly c-)axis component, respectively. η is a small coefficient concerned with the canting mechanisms. The magnitude of η is the degree of moment canting and actually about 10^{-3} in the present case.[7] Thus we can derive the characteristics of L and χ_s of MnF2H, directly and accurately by a conventional magnetic measurements especially in the neighbourhood of the critical temperature T_N.

The ratio of effective inter-layer interaction between A planes through the intermediate paramagnetic B ions to intra-layer interaction is estimated to be 10^{-3}.[8] The lowest spectral term of the free Mn^{2+} ion is $^6S_{5/2}$ and its ground state is expected to suffer negligibly small crystalline field splitting ($< 0.05\ cm^{-1}$) as reported in the ESR experiment of Mn^{2+} ions.[9] The g-factors for the Mn^{2+} ions on the A and B planes are $g_A = 2.005 \pm 0.004$ and $g_B = 1.993 \pm 0.010$, respectively. Therefore, the A planes of MnF2H may be approximated as a 2d isotropic Heisenberg antiferromagnetic system.

It is interesting to examine the influence of heterogeneity or such a modification of inter-plane interaction on the ordering of an especially Heisenberg-like system. Because, a 2d Heisenberg

system does not order at a finite temperature and any small purturbation may give a remarkable effect on the onset of ordering. For this purpose, the essential is the separate determination of two subsystem quantities or susceptibility, spontaneous magnetization and so on.

All the previous experiments tell us that the thermal and magnetic properties of MnF2H are well explained by a simple superposition of those for a quadratic Heisenberg antiferromagnet and an ideal paramagnet above T_N indicating that the interactions are negligible not only among B ions but also between the subsystems. Early susceptibility measurement[1] derived $\gamma = 1.7$ for the staggered susceptibility in the temperature range $1 \times 10^{-3} < \varepsilon (= |T/T_N - 1|) < 1 \times 10^{-2}$, which is very close to 1.75 for 2d Ising universality class. While the previous NMR[11] and neutron diffraction[2] showed that the growth of the staggered magnetization of A subsystem L_A below T_N, follows an exponential law and a critical index of $\beta = 0.23 \pm 0.01$ in the measured temperature range $4 \times 10^{-2} < \varepsilon < 5 \times 10^{-1}$. This value of β is different from both 0.125 for 2d Ising model and 0.31 or 0.35 for 3d Ising or 3d Heisenberg model, respectively.

Such an intermediate value of β may be associated with the characteristic inter-planer structure of this compound mentioned above. Indeed, the analysis of neutron diffraction derived a small but finite (about 10 % of L_A) spontaneous magnetization L_B below T_N indicating a weak interaction between the A and B subsystems. So in this chapter we tried to examine the proton NMR on deuterated salt MnF2D in detail to determine the uniform subsystem susceptibility χ_{uA} and χ_B above T_N separately, and the spontaneous subsystem magnetization L_A and L_B below T_N, respectively. We also tried a

simultaneous accurate measurement of susceptibility and spontaneous magnetization of MnF2H at zero field in the immediate neighbourhood of T_N by using a SQUID magnetometer.

§III-2. Experimental results and analysis

III-2.1 Separate observation of subsystem susceptibilities above T_N[16)]

The Mn ion system in the A planes makes a long range order at T_N (= 3.686 K) but that in the B planes still behaves paramagnetically down to the temperature far below T_N.[12)] The inter-planer correlation is brought by paramagnetic ions in the B plane. It is therefore interesting to observe the temperature dependence of each subsystem susceptibility χ_A or χ_B, respectively. The separation, however, has not been successful by bulk susceptibility measurement[1,13)] and also by conventional proton NMR.[14)] In principle, it is found possible when the NMR signal is detected in the external field along the selected directions as explained below. Here we report a successful trial on χ_A and χ_B of $Mn(HCOO)_2 \cdot 2D_2O$ (MnF2D), the heavy water substituted salt of hydrated one.

There are two crystallographically non-equivalent protons in the unit cell of MnF2D, which correspond to proton No.5 and No.6 in the hydrated salt.[14)] The internal fields for these protons are caused by the ionic moments in both A and B subsystems $\vec{m}_A$ and $\vec{m}_B$. The resonance line shift for these protons due to the internal field is expressed by

$$\Delta H_i(\theta) = C_{iA}(\theta) \cdot m_A + C_{iB}(\theta) \cdot m_B, \quad (i = 5 \text{ or } 6), \qquad (3.3)$$

and

$$C_{iI}(\theta) = \alpha_{iI} \cdot \cos 2(\theta - \theta_{iI}^{max}) + \beta_{iI}, \quad (I = A \text{ or } B), \qquad (3.4)$$

where ∥ indicates the direction of external field. Quantities m_A and m_B are the magnitudes of ionic moments $\vec{m}_A$ and $\vec{m}_B$ and proportional to χ_A and χ_B, respectively. When the external field is in the zx= plane, α_{iI}, β_{iI} and θ_{iI}^{max} are expressed by the components of dipole sum tensor $\tilde{d}_{iI}$ as

$$\alpha_{iI} = [(d_{iI}^{xx}-d_{iI}^{zz})^2 + (2d_{iI}^{xz})^2]^{1/2}, \tag{3.5}$$

$$\beta_{iI} = d_{iI}^{xx} + d_{iI}^{zz}, \tag{3.6}$$

and

$$\theta_{iI}^{max} = 1/2\tan^{-1}[2d_{iI}^{xz}/(d_{iI}^{xx} - d_{iI}^{zz})]. \tag{3.7}$$

The dipole sum tensors in para state are shown as D^+ in Table III-2, including those in ordered state as D^-. The relations in the case of external field in the xy- and yz-planes are obtained by cyclic changes of suffix x, y, z. By using the fact that the dipole sum tensor is traceless or

$$d_{iI}^{xx} + d_{iI}^{yy} + d_{iI}^{zz} = 0, \tag{3.8}$$

we can easily show the inequality $\alpha_{iI} > \beta_{iI}$ for at least two of three cases where the external field is in the xy-, yz- or zx-plane. If $\alpha_{iI} > \beta_{iI}$ in the zx-plane, coefficient C_{iI} is necessarily zero at a special angle θ_{iI}^0. In the case of $\theta = \theta_{iA}^0$ or θ_{iB}^0, the line shift ΔH_i is caused by only m_B or only m_A and proportional to only χ_B or only χ_A, respectively.

Practically for proton No.6, we obtain $\theta_{6A}^0 = 34°$ from a' (⊥bc-plane) to c-axis. The temperature dependence of ΔH_6 for $\theta = 34°$, which should give directly the temperature dependence of χ_B, is shown in Fig.III-2. The solid line shows the Curie law for S =

Table III-2.

The dipole sum tensor of $Mn(HCOO)_2 \cdot 2D_2O$

($\times 10^{22}$ cm^{-3}) ($D_A^+ = D_{A1} + D_{A2}$ etc.)

		x	y	z	
H_5	D_A^+	6.97	0.14	-0.30	x
			-1.26	-8.44	y
				-5.70	z
	D_B^+	-2.49	0.56	-0.38	
			1.35	0.68	
				1.14	
	D_A^-	-0.12	2.02	2.94	
			-1.98	-0.068	
				2.10	
	D_B^-	-0.85	0.65	-0.85	
			0.29	0.11	
				0.56	
H_6	D_A^+	-4.59	0.25	2.70	
			3.00	-0.18	
				1.59	
	D_B^+	2.85	0.32	0.25	
			-2.83	0.27	
				-0.02	
	D_A^-	5.00	-0.31	-3.78	
			-2.86	0.10	
				-2.14	
	D_B^-	-0.49	-0.39	1.36	
			5.98	-0.12	
				-5.49	

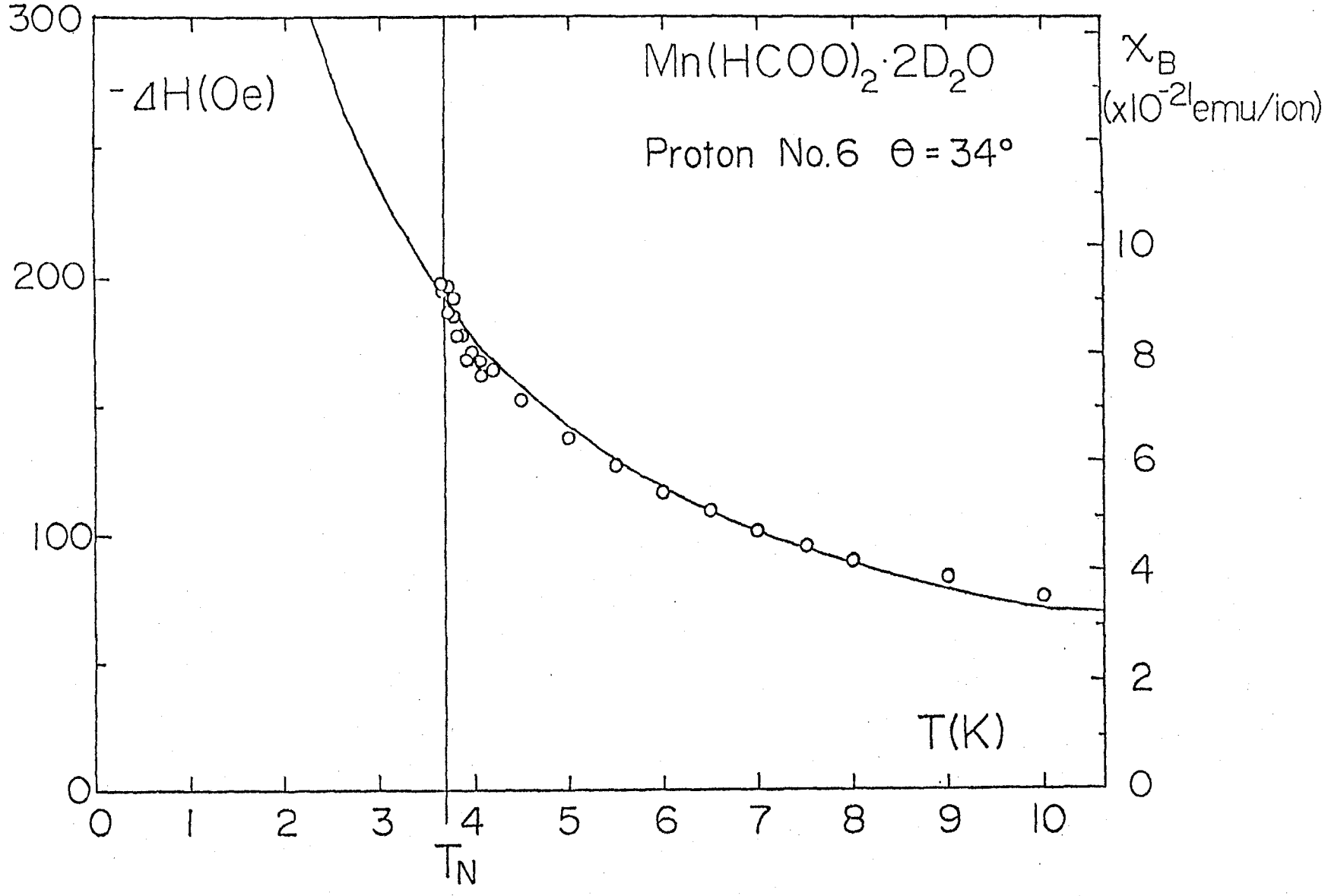

Fig.III-2. Temperature dependence of the NMR line shift for proton No.6 at θ = 34° from a' to c-axis inder H_0 = 4.7 kOe.

5/2 and g = 2.0. The agreement with experimental result is very good considering that no adjustable parameter is included there. It means that down to T_N the Mn ions in the B plane are quite independent not only of each other within the plane but also of Mn ion system in the A planes, the short range order of which is highly developed near T_N as seen below in the χ_A-T curve. For proton No.5, θ^0_{5B} = 61° is found. Figure III-3 is the ΔH_5-T curve at the angle, which corresponds to χ_A-T curve. A remarkable is that χ_A shows a broad maximum at about 7 K and decreases down to T_N as temperature decreases. The characteristic temperature dependence of χ_A above T_N should be taken as that of the 2d Heisenberg antiferromagnet of S = 5/2, refering the very weak anisotropy in the system. Tentatively, the experimental result is compared with a theoretical estimate[15] by high temperature series expansion, although the latter may be reliable only above the temperature around which χ takes its maximum. The only adjustable parameter J/k is taken here as -0.4 K, which is consistent with the previous experimental value -0.35 K.[8]

Finally it should be noted that the sum of obtained χ_A and χ_B is found to be in agreement with the result by bulk susceptibility measurement. The present method is generally applicable to other multi-sublattice systems. Especially, in crystallographic two sublattice system, it is useful in order to observe the behaviour of only staggered mode separately.

III-2.2 Spontaneous subsystem magnetizations below T_N

The NMR frequencies for two protons in MnF2D at zero field

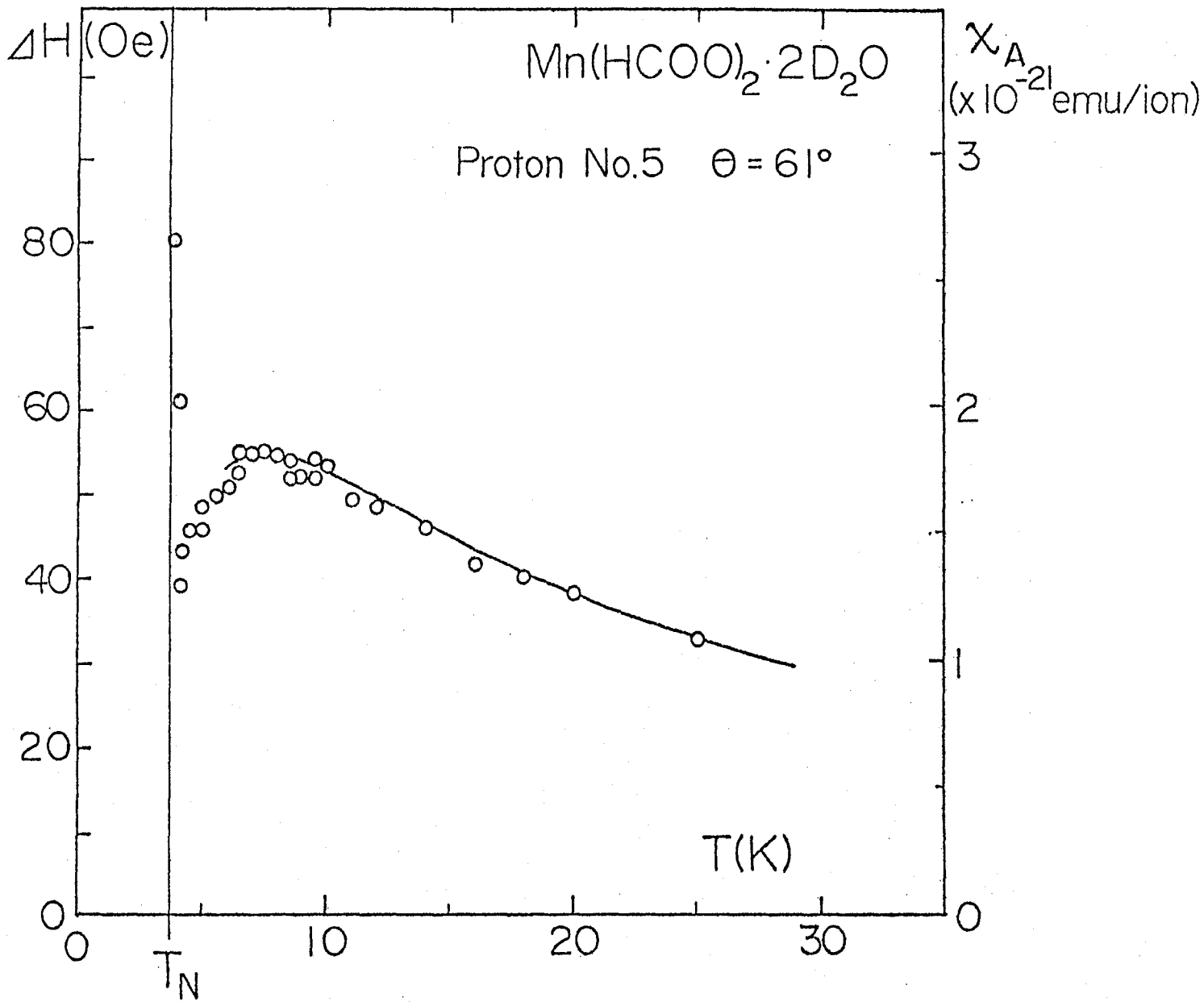

Fig.III-3. Temperature dependence of the NMR line shift for proton No.5 at θ = 61° from a'- to c-axis under H_0 = 4.7 kOe.

below T_N are determined by the dipole-dipole interactions with the surrounding Mn ions in both A and B planes. The dipole sum tensors in ordered state are summarized as $\bar{D}$ in Table III-2. In principle, we can derive the spontaneous subsystem staggered magnetizations L_A and L_B separately by analizing the resonance frequencies for two protons No.5 and No.6 in MnF2D.

The use of deuterated salt instead of hydrated one is impotant and noteworthy here. Because, in the hydrated salt six NMR lines gather to a narrow frequency range with increasing the width as temperature approaches to T_N. It results in a difficulty of separation of individual line and thus a large uncertainty in determining the resonance frequency of each line. In deuterated salt, while, the number of lines is reduced to only two. The present success in extending the lower limit of measuring temperature one decade closer to T_N than in earlier experiment[11] is indeed owing to this deuteration.

In order to check the influence of deuteration on crystal and spin structure, the angular dependence of NMR frequencies (patterns) are investigated under the condition that the applied static field intensity H_0 is much weaker than the local dipole fields H_d at the proton sites. Figure III-4(a) and (b) are the patterns at 2.2 K ($\sim 0.6T_N$) at H_0 = 50 Oe in the ac- and bc-plane, respectively. The black and white circles show the data for the deuterated and the hydrated salts, respectively. Clearly both data are in good agreement, which assures that the spin structure of MnF2D is just the same as that of MnF2H.

To investigate the growing feature of the spontaneous subsystem magnetization of both A and B systems, the temperature dependences

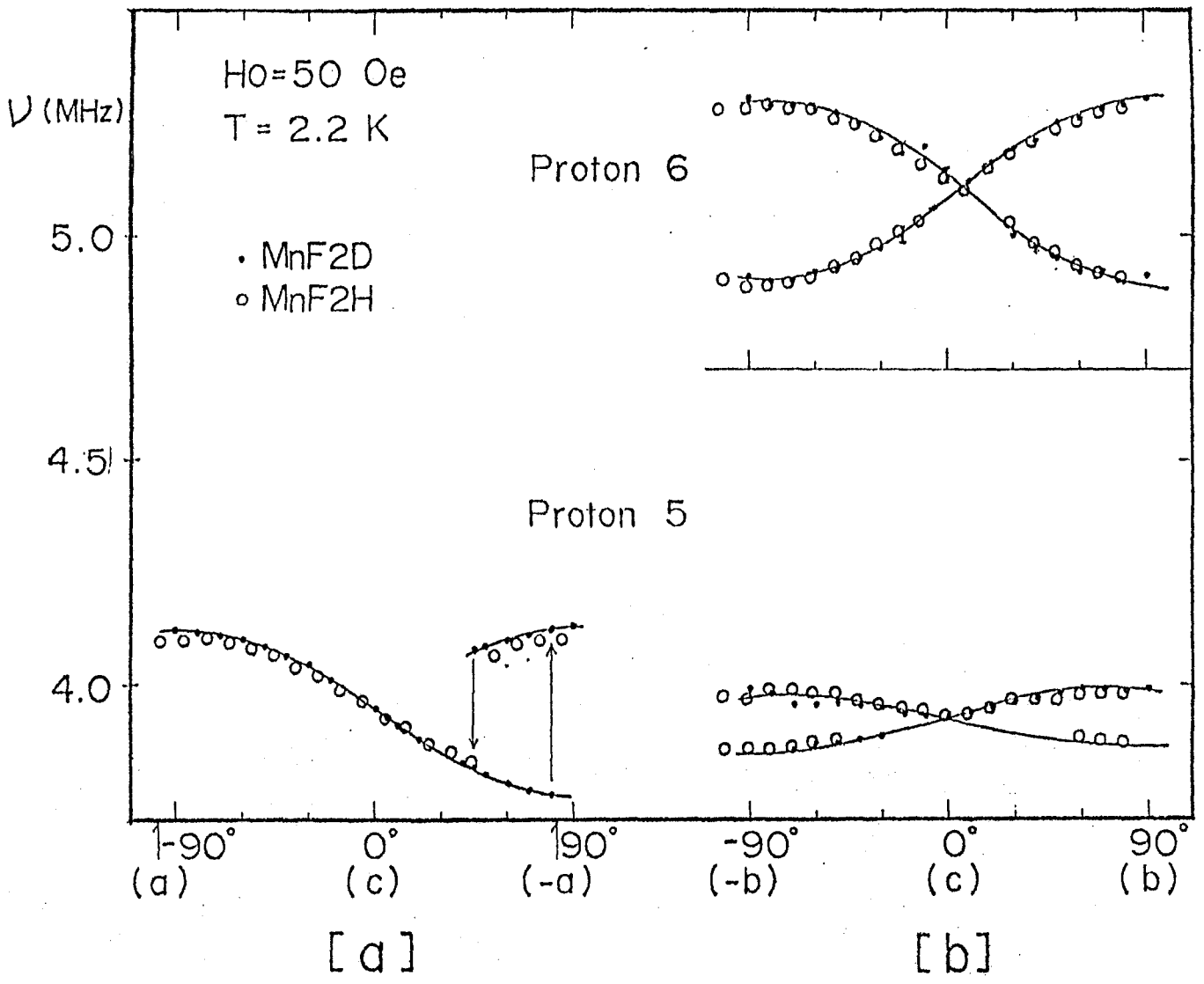

Fig.III-4. Angular dependence patterns of the NMR line shift for the deuterated (•) and the hydrated (o) salts at T = 2.2 K under H_0 = 50 Oe. (a) ac- (b) bc-plane.

of NMR frequencies at zero field are observed. The result is shown in Fig.III-5.

The resonance frequencies of proton No.5 and No.6 are generally expressed by

$$\omega_i = |\gamma \cdot H_d^i|, \qquad (i = 5,6) \tag{3.9}$$

and

$$H_d^i = \sum_I (\tilde{D}_I^{i+} \cdot M_I + \tilde{D}_I^{i-} \cdot L_I), \tag{3.10}$$

where $\tilde{D}_I^{i+} = \tilde{D}_{I1}^i + \tilde{D}_{I2}^i$, $\tilde{D}_I^{i-} = \tilde{D}_{I1}^i - \tilde{D}_{I2}^i$, (I = A,B) and $\tilde{D}_{I1}^i$ and $\tilde{D}_{I2}^i$ are the dipole sum tensors from 1 and 2 sublattice points in I subsystem, respectively. M_I and L_I are the uniform and the staggered magnetizations of I subsystem. In the present antiferromagnet, the coupling between the uniform and the staggered moments is known very weak and contribution from M_A and M_B are negligible. So in this case, ω_i is determined by the magnitudes L_A and L_B and expressed in the form as

$$\omega_i = L_A \cdot F_i(\eta), \qquad (i = 5,6) \tag{3.11}$$

where η is the ratio L_A/L_B. $F_i(\eta)$ is determined by $\tilde{D}_A^{i-}$ and $\tilde{D}_B^{i-}$ and a function of only η. By applying the experimental data in Fig.III-5 to equation (3.11), L_A and η are obtained.

Figure III-6(a) is the temperature dependence of L_A in both logarithmic scale. It tells us that the spontaneous staggered magnetization of A subsystem L_A^0 follows two exponential laws. In the temperature range $2 \cdot 10^{-2} < \varepsilon < 5 \cdot 10^{-1}$, an exponent $\beta = 0.23 \pm 0.01$ which is in good agreement with the previous result 0.22 ± 0.01 from NMR and neutron diffraction. While in the temperature range

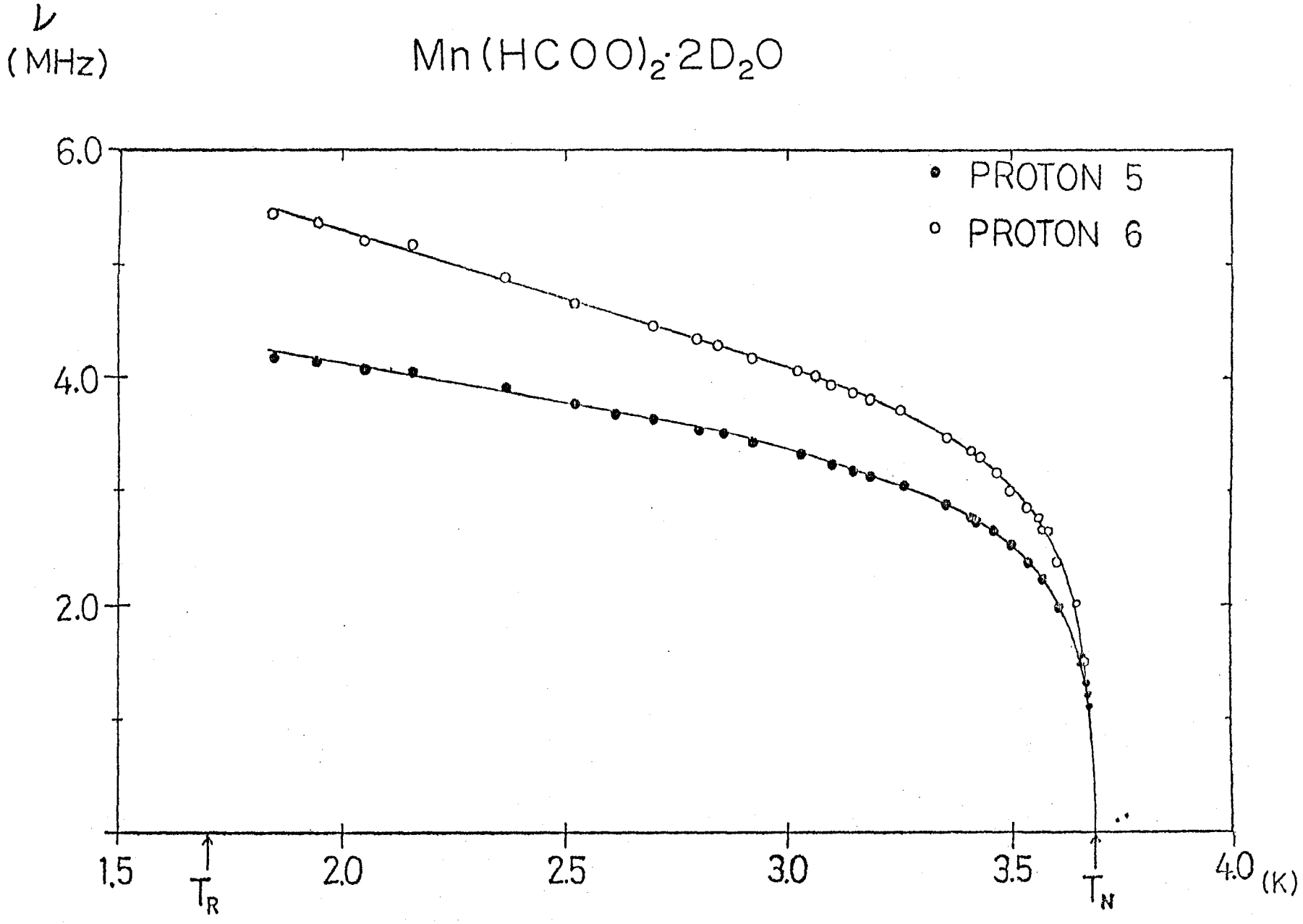

Fig.III-5. Temperature dependence of proton NMR frequencies at zero external field in the ordered state.

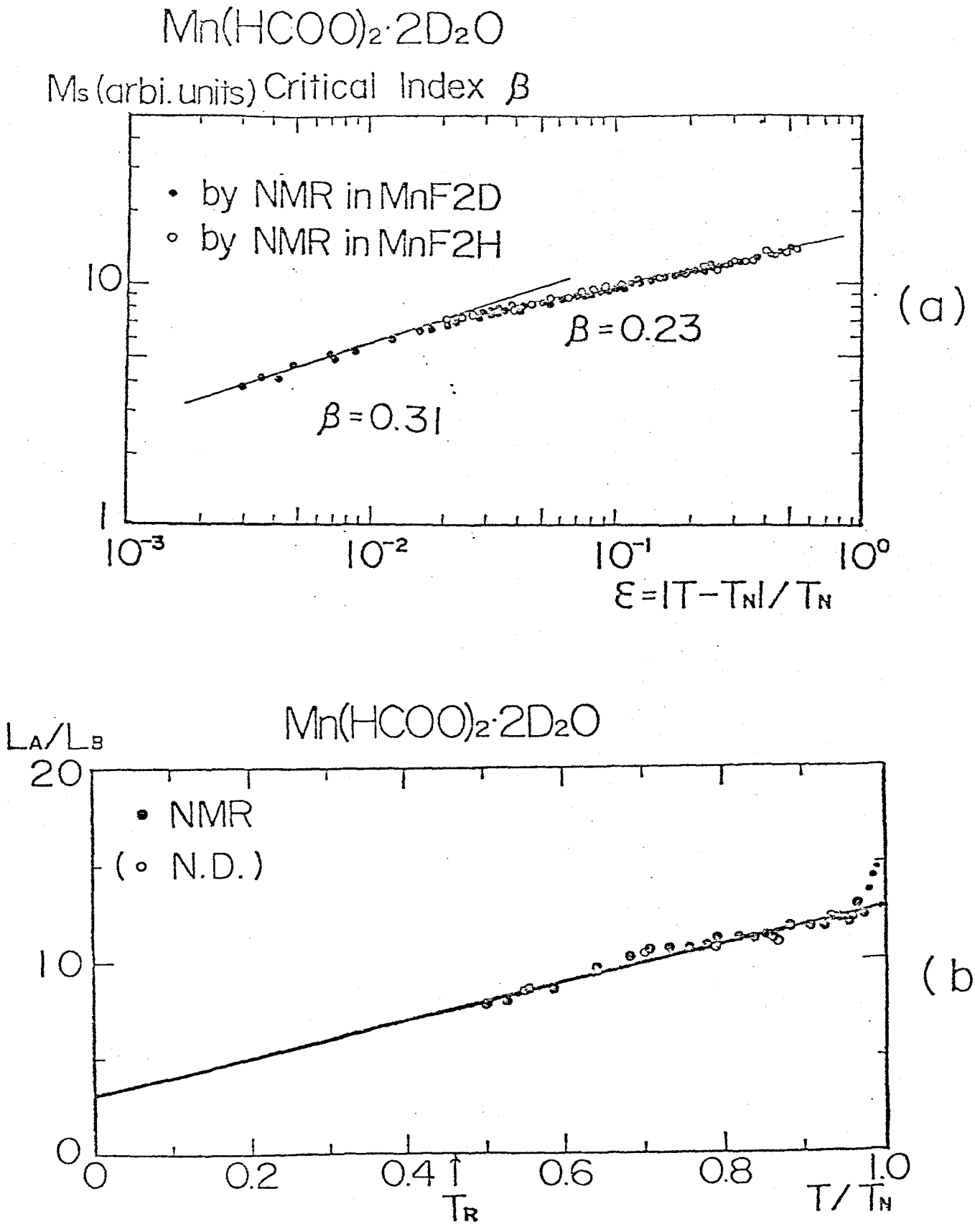

Fig.III-6. (a) Temperature dependence of L_A in both logarithmic scale.

(b) Temperature dependence of $\eta \equiv L_A / L_B$.

closer T_N i.e. for $3 \cdot 10^{-3} < \varepsilon < 2 \cdot 10^{-2}$, another exponent $\beta = 0.31 \pm 0.02$ is found. It indicates a crossover effect at the temperature $\varepsilon^* = 2 \cdot 10^{-2}$.

Figure III-6(b) is the temperature dependence of η, which tells us that the ratio L_A/L_B increases linearly with temperature as $T \to T_N$. The ratio η estimated by using the previous neutron diffraction data in reference 2) is normalized and also plotted in the same figure by white circles, which are in good agreement with the present data.

III-2.3 Simultaneous measurement of susceptibility and spontaneous magnetization by a SQUID magnetometer

The spontaneous magnetization M_s and the susceptibility χ of MnF2H are very sensitive to the applied field in the neighbourhood of T_N reflecting the non-linear characteristics of the corresponding staggered quantities. The essentials are therefore a perfect compensation of residual DC field H_r including earth field and a suppression of exciting AC field intensity h to a negligibly weak level in order to assure the linear response in susceptibility measurement. All the zero field measurements are thus made at negligibly small H_r and h less than 5 mOe.[17] Necessary, a high sensitive measurement is wanted and we used a SQUID magnetometer.

In order to obtain the spontaneous magnetization M_s, so called "field cooling method" is applied. The magnitude of M_s depends usually on the cooling field H_c but is constant in high field region ($H_c \gtrsim 50$ mOe for the present case). After decreasing this field to a negligible value by a proper compensation, M_s and χ are measured simultaneously with increasing temperature towards and accross T_N.

An important and noteworthy here is the simultaneous measurement of M_s and χ in a single run of increasing temperature on a same single crystal. Because, the determination of critical exponent depends strongly on the position of T_N especially in the immediate neighbourhood of T_N. Independent measurements of M_s and χ necessitate independent determinations of T_N for each case, which may introduce some accidental or systematic errors due to a small but non-negligible deviation of experimental conditions for these measurements.

It is confirmed by a separate observation of subsystem susceptibilities χ_{uA} and χ_B by NMR in III-2.1 that a very sharp needle-like anomaly of χ at T_N comes from χ_A and shows the divergent nature of the staggered susceptibility χ_{sA}. The contributions of χ_B and χ_{uA} to the total susceptibility χ are not singular and a slowly varying quantities with T around T_N. So the temperature dependence of residual part $\Delta\chi$ in the immediate neighbourhood of T_N shows just the singularity of χ_{sA}. It is also confirmed by a separate determination of L_A and L_B by NMR in III-2.2 that L_B is proportional to L_A and the proportional constant is a slowly varying quantity with T around T_N. So the temperature dependence of M_s in the immediate neighbourhood of T_N shows just the singularity of L_A.

Figure III-7 shows the temperature dependences of $\Delta\chi$ and M_s in the neighbourhood of T_N. These quantities are measured simultaneously as mentioned above. The correspondence of the temperature scale for these quantities is quite exact. A divergent anomaly happens at T_N = 3.686 K. Correspondingly, M_s is noticed to disappear at the temperature as temperature increases. Fig.III-8(a)

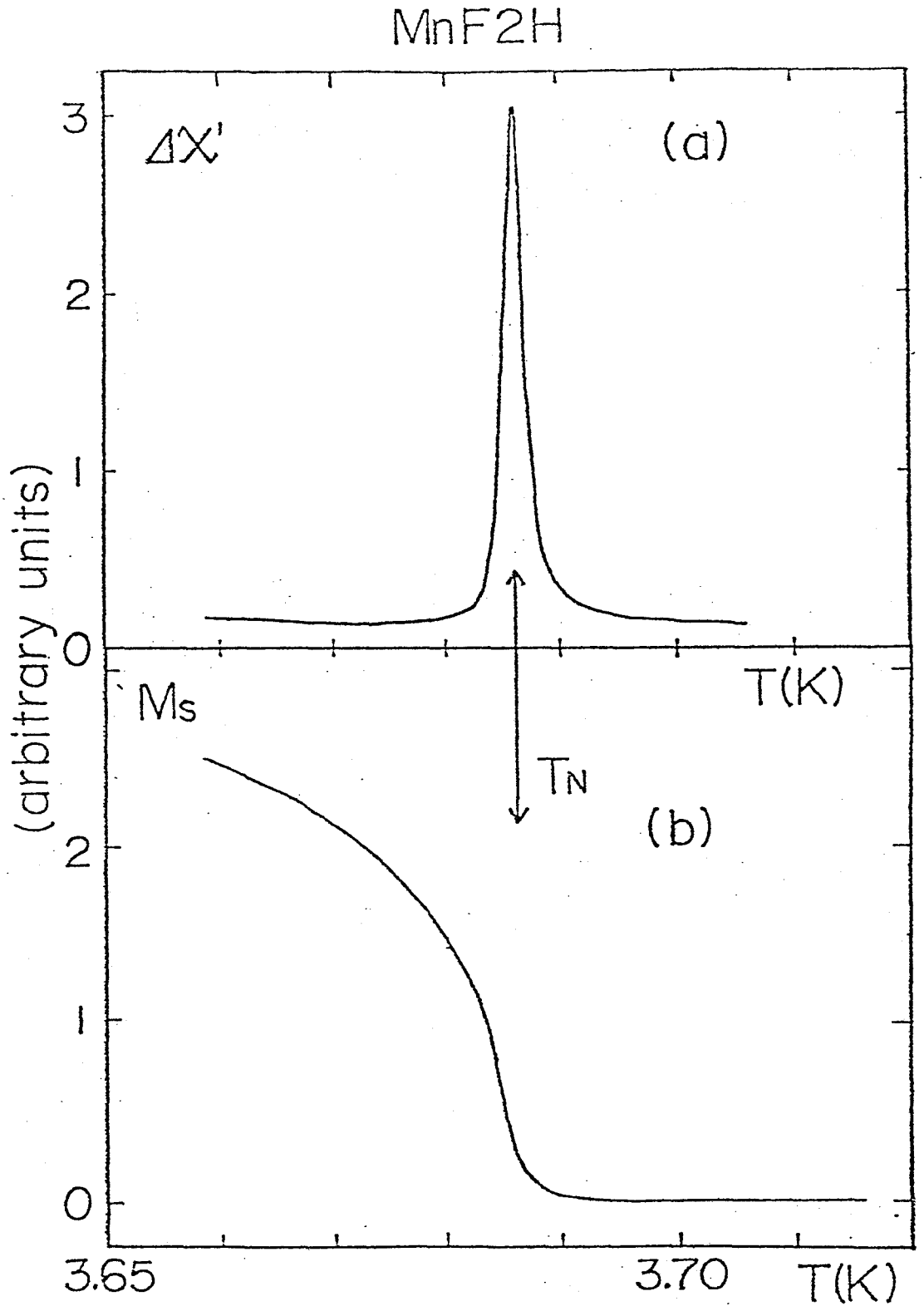

Fig.III-7. Temperature dependences of (a) $\Delta\chi$ and (b) M_s in the vicinity of T_N.

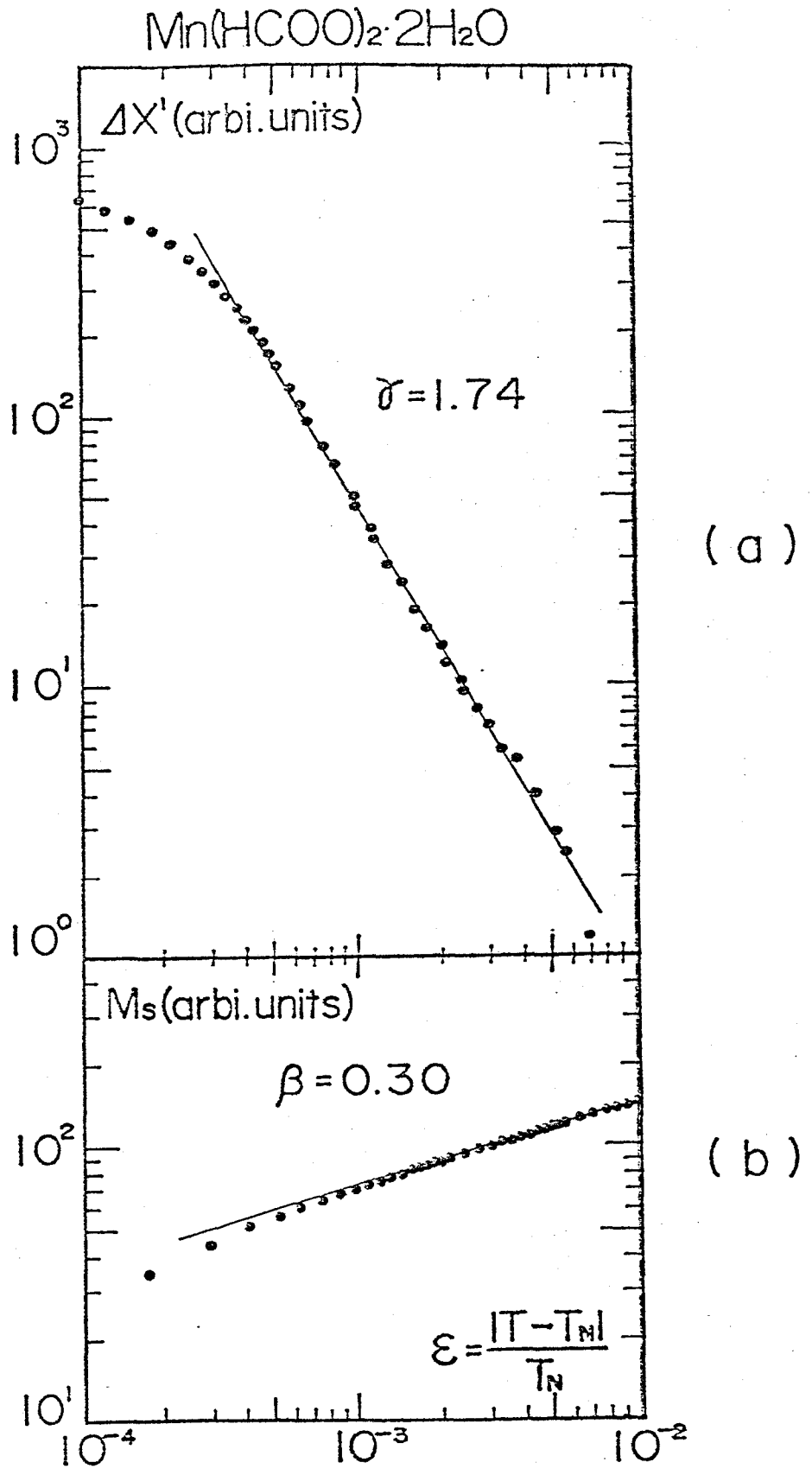

Fig.III-3. Both logarithmic plots of (a) $\Delta\chi - \varepsilon$ and (b) $M_s - \varepsilon$.

is the both logarithmic plot of $\Delta\chi$-ε. It tells us that χ_{sA} follows an exponential law with a critical index $\gamma = 1.74 \pm 0.1$ down to the temperature $\varepsilon = 5 \cdot 10^{-4}$, below which a rounding occurs. The result is consistent with that in the early measurement except that the rounding temperature ε_r in the present case is much lower than the previous one $1 \cdot 10^{-3}$.[1] So, we conclude that the apparent rounding phenomena in the early measurement is attributed to the residual field effect and not a crossover to any other universality class at all.

Figure III-8(b) is the both logarithmic plot of M_s-ε. It tells us that L_A follows an exponential law with a critical index $\beta = 0.30 \pm 0.02$ in the temperature range down to $\varepsilon = 5 \cdot 10^{-4}$. It is in good agreement with $\beta = 0.31 \pm 0.02$ obtained from recent NMR on the deuterated salt in the temperature range $3 \cdot 10^{-3} \lesssim \varepsilon \lesssim 2 \cdot 10^{-2}$ as shown in Fig.III-6(a) for comparison. The present simultaneous and careful measurement of M_s and χ is in good agreement with the previous independent measurements of these quantities by different methods in the common temperature range, and tells us that the critical index γ for the staggered susceptibility above T_N is 1.74 ± 0.1 and β for the spontaneous staggered magnetization below T_N is 0.30 ± 0.02 in the same temperature range $5 \cdot 10^{-4} \lesssim \varepsilon \lesssim 1 \cdot 10^{-2}$. These γ and β are very close to the values for two different universality classes i.e. 2d Ising and 3d Ising ones, respectively. Such a characteristic critical phenomena asymmetric against T_N is apparently inconsistent with the scaling law and the universality in the conventional sense.

§III-3. Discussion

As seen in §III-2, the present result revealed that the exponent of spontaneous staggered magnetization of A subsystem is 0.30 ± 0.02 in the immediate neighbourhood of T_N. The value of β is in close agreement with that for 3d Ising model and not so much different from those for 3d Heisenberg and 3d XY models. While another exponent $\beta = 0.23$ in the temperature range a little far from T_N, is different both from 2d Ising model and from any 3d model and quite intermediate.

The latter exponent $\beta = 0.23$ can hardly be taken as an apparent value in the crossover temperature region from one for 3d Ising model to the other for 2d Ising model because the anomaly at $\varepsilon^* = 2 \cdot 10^{-2}$ looks like a kink and the following L_A-ε plot is very linear over a wide temperature range, as seen in Fig.III-6(a). This characteristic exponent is the same as that in CuFUD or CuF4D in Chap.II. So, the origin of this characteristic exponent may be regarded as the new universality class which is caused by 2d Heisenberg model with some weak symmetry breaking interactions.

While, the former exponent $\beta = 0.30$ seems to be reasonable refering the observed 3d long range order below T_N by previous neutron diffraction[2] and to indicate that the ordering of A subsystem proceeds in a 3d way. However, it is not simply the case and the situation is quite puzzling as mentioned later.

The present result also reveals that the spontaneous magnetization of B subsystem L_B appears below T_N and that the growth rate is proportional to that of L_A with a coefficient which depends linearly on temperature. Such a growing feature of L_B is very similar to the nuclear spin polarization process under the hyperfine

field from the ordered electron system. Analogously, if we attribute the obtained L_B to the local field induced polarization from the ordered A subsystem, we get a local field of about 1.4 kOe at a B ion site, which is about 1 % of the exchange field in A subsystem.

Actually, the existence of such a local field can reasonably explain the shottky-type heat capacity anomaly of MnF2H observed previously at very low temperature ($\sim 0.1 \cdot T_N$) far from T_N. Looking back on the ideally paramagnetic behaviour of B subsystem above T_N mentioned in III-2.1, we strongly believe that B subsystem does not give any essential contribution at all to the onset of phase transition of A subsystem at T_N. In other wards, the modification of inter-plane interaction by a paramagnetic ion could not affect primarily on the phase transition of such a quasi 2d system. The appearance of spontaneous magnetization of B subsystem is then reasonably well understood by a resultant secondary effect.

As mentioned before, the critical index $\beta = 0.30$ of A subsystem in the immediate neighbourhood of T_N is surprising as follows. The exponent suggests that the most dominant purturbation on the onset of phase transition of A subsystem is the inter-plane interaction. According to the scaling law and the universality,[19] which are well known to be two fundamental laws to describe the so called second order phase transition, we expect that a critical index for the susceptibility γ should be 1.31 for 3d Ising model. Early susceptibility measurement and the present one by SQUID, however, gave $\gamma = 1.74$ for the staggered susceptibility of A subsystem in the intermediate neighbourhood of T_N. The above value is close to 1.75 for 2d Ising model and quite in disagreement with above expectation.

Now, one may think that the present result is still compatible with the established laws (scaling law and the universality) Ising to 3d Ising universality classes into account. Then the crossover temperature ε^* from 2d Ising to 3d Ising for χ_s above T_N should be taken to be less than $5 \cdot 10^{-4}$. While, ε^* for L_A below T_N is $2 \cdot 10^{-2}$ and roughly two order of magnitude larger than that for χ_s. We can not have any special reason for such a large asymmetry of crossover temperatures above and below T_N so far. Indeed, the values of ε^* for susceptibility and spontaneous magnetization have been predicted to be the same as reasonably acceptable. Besides, outside the $\varepsilon^* = 2 \cdot 10^{-2}$, we find an exponent $\beta = 0.23$, which is quite different from 0.125 for 2d Ising universality class. Thus, we can not explain the present characteristic facts simply by a dimensionality crossover effect.

As mentioned above, the critical phenomena of MnF2H is quite asymmetric and apparently inconsistent with the scaling law and the universality in the conventional sense. The viewpoint from dimensionality crossover can not be helpful at all for the characteristic phenomena. Manganese ion has $(3d)^5$ electronic configuration and is in so called S-state with $S = 5/2$. Besides, it is surrounded by six oxigen atoms in the form of nearly octahedron and originally very isotropic. For such a S-state ion system with large spin number, the main contribution to the anisotropy is dipole-dipole interaction usually. In a single quadratic antiferromagnet, the dipole anisotropy is of Ising-type and the direction is perpendicular to the plane. A rather strong anisotropy of Ising-type perpendicular to the plane in K_2MnF_4[4] or Rb_2MnF_4[18] would be explained by this

interaction.

While, in MnF2H, the situation is different. The Ising-type anisotropy by dipole-dipole interaction is known here to be compensated by another planer-type anisotropy even a little excessively and can not be the main origin of the symmetry at all, from the fact that the first and second easy directions below T_N are nearly in the plane. The appearence of such a planer-type anisotropy in A plane is attributed to a slight distortion of the octahedral crystal field symmetry by oxgen atoms sorrounding a A ion site. Then the Ising-type anisotropy in the plane will be reduced to a weak asymmetry of the crystal field within the A plane and thus much weaker than the residual planer anisotropy. Besides, this asymmetric crystal field should be inequivalent at two sublattice points in the A plane, which will reduce the Ising-type anisotropy in the plane to some extent and instead produce an antisymmetric interaction with an inequivalence of g-tensors, between the A ions at the two sublattice points. Indeed, the existence of very weak moment canting interactions in this salt, as mentioned in §III-1, supports this speculation.

Such a situation in MnF2H that a multiple compensation of several symmetry breaking factors results in a very weak Ising-type anisotropy is remarkable and quite different from those in other simple Heisenberg-like systems. The distinguishable critical phenomena asymmetric against T_N might be attributable to this characteristic situation.

As mentioned in §III-1, the interplane interaction is decorated by the paramagnetic ion. As seen in §III-2, it seems to suggest

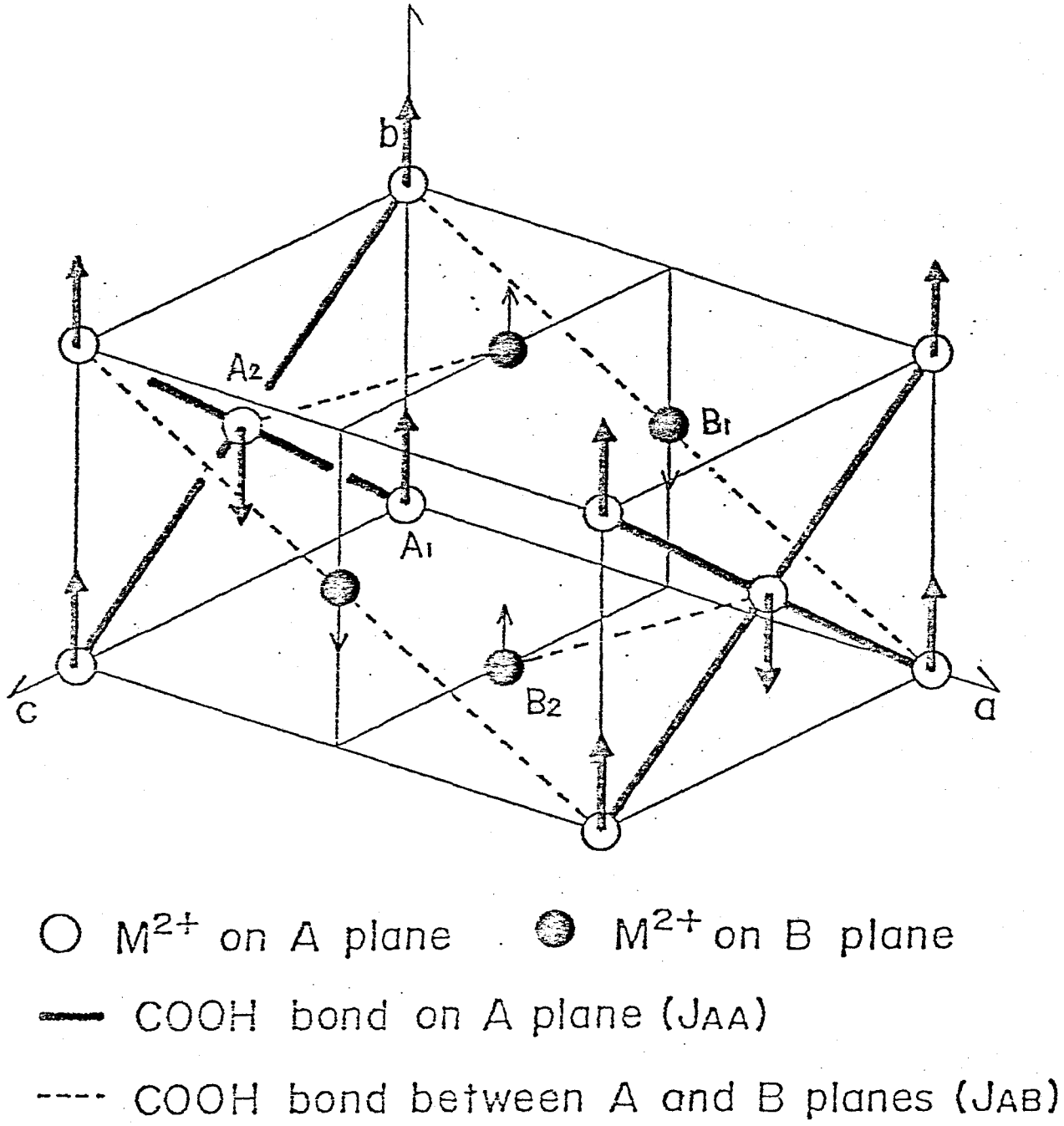

Fig. III-9. A schematic crystal structure of Mn formate dihydrate and spin structure below T_N.

strongly that such decorating paramagnetic ions do not give any essential contribution to the onset of phase transition of A subsystem at T_N and that such a decoration does not modify at all the original natures of superexchange interaction formed by only nonmagnetic ions.

Actually, in many decorated 2d Ising systems, no essential change of critical phenomena have been reported so far from those of nondecorated simple systems. However, a 2d Heisenberg system does not order at all by itself. Besides, the present decorating ion is just on the intermediate of interplane interaction path between such 2d Heisenberg planes, which is an essential symmetry breaking purturbation. So such a modification might give a remarkable influence on the phase transition and reveal some characteristic feature which have never expected and never really observed so far in any simple systems.

References (III)

1) M. Matsuura, Y. Ajiro and T. Haseda: J. Phys. Soc. Jpn. 26 (1969) 665.

2) J. Skalyo,Jr., G. Shirane and S. A..Friedberg: Phys. Rev. 188 (1969) 1037.

3) Y. Yamamoto, M. Matsuura and T. Haseda: J. Phys. Soc. Jpn. 43 (1977) 1550.

4) R. J. Birgeneau, H. J. Guggenheim and G. Shirane: Phys. Rev. B8 (1973) 304.

5) K. Osaki, Y. Nakai and T. Watanabe: J. Phys. Soc. Jpn. 19 (1964) 717

6) M. Matsuura and Y. Ajiro: J. Phys. Soc. Jpn. 41 (1976) 44.

7) K. Yamagata: J. Phys. Soc. Jpn. 22 (1967) 582.

8) K. Takeda, T. Haseda and M. Matsuura: Physica 52 (1971) 225.

9) H. Morigaki and H. Abe: J. Phys. Soc. Jpn. 23 (1967) 462.

10) Y. Ajiro: J. Phys. Soc. Jpn. 27 (1969) 829.

11) H. Yamakawa: thesis, Osaka University (1977).

12) M. Matsuura, H. W. J. Blöte and W.JJ. Huiskamp: Physica 50 (1970) 444.

13) H. Abe and K. Torii: J. Phys. Soc. Jpn. 20 (1965) 183.

14) H. Abe and M. Matsuura: J. Phys. Soc. Jpn. 19 (1964) 1867.

15) M. E. Lines: J. Phys. Chem. Solids 31 (1970) 101.

16) K. Kcyama, N. Terata and M. Matsuura: J. Phys. Soc. Jpn. 51 (1982) 2697.

17) M. Matsuura, K. Koyama and Y. Murakami: J. Phys. Soc. Jpn. 52 (1983) Suppl.37.

18) R. J. Birgeneau, H. J. Guggenheim and G. Shirane: Phys. Rev. 1 (1970) 2211.

19) See Chap.I or ref.9) in Chap.I.

Chapter IV. Ordering of $Mn(HCOO)_2 \cdot 2H_2O$ and $Mn(HCOO)_2 \cdot 2D_2O$ under the field

IV.A. Magnetic phase boundary

§IV.A-1. Introduction

One of the current problems in two-dimensional (2d) XY or Heisenberg spin systems is in their attractive features of new type of phase transition or ordered phase. A crossover phenomenon of spin dimensionality from the Heisenberg (or XY) spin to the XY (or Ising) spin in the external magnetic field has been expected[1] and observed in real quasi-1d antiferromagnets.[2-4] The same phenomenon has been predicted also in 2d systems.

Recently, we have recognized that $Mn(HCOO)_2 \cdot 2H_2O$ (MnF2H) is an excellent realization of 2d Heisenberg antiferromagnet and we suppose that it may give us some possibilities of finding new cooperative phenomena mentioned above. A number of works have been carried out on this compound because of the variety of interests. Nevertheless, the magnetic phase diagram is not yet clear. The purposes of the first half of this chapter is to establish the fully mapped magnetic phase diagram in the external magnetic field applied along the spin easy and hard axes, and to determine the magnetic structure in various phases and the mechanisms of transitions by the measurements of proton NMR. In order to determine the phase boundary, the heat capacity and the magnetic susceptibility were measured simultaneously in the superconducting magnet which could generate the field up to 115 kOe. The intrinsic 2d Heisenberg or XY behaviours observed in the field will be given in the latter half of this chapter.

§IV.A-2. Experimental results of heat capacity and susceptibility

IV.A-2.1 The paramagnetic contribution of Mn^{2+} ions on the B-planes

Evidence for the paramagnetic behaviours of the Mn^{2+} ions on the B-planes have been observed in various studies such as adiabatic demagnetization,[5] susceptibility,[5,6] neutron diffraction[7] and magnetic heat capacity.[8] In order to extract the contribution of the 2d A-planes in a finite field, we shall present a procedure for separating the paramagnetic contribution of the Mn^{2+} ions on the B-planes from the observed physical quantities, taking the case of magnetic heat capacity as an example.

The overall behaviour of the magnetic heat capacity of MnF2H in zero field is shown in Fig.IV.A-1 against reduced temperature T/T_N (T_N = 3.69 K).[9] The Schottky anomaly C_B at low temperatures indicated by the broken line corresponds to the paramagnetic contribution from the B-planes. The 2d A-planes order at T_N and their magnetic contribution C_A appears mainly at higher temperatures than 1 K ($T/T_N \gtrsim 0.3$).* In the field $\vec{H}_e$, the paramagnetic Mn^{2+} gives a Schottky-type heat capacity C_B which can be expressed as

$$C_B(t)/R = (S\ t)^2 \cdot B_S'(S\ t)$$

$$B_S'(u) = dB_S(u)/du$$

$$= -\left(\frac{2S+1}{2S}\right)^2 \mathrm{cosech}^2\left(\frac{2S+1}{2S}u\right) + \left(\frac{1}{2S}\right)^2 \mathrm{cosech}^2\left(\frac{u}{2S}\right), \quad (4.1)$$

with $t = g\mu_B|\vec{H}_e|/k_BT$ and $u = S \cdot t$, where R, S and $B_S(u)$ are the gas

*) The lattice heat capacity C_L of this sample is known to be much smaller than the magnetic one (only less than 1 % of the magnetic heat capacity at T_N)[9,10,11] and is subtracted here.

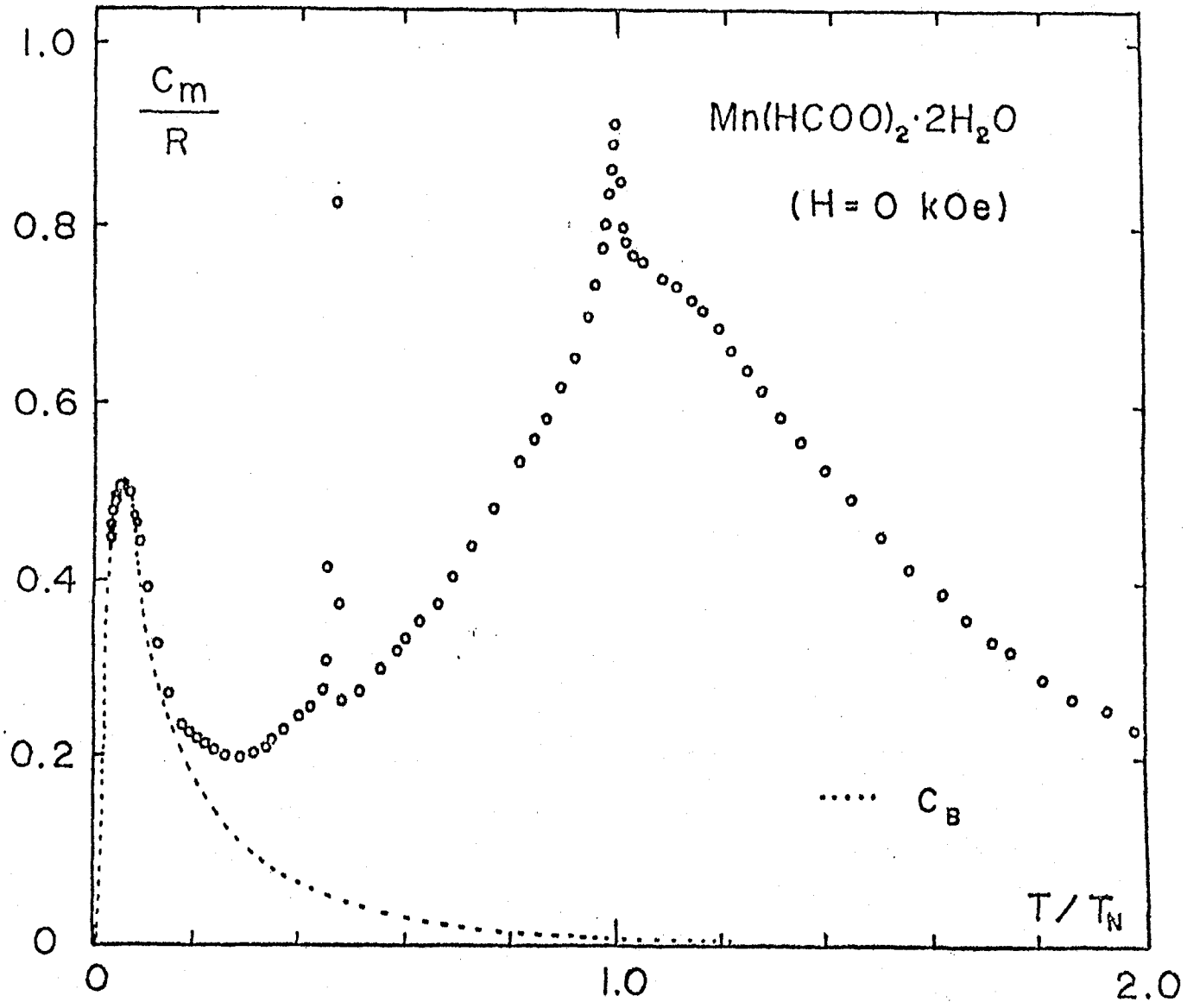

Fig.IV.A-1. Magnetic heat capacity of $Mn(HCOO)_2 \cdot 2H_2O$ against the reduced temperature in zero field.[9,10] C_B indicates the contribution from paramagnetic Mn^{2+} ions in the B-planes.

constant, the spin value of Mn^{2+} ions (S = 5/2) and the Brillouin function, respectively. We can reproduce the observed heat capacity at low temperatures by the use of eq.(4.1) (broken line in Fig.IV.A-1) with $|\vec{H}_e|$ = 2.6 kOe ($\equiv|\vec{H}_l|$), although the detailed experimental analysis down to the lowest temperature has been carried out in ref.8. This implies that in zero field, the Mn^{2+} ions on the B= planes are under the influence of an effective (local) field $\vec{H}_l$ at low temperatures where the Mn^{2+} ions on the A-planes are in ordered state. The origin of $\vec{H}_e$ has been discussed somewhere.[5,8,11] The value $|\vec{H}_l|$ = 2.6 kOe is consistent with that estimated from the adiabatic demagnetization experiment for Mn^{2+} ions on the B-planes.[5] In a finite external field $\vec{H}$, we can estimate C_B from eq.(4.1) by putting

$$|\vec{H}_e| = |\vec{H} + \vec{H}_l|. \tag{4.2}$$

The temperature T_m which gives the maximum value of the Schottky heat capacity shifts to the higher temperature with increasing H as,

$$g\mu_B|\vec{H}_e|/k_BT_m = 1.20 \tag{4.3}$$

For example, the calculated temperature dependence of C_B at H = 20 kOe is shown in Fig.IV.A-2 by the dotted line whose maximum comes around 2.3 K. By subtracting C_B from the total magnetic heat capacity in this way, we can extract C_A for the 2d A-planes. In Fig.IV.A-2, the values of C_A are plotted for H = 20 kOe applied along the spin easy (b-)axis and the hard (a*-)axis. It should be remarked that the heat capacity C_A for H = 20 kOe exhibits quite a different shape from that for H = 0 kOe (Fig.IV.A-1). The detailed discussion

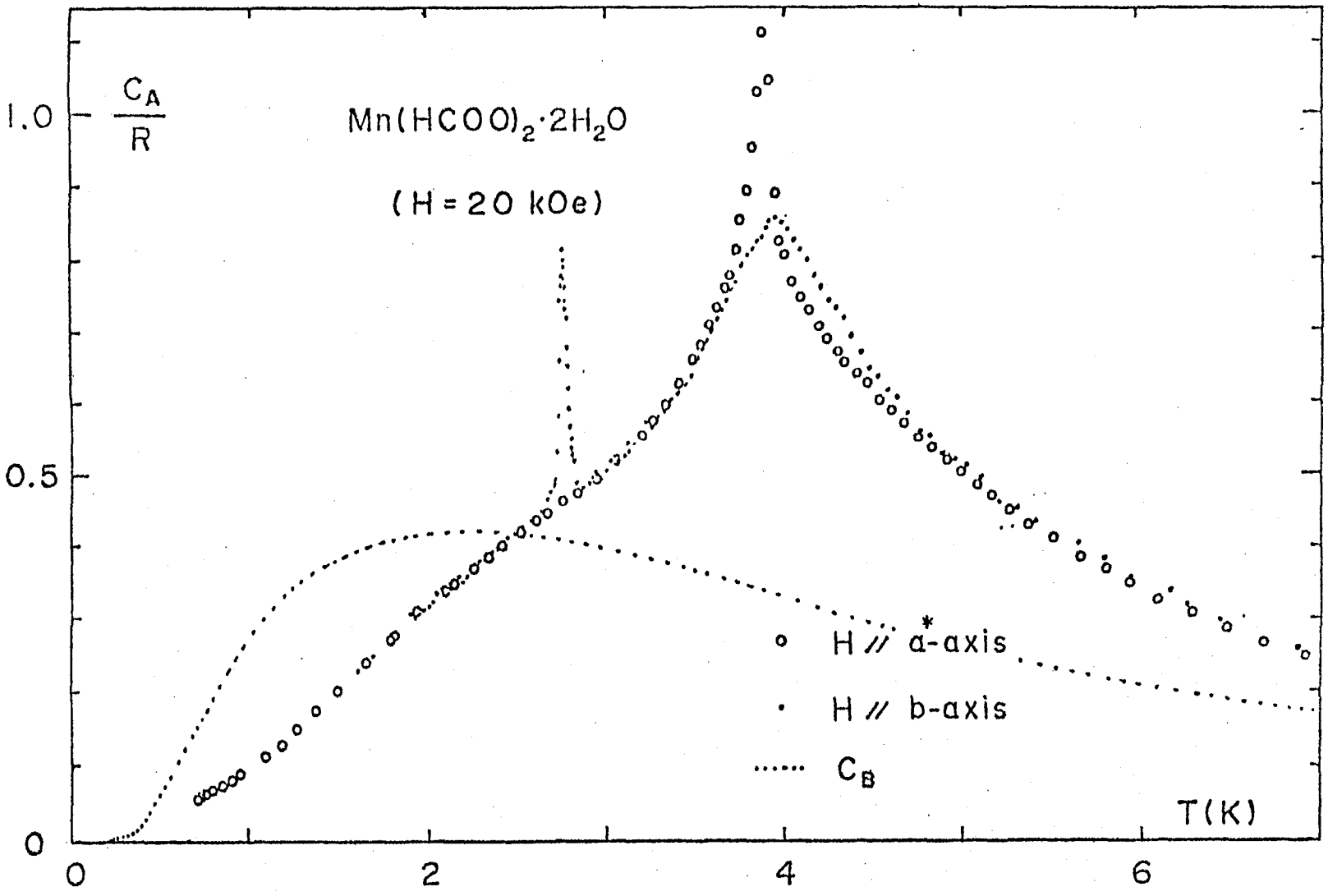

Fig.IV.A-2. Magnetic heat capacities of the 2d A-planes (C_A) and of the paramagnetic B-planes (C_B) in a fixed field H = 20 kOe.

about the absolute values of C_A and their variation in fields will be given in the latter half of this chapter.

The temperature dependence of magnetic entropy for the 2d A= planes can be evaluated by the relation

$$S_A(T)/R = \int_0^T (C_A/R \cdot T)\, dT. \qquad (4.4)$$

In carring out the integration in eq.(4.4), the experimental values of C_A are used in the temperature range $1.0 < T < 8.0$ K (see Fig. IV.A-2), where we presume that almost all of $S_A(T)$ will be consumed. For the higher temperatures in the paramagnetic state $T \geq 8$ K, we may assume $C_A = bT^{-2}$. At lower temperatures $T \leq 1$ K, we tentatively extrapolate C_A as $C_A = aT^2$ as can be expected from 2d antiferromagnetic spin wave theory.[10] We notice in Fig.IV.A-3 that the ambiguity of $S_A(T)$ derived under these assumption (indicated with dotted line) is much smaller than the entropy change for $1.0 < T \leq 8.0$ K (solid line). It can be seen that $S_A(T)/R$ seems to reach the theoretical value $(1/2)\cdot\ln(2S + 1)$ for the 2d A-planes as $T \to \infty$. It should be noted that about one half of magnetic entropy for the A-planes still remains above T_N, reflecting the two-dimensionality of the system.

In the same way as employed above, we can estimate the paramagnetic contribution which may appear in other physical quantities such as susceptibility. Here we should note that the Mn^{2+} ions on the B-planes behave paramagnetically and do not exhibit any tendency of phase transition in a finite field and in the present temperature range.

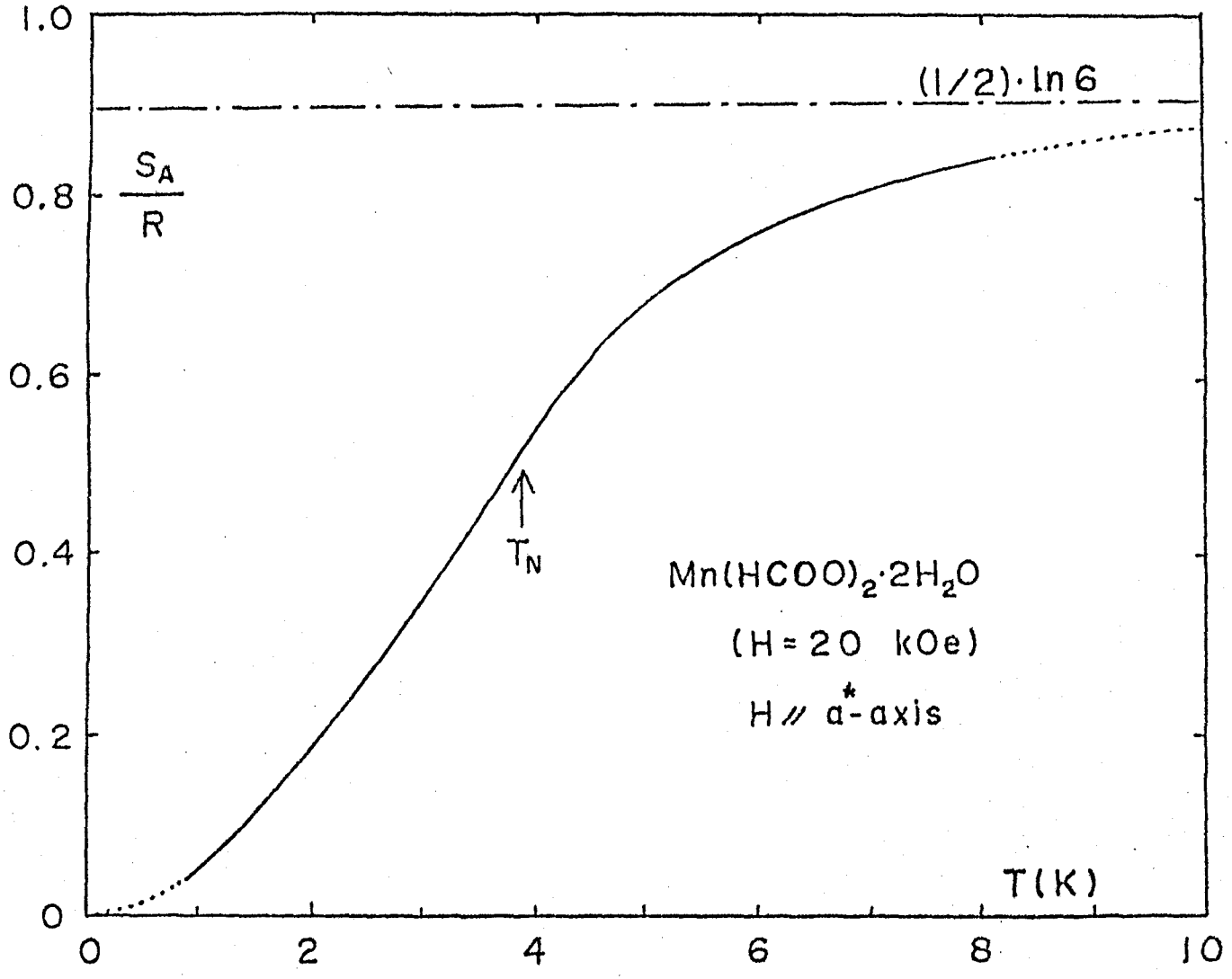

Fig.IV.A-3. Temperature dependence of the magnetic entropy of the 2d A-planes in the field H = 20 kOe.

IV.A-2.2 Determination of the magnetic phase boundary for the two-dimensional A-planes

In zero field, the Mn^{2+} ions on the A-planes set into antiferromagnetic ordered state accompanying a small but sharp heat capacity peak at T_N = 3.69 K (Fig.IV.A-1). The spin structure in the ordered phase is schematically drawn in Fig.IV.A-4.[12] It takes the H-phase in the range $T_N > T > T_r \equiv 1.7$ K, where the magnetic moments are almost along the easy (b-)axis slightly canting towards the c-axis. At $T = T_r$ there occurs a spin axis reorientation which exhibits quite a sharp heat capacity peak as in Fig.IV.A-1 (at $T/T_N = 0.46$), and below $T < T_r$ the L-phase is realized.

In this section we will determine the T-H phase diagram of this 2d system for the field applied along the spin easy (b-)axis and the hard (a*-)axis. The phase boundary concerning with the spin axis reorientation, which occurs in low fields $H \leq 4$ kOe, has been studied[12] and only the results will be shown here (Figs.IV.A-6 and 7). First we will mention about the results for H// b-axis. Figure IV.A-5 shows the field dependence of the magnetic heat capacity in the vicinity of the Néel temperature $T_N(H)$. The small but sharp peak at $T_N(0)$ = 3.69 K shifts towards low temperature rather sensitively with increasing field, keeping and growing its sharpness. When H = 20 kOe, this peak appears at $T_N(H)$ = 2.75 K as seen in Fig.IV.A-2. Tracing down the shift of this peak on the T-H plane, we have phase boundary curves between P & H, P & M, and Z & M phases as in Figs.IV.A-6 and 7. In our susceptibility measurement in the process of field sweep at a constant temperature below $T_N(0)$, we can detect this boundary between M and Z as in

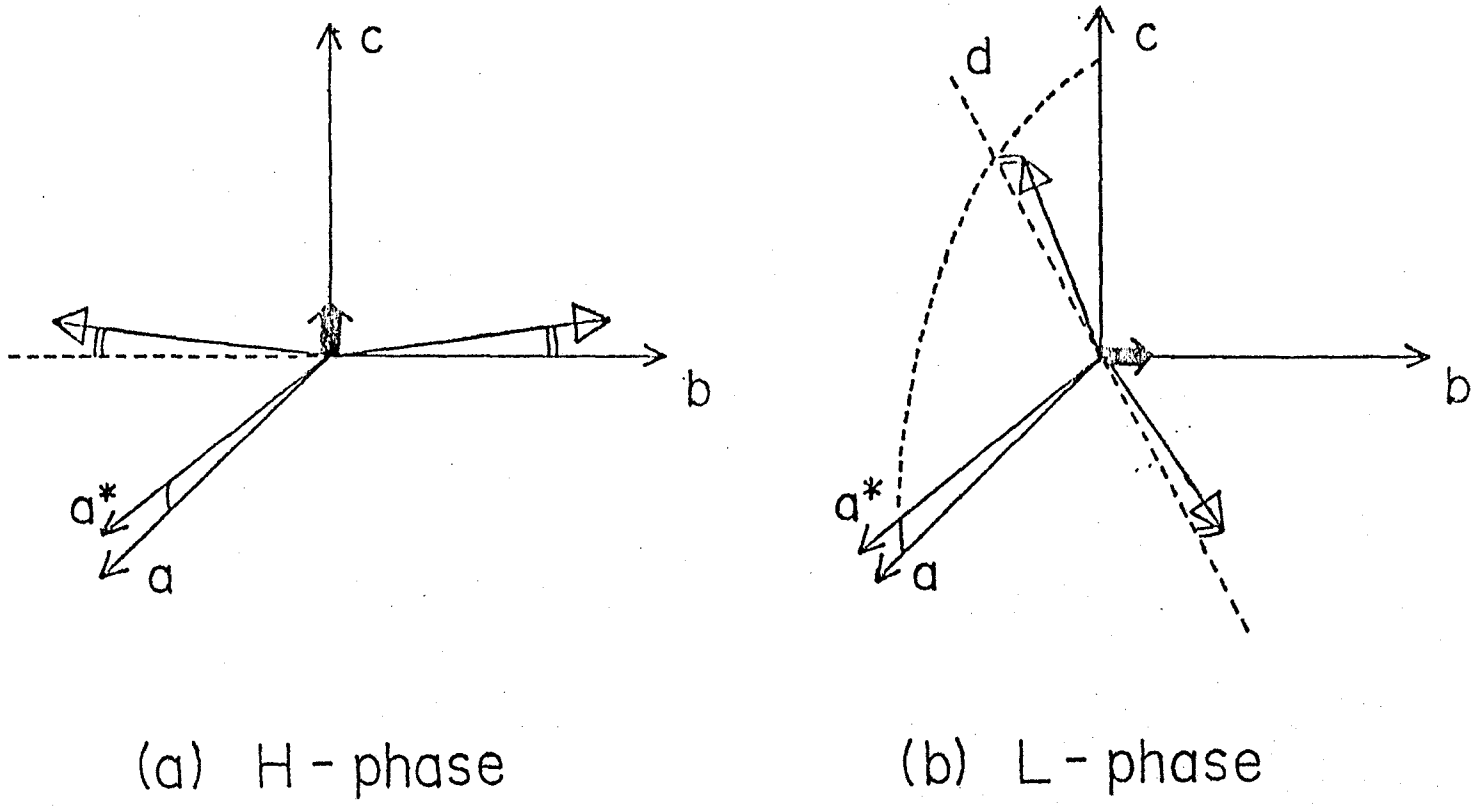

Fig.IV.A-4. Schematic description of the spin structure in the ordered state of $Mn(HCOO)_2 \cdot 2H_2O$. (a) H-phase: $T_N > T > T_r$. (b) L-phase: $T < T_r$.

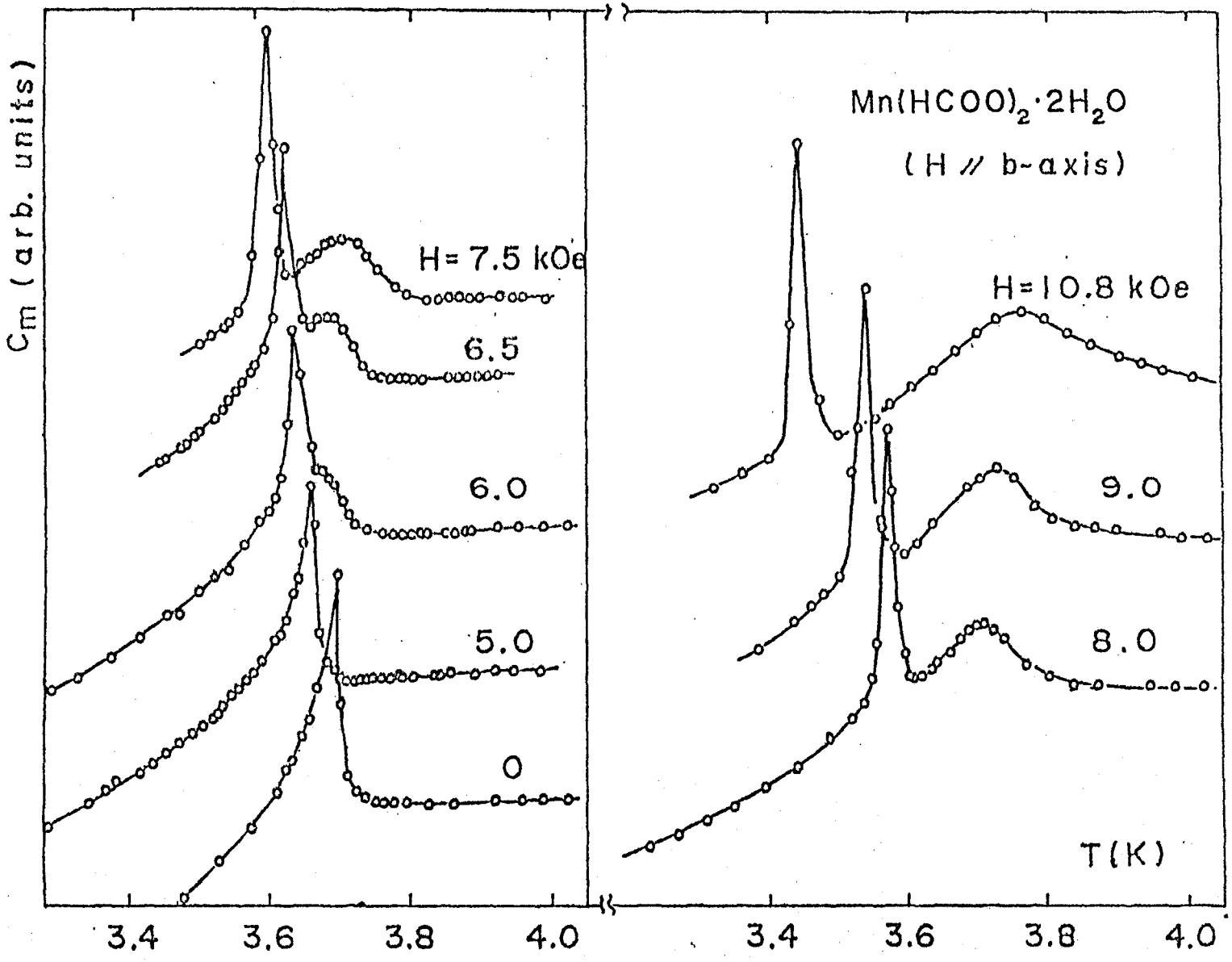

Fig.IV.A-5. Variation of the heat capacity near T_N(II) in the field applied along b-axis (arbitrary units).

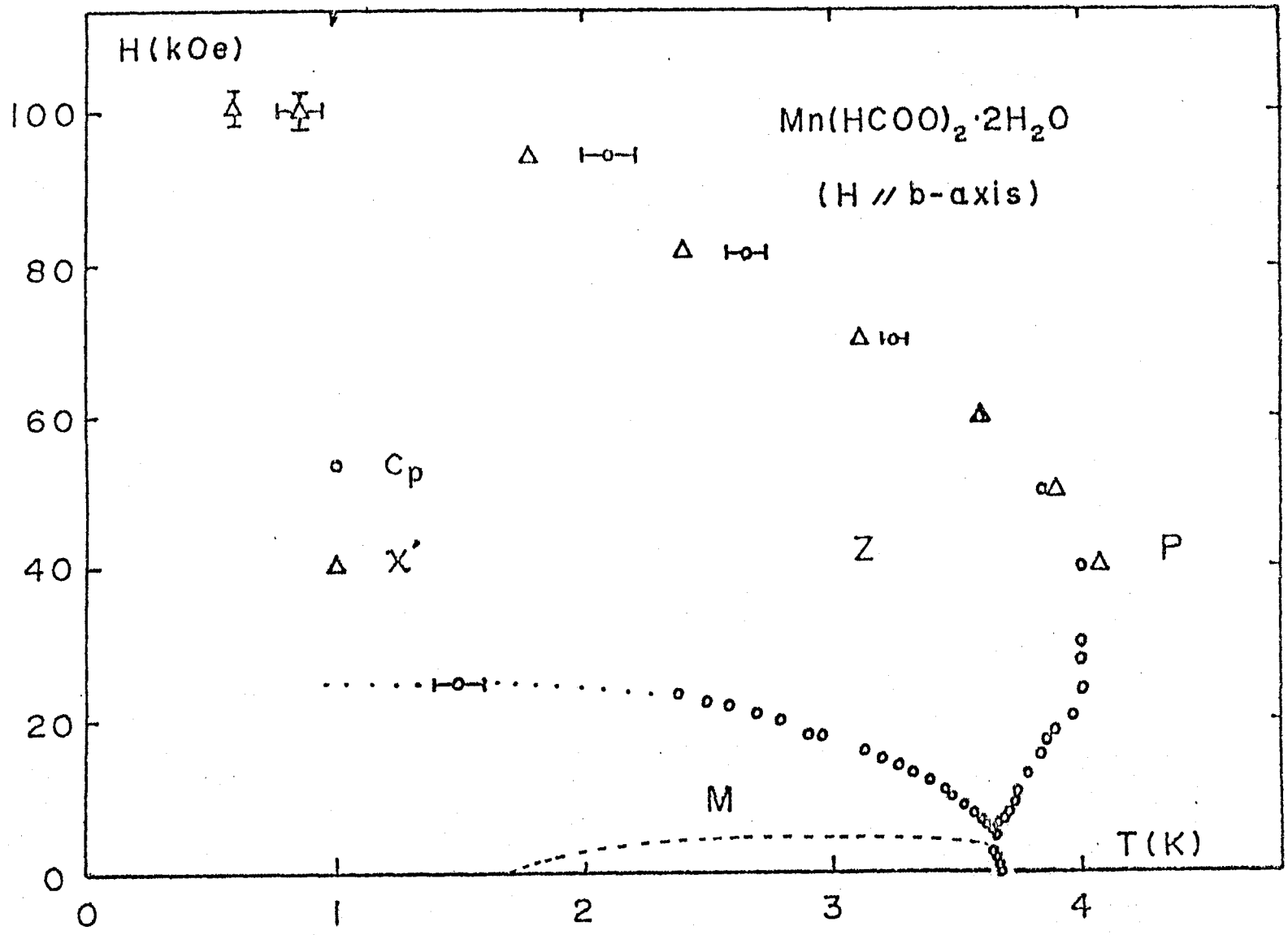

Fig.IV.A-6. T-H phase diagram of the 2d A-planes for the spin easy (b-)axis. The spin axis reorientation occurs on the boundary between M and H.[12] The closed area is enlarged in Fig.IV.A-7.

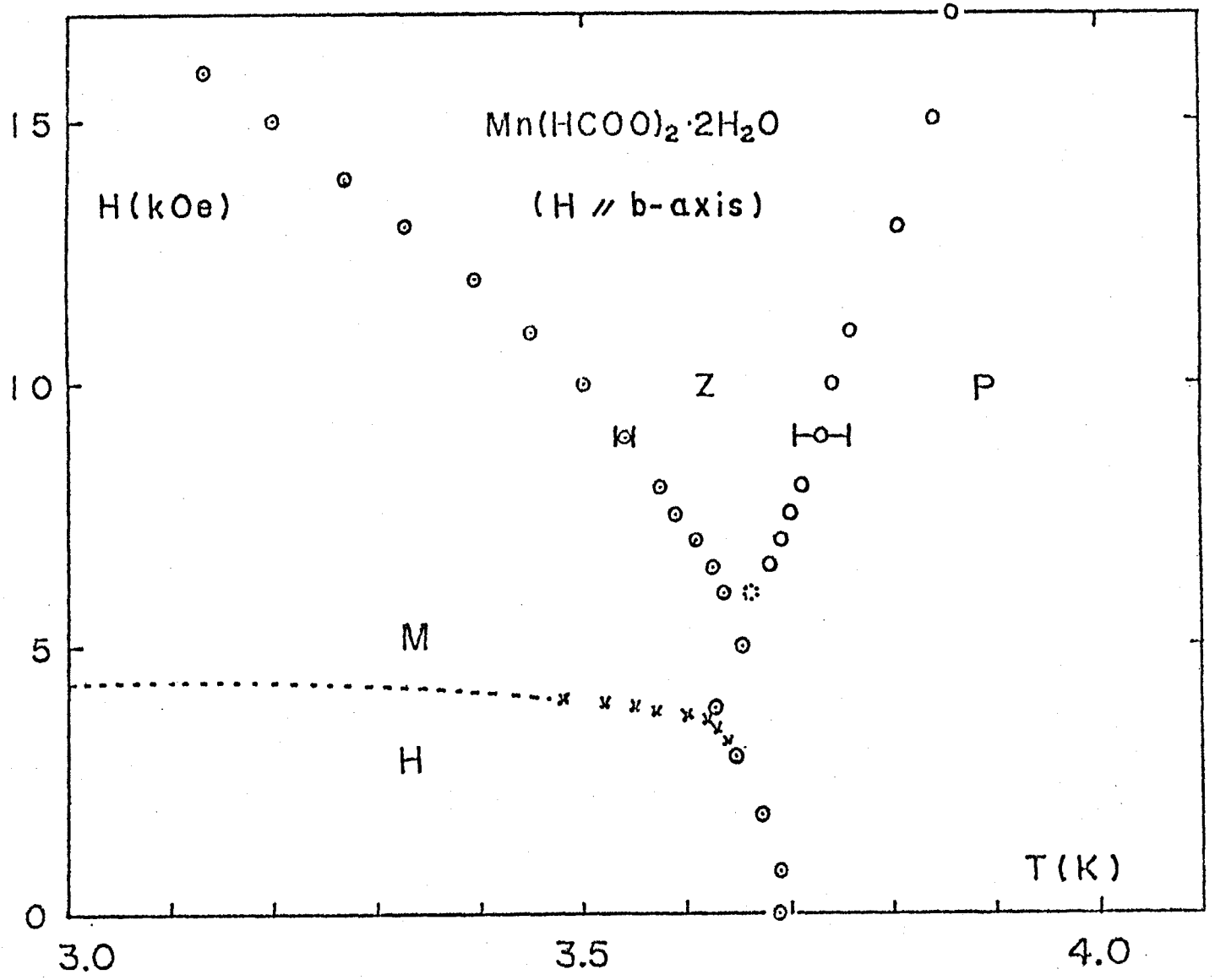

Fig.IV.A-7. T-H phase diagram of the 2d A-planes for the b-axis.

Fig.IV.A-8 (at H = 25 kOe; T = 1.51 K). This boundary coincides with that determined from the independent measurement of susceptibility.[13] The phase transition which crosses this boundary may be of the first kind judging from the sharp heat capacity peak like a delta-function.

Turning back to Fig.IV.A-5, we note that another broad shoulder begins to grow on the higher temperature side of the heat capacity peak for the field higher than 6.0 kOe. This broad maximum shifts to the higher temperatures, separating from the sharp peak, with increasing field. When H = 20 kOe, this comes up around 3.95 K with its cusp-like shape as in Fig.IV.A-2. For H > 40 kOe, this heat capacity maximum turns to shift to lower temperatures as in Fig.IV.A-9. We can observe also the corresponding shift of the broad maximum in the susceptibility measurements as in Fig.IV.A-10. The trace of these maximum points describes a phase boundary curve between P and Z phases in Figs.IV.A-6 and 7. This boundary can be detected by the susceptibility measurement in the process of field sweep at a constant temperature as in Fig.IV.A-8 (at H = 100 $\pm$ 5 kOe; T = 0.59 K). The constant susceptibility for H $\leq$ 95 kOe in Fig.IV.A-8 seems to correspond to the perpendicular susceptibility. For H > 100 kOe, the susceptibility falls down due to the paramagnetic saturation. The phase boundary curve obtained just above may correspond to the phase transition of the second kind. From the graphical estimation in Fig.IV.A-6, we expect the critical field at T = 0 K to be $H_c^{//}$ = 105 $\pm$ 5 kOe.

In the same way as mentioned above, we can get the phase boundary for the field applied along the hard (a*-)axis. Figure IV.A-11

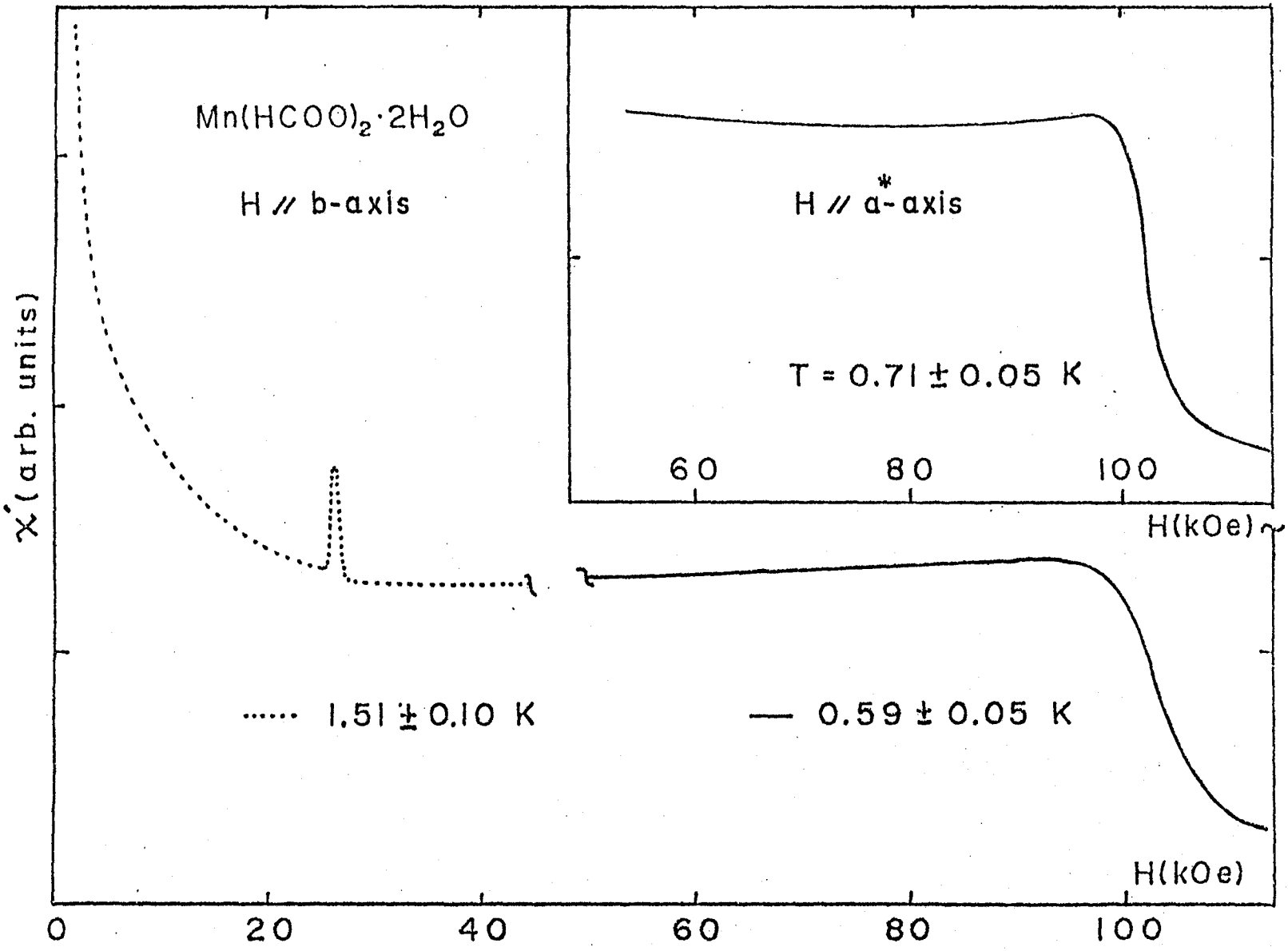

Fig.IV.A-8. Magnetic susceptibility at constant temperatures (H-sweep).

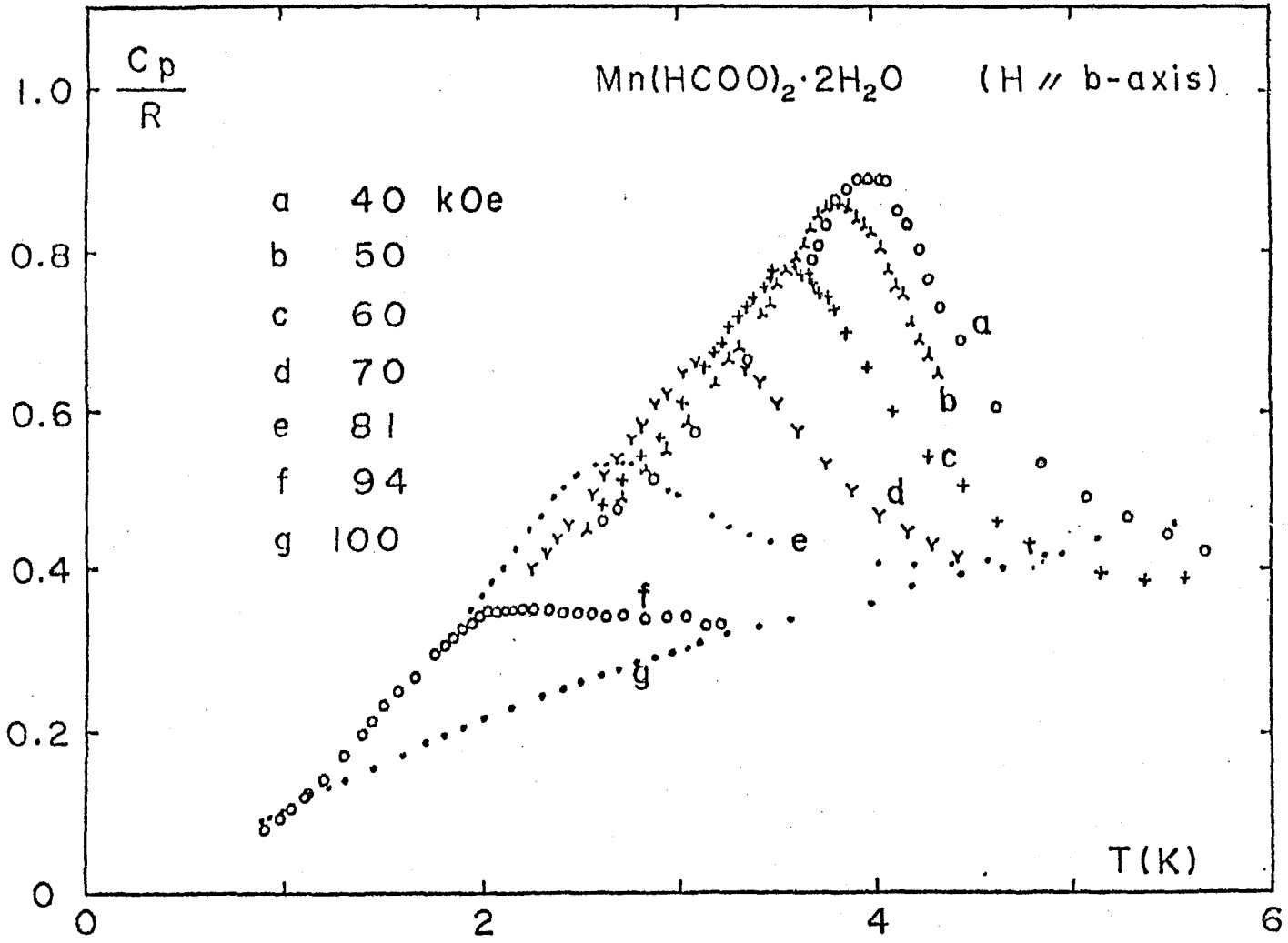

Fig.IV.A-9. Heat capacity of $Mn(HCOO)_2 \cdot 2H_2O$ in the field applied along the b-axis.

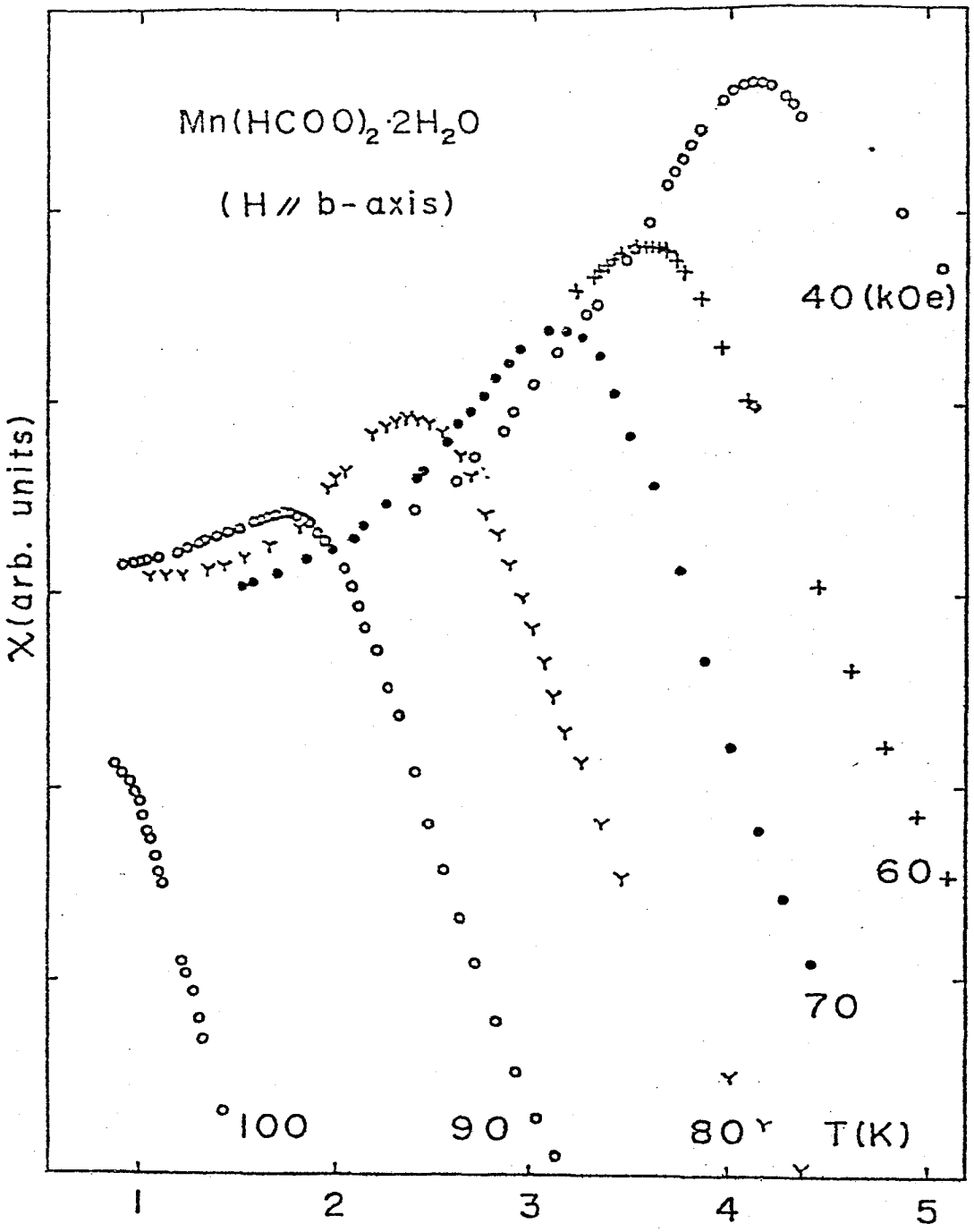

Fig.IV.A-10. Magnetic susceptibility in constant fields applied along the b-axis (T-sweep).

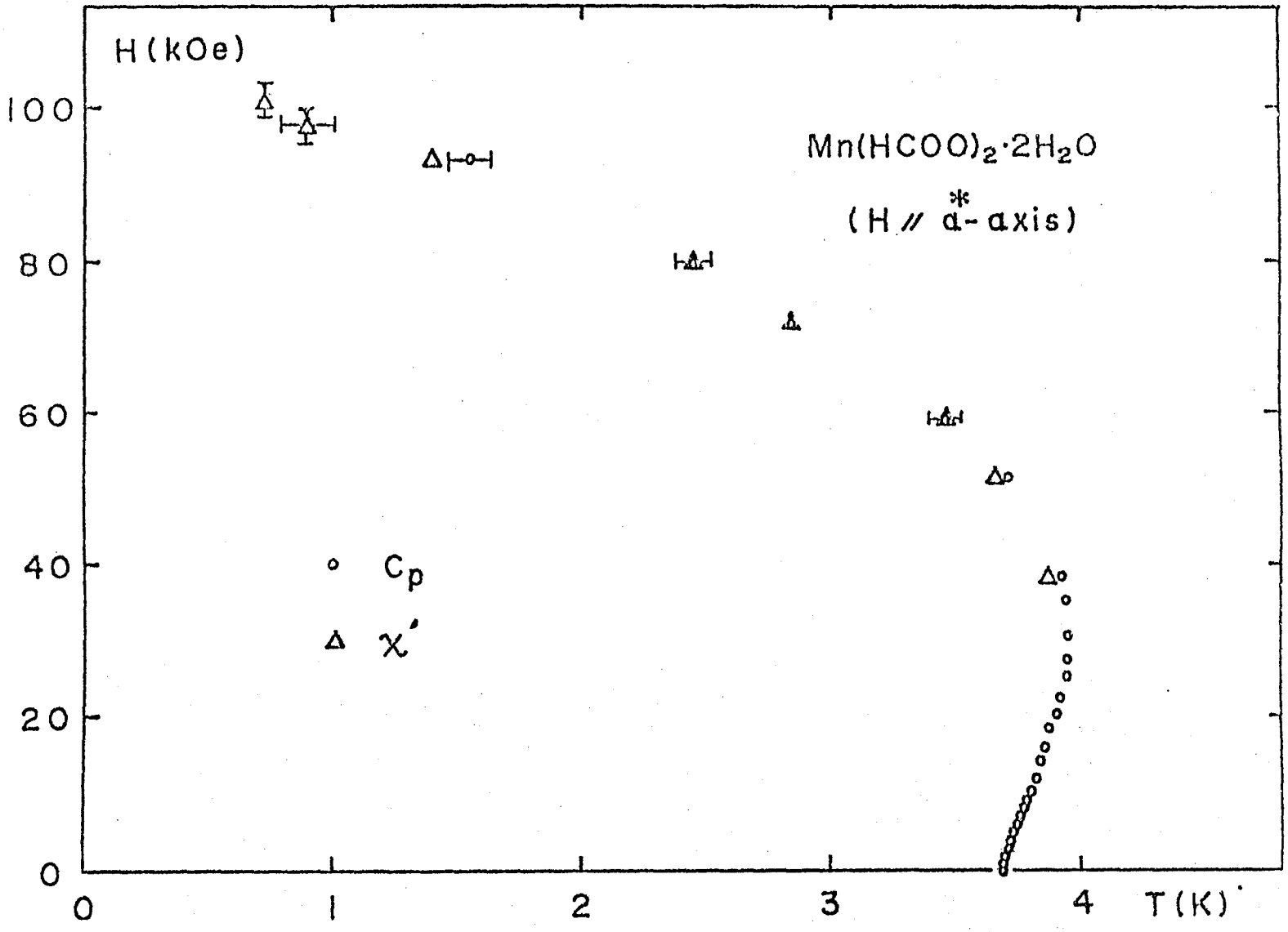

Fig.IV.A-11. T-H phase diagram of the 2d A-planes for the spin hard (a*-)axis.

shows the overall phase boundary determined by the measurements of heat capacity (Fig.IV.A-12 and 13), and susceptibility (Fig.IV.A-14: T-sweep, and Fig.IV.A-8: H-sweep). There is only one boundary in this case, as it should be for H// hard axis of the usual antiferromagnet. It is a remarkable feature that $T_N(H)$ goes up with increasing field up to 35 kOe ($T_N(H) = 1.10 \cdot T_N(0)$). From the graphical estimation in Fig.IV.A-11, we expect the critical field at T = 0 K to be $H_c^{\perp} = 105 \pm 5$ kOe.

IV.A-2.3 Evaluation of the intra-layer exchange constant

Here we estimate the magnitude of intra-layer exchange constant $|J|$ from the evaluated critical field $H_c^{//}$ and $H_c^{\perp}$. Assuming a two-sublattice antiferromagnet with anisotropy energy K (defined in unit volume),* the critical field can be derived in the molecular field approximation to be

$$H_c^{//} = 2\lambda M - \frac{K}{M} , \qquad (4.5)$$

$$H_c^{\perp} = 2\lambda M + \frac{K}{M} , \qquad (4.6)$$

respectively, with

$$\lambda = 4z|J|/N_A(g\mu_B)^2 ,$$

$$M = (N_A/2) \cdot g\mu_B S ,$$

*) This assumption may not be proper for the description of the phase boundary for the lower fields. The most dominant value $|J|$, however, can be evaluated regardless of the small anisotropy or the canting interaction which mainly work for describing the phase boundaries in much lower field $H \ll H_c^{//}$ or $H_c^{\perp}$.

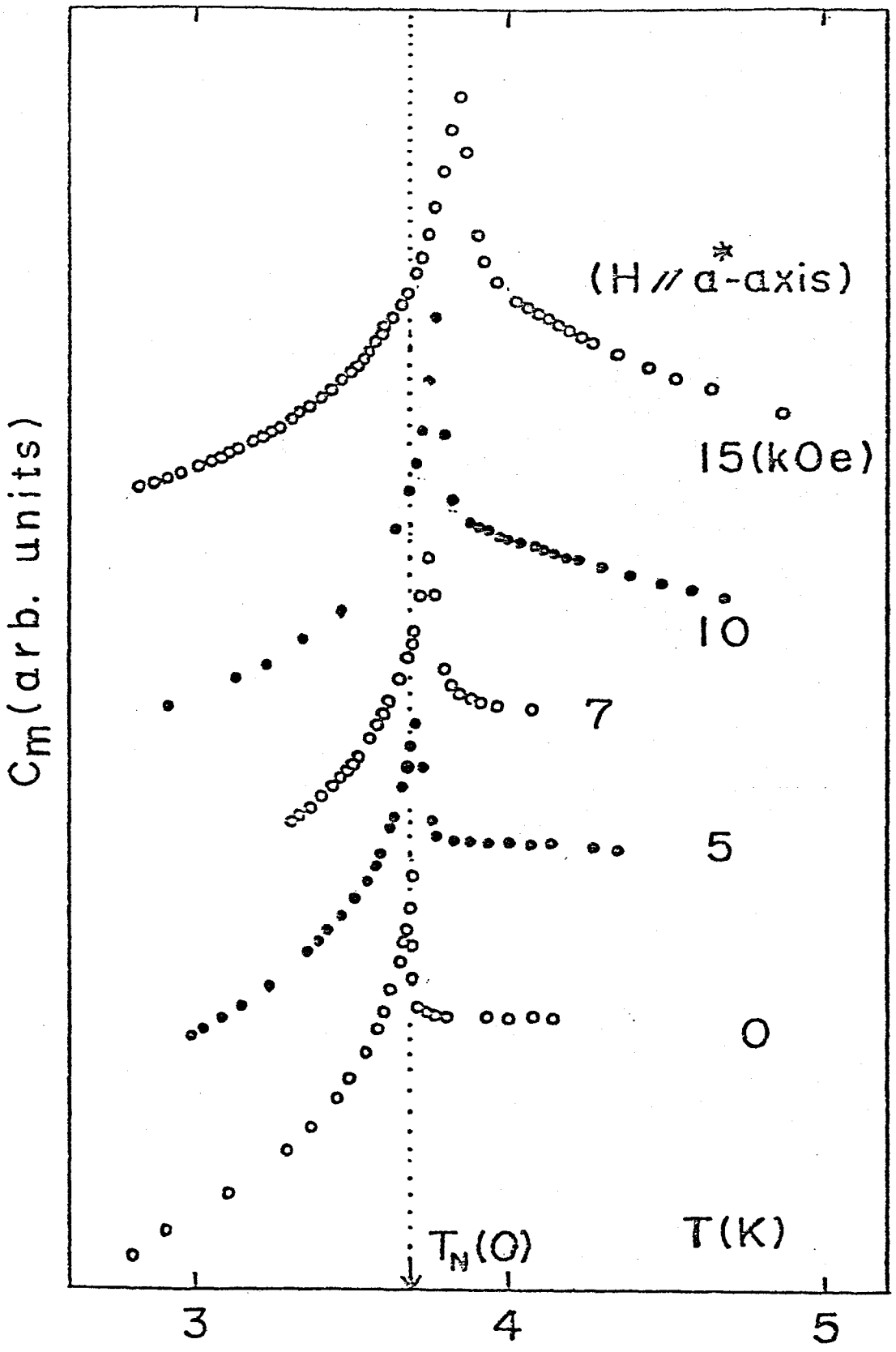

Fig.IV.A-12. Variation of the heat capacity near $T_N(H)$ in the field applied along the a*-axis.

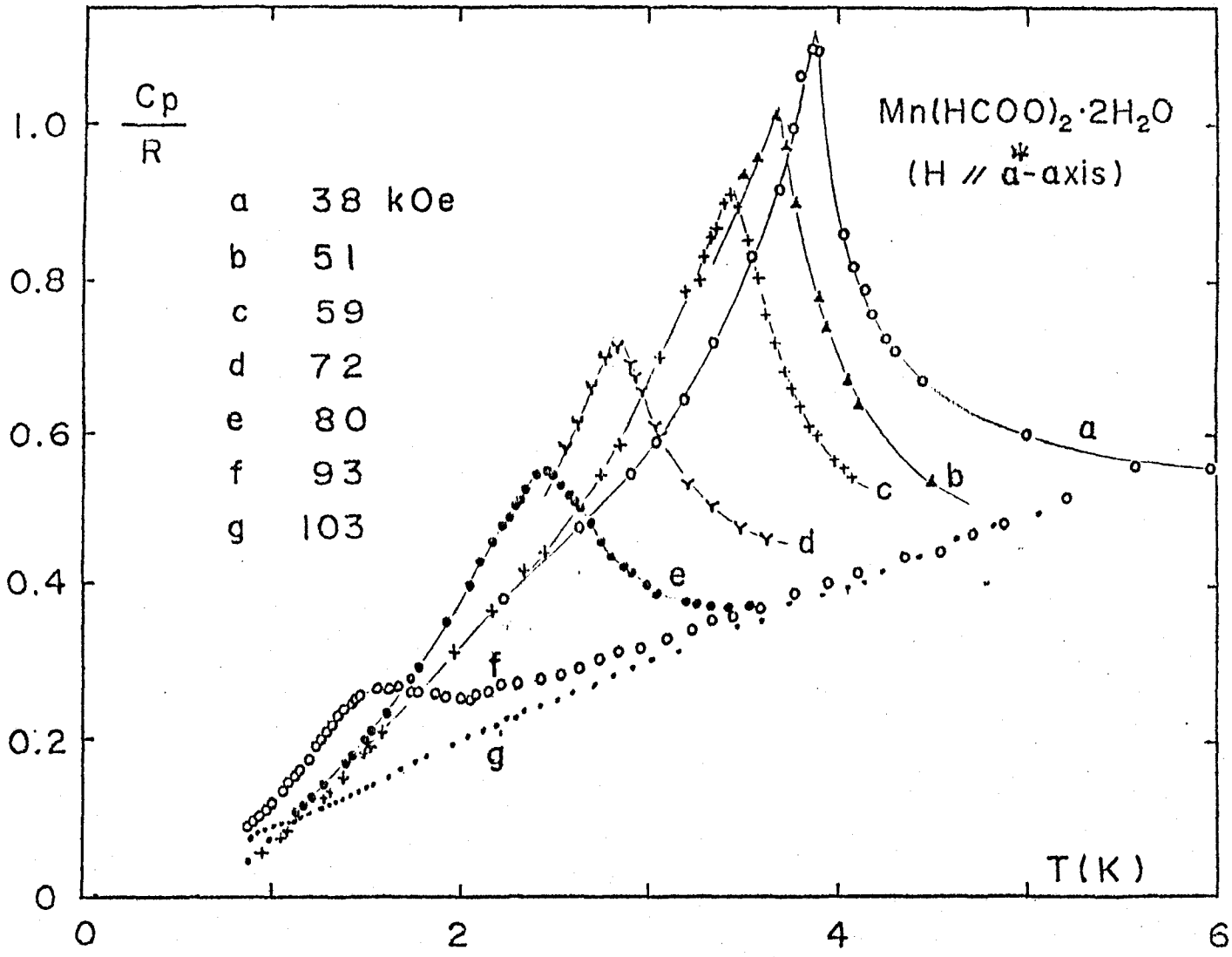

Fig.IV.A-13. Heat capacity of $Mn(HCOO)_2 \cdot 2H_2O$ in the field applied along the a*-axis.

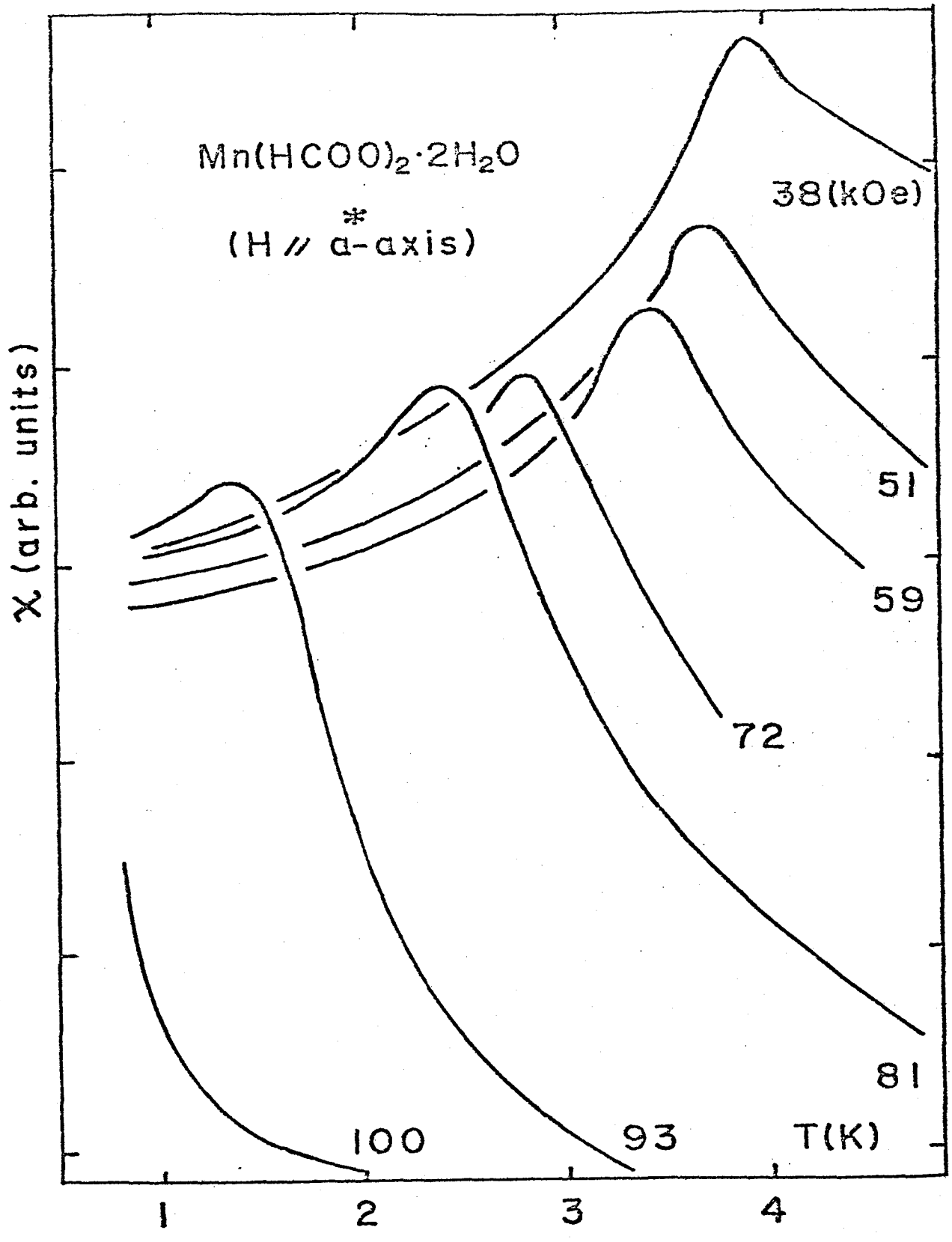

Fig.IV.A-14. Magnetic susceptibility in constant fields along the a*-axis (T-sweep).

where z and N_A are the number of nearest neighbour spins and the Avogadro's number, respectively. If we put our experimental values $H_c^{//} = H_c^{\perp} = 105 \pm 5$ kOe in eqs.(4.5) and (4.6), we get

$$|J|/k_B = 0.35 \pm 0.02 \text{ (K)},$$

$$K/M < 5 \text{ (kOe)}.$$

The estimated value $|J|$ is in good agreement with that determined from other experiments.[9,10,11)]

§IV.A-3. Experimental results of proton NMR and analysis

IV.A-3.1 Temperature dependence across the various phases

When the external field of 10 kOe is applied along the spin easy (b-)axis, it is known from Fig.IV.A-7 that the phase transitions between para state (P) and Z phase and between Z and M phase should occur. The temperature dependence of the proton NMR line shift of MnF2D under this field is shown in Fig.IV.A-15. The transition temperatures between P and Z and between Z and M determined by the results of heat capacity are also indicated in the same figure. The line shift by the uniform moment of paramagnetic B ions are calculated using Brillouin function and shown in Fig.IV.A-15 by the dotted line. It is understood to saturate towards T = 0 K unlike Curie's law dependence (CH/T), where C, H and T are the Curie's constant, magnetic field and temperature, respectively. The line shift caused by the induced staggered moment appeares even above the transition temperature from para state to Z phase. The maximum point of temperature change rate of line shift corresponds to the broad peak of heat capacity. The jump point of line shift is the transition temperature from Z to M phase and corresponds to

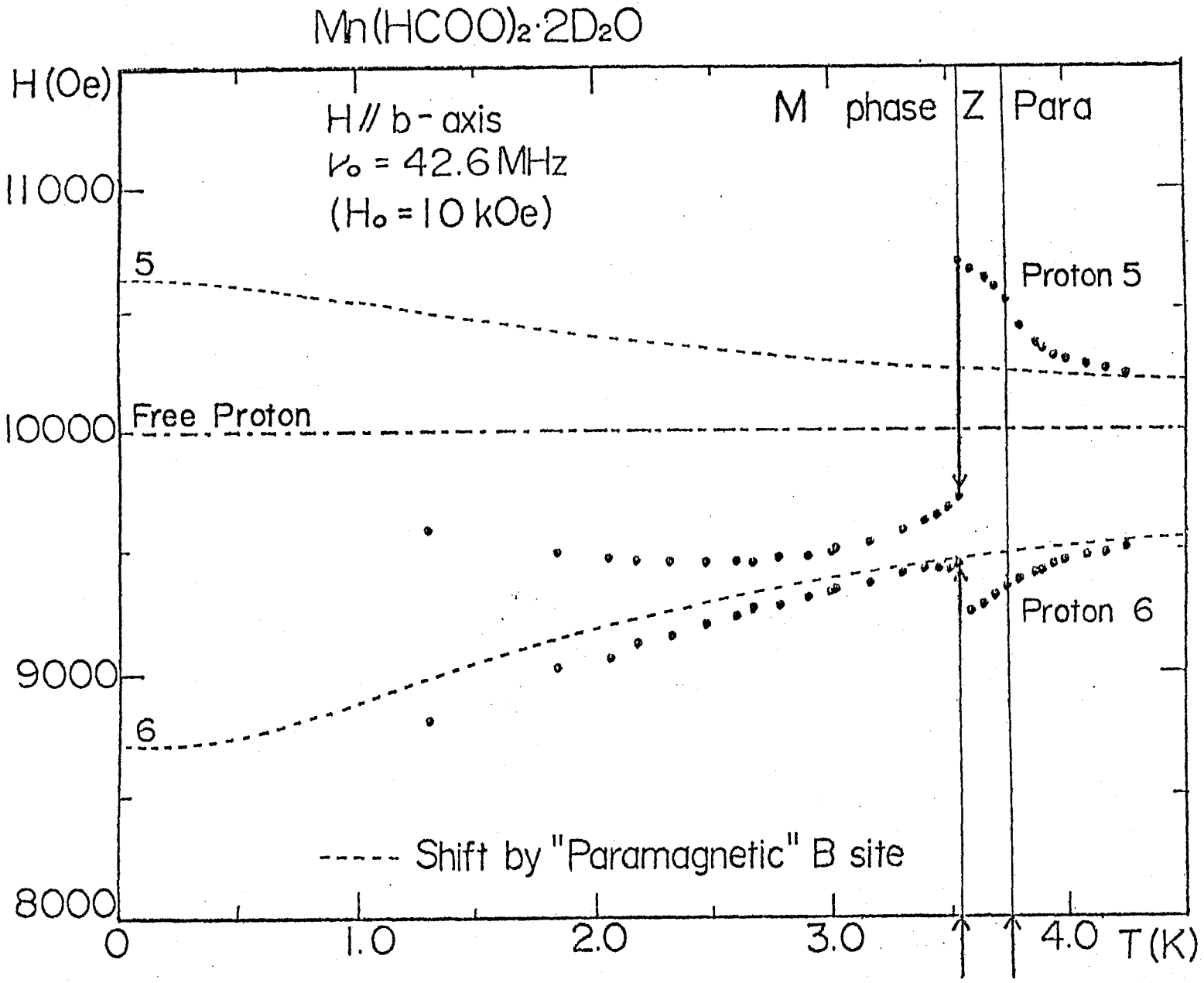

Fig.IV.A-15. Temperature dependence of the proton NMR line shift under the field of 10 kOe along the b-axis.

the sharp peak of heat capacity. The proton lines do not split in both Z and M phases, which indicates that antiferromagnetic axes in both phases are perpendicular to the external field (//b-axis) from the consideration of symmetry. When the external field of 5 kOe is applied along b-axis, the phase transition only between para state and M phase occurs, and the result is shown in Fig.IV.A-16. The line shift caused by the staggered moment begins to appear below the transition temperature, which corresponds to the sharp peak of heat capacity. When the external field of 1 kOe is applied along b-axis the phase transition between para phase and H phase occurs, and the result is shown in Fig.IV.A-17. The line shift by the staggered moment appears below $T_N(H)$. It is shown that antiferromagnetic axis in H phase is parallel to the b-axis from the doublet splitting of proton NMR line, and consistent with the result from other experiments.[14)]

To sum up, antiferromagnetic axes in Z and M phases are perpendicular to the external field which is applied along the b-axis and that in H phase is parallel. Spin structure changes continuously with temperature between paramagnetic phase and Z phase. While, between Z and M phases or H and M phases, spin structure change suddenly, which suggest the first order phase transition.

IV.A-3.2 Angular dependence pattern in Z and M & H phases

The angular dependence patterns in a*b-plane were observed for several temperatures. The pattern at T = 3.6 K under the field of 10 kOe is shown in Fig.IV.A-18. It is found from the phase boundary (e.g. Fig.IV.A-6 and 7) that Z phase is recognized at this

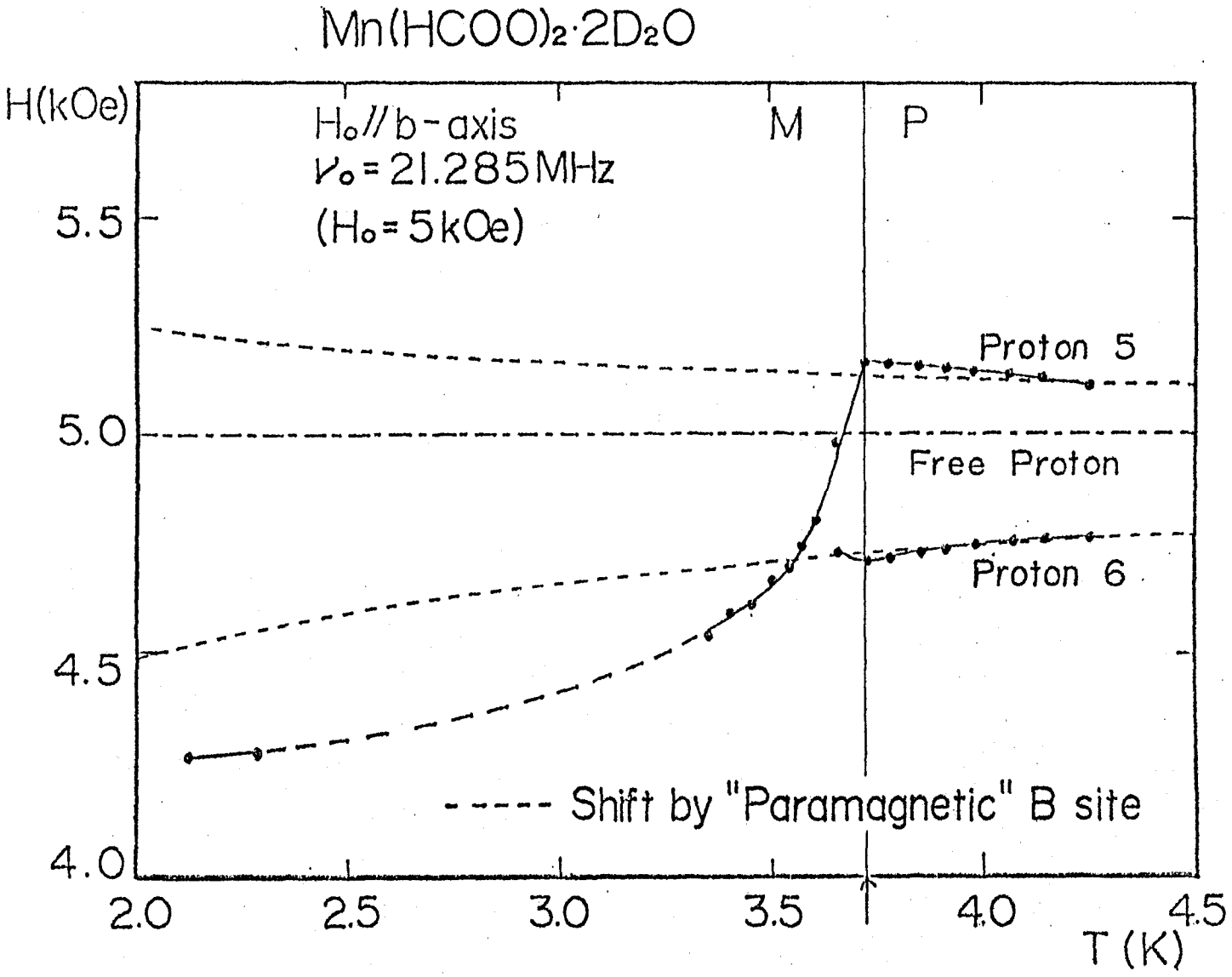

Fig.IV.A-16. Temperature dependence of the proton NMR line shift under the field of 5 kOe along the b-axis.

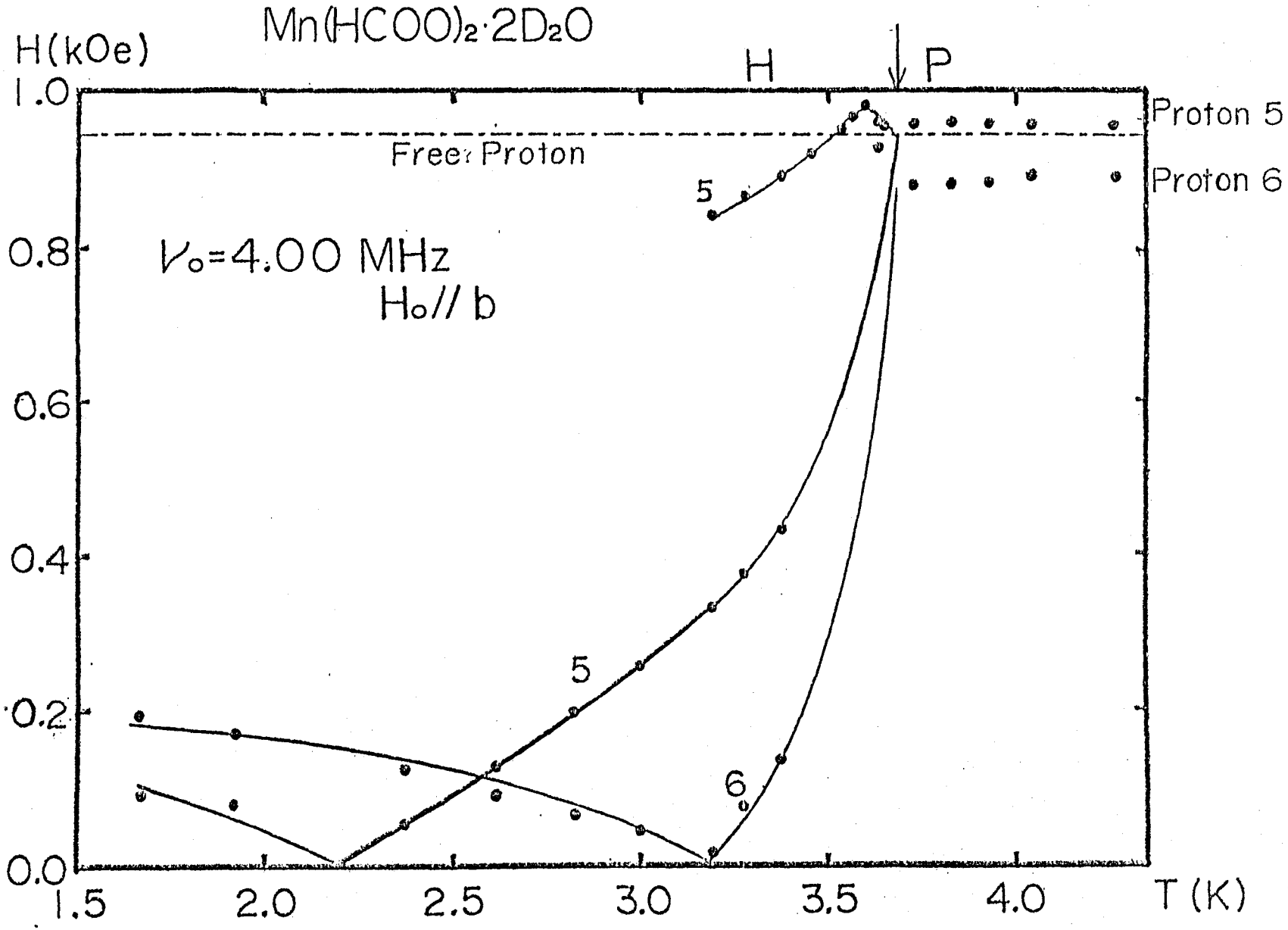

Fig.IV.A-17. Temperature dependence of the proton NMR line shift under the field of 1 kOe along the b-axis.

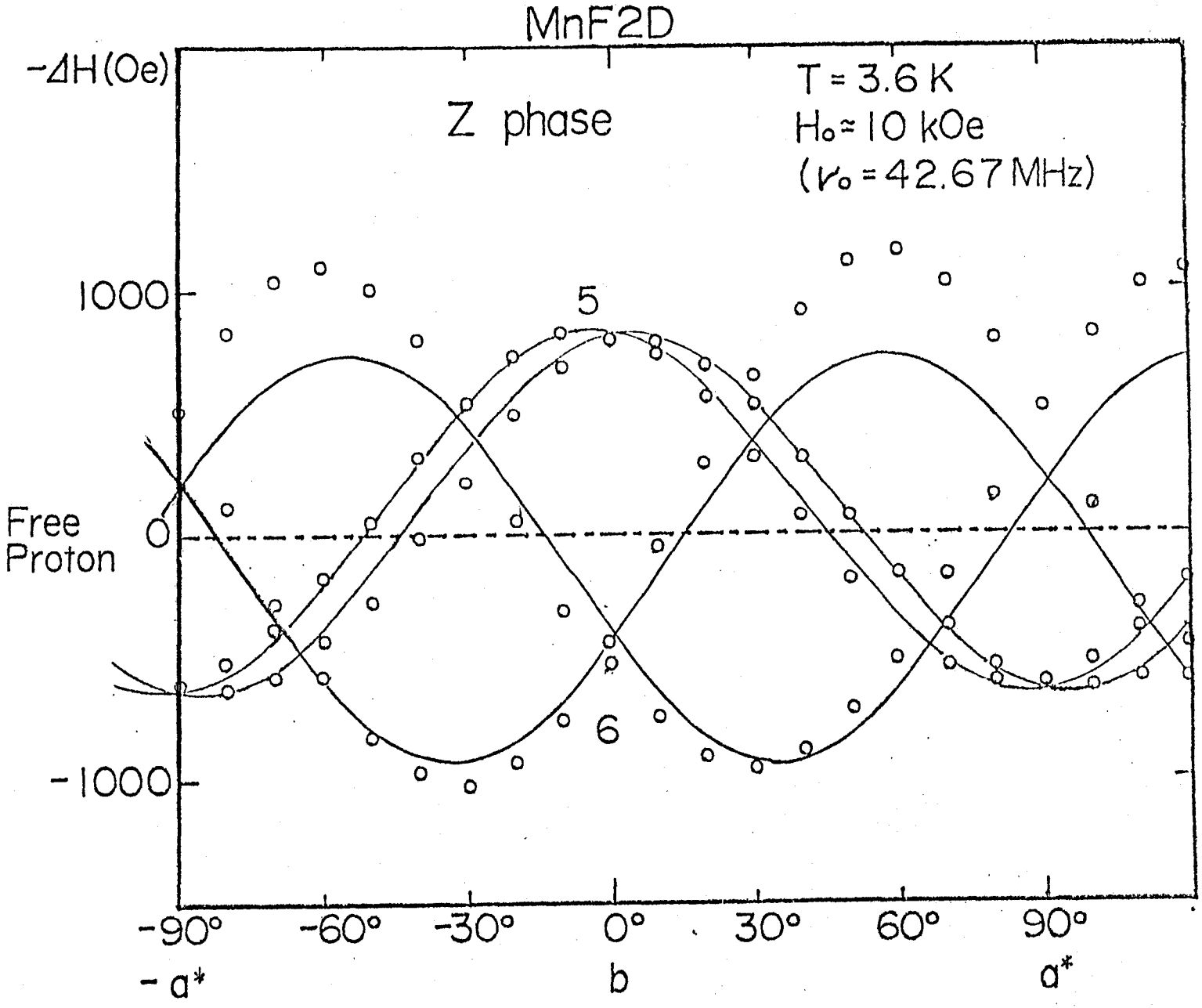

Fig.IV.A-18. Angular dependence pattern at T = 3.6 K under the field of 10 kOe.

temperature and field for at least b-axis. This pattern is 180° periodic and continuous without jump. Therefore it is considered that Z phase is recognized also for a*-axis. Solid line is the calculated shift as that staggered moment parallel to the a*-axis is induced by the b-axis component of external field. Line shift by the paramagnetic B ions is of corse contained. Staggered susceptibility χ_s^{ef} is selected 3.5×10^{-24} emu/ion as the parameter. The calculation curve is roughly agreement with the experimental result (open circles). Especially near the b-axis there is hardly descrepancy between them.

The pattern at T = 1.4 K under the field of 10 kOe is shown in Fig.IV.A-19. It is found from the phase boundary (e.g. Fig.IV. A-6, 7 and 9) that M phase is recognized for the b-axis and H phase for the a*-axis at this temperature and field. There is a jump of shift near 70° from the b- to the a*-axis which is caused by the phase change. Considering that the staggered moment of A subsystem effects the line shift of proton No.5 more than that of No.6 at H // b-axis, it is understood qualitatively that the antiferromagnetic axis in M phase is almost opposite to that in Z phase. As the result of calculations, the antiferromagnetic axis in M phase changes gradually as the change of direction of the external field in b-a* plane. Similar circumstance is realized also in H phase.

IV.A-3.3 Field dependence of the direction of antiferromagnetic axis in M phase

It is considered from the analysis in IV.A-3.2 that the antiferromagnetic axis changes continuously by the field and temperature

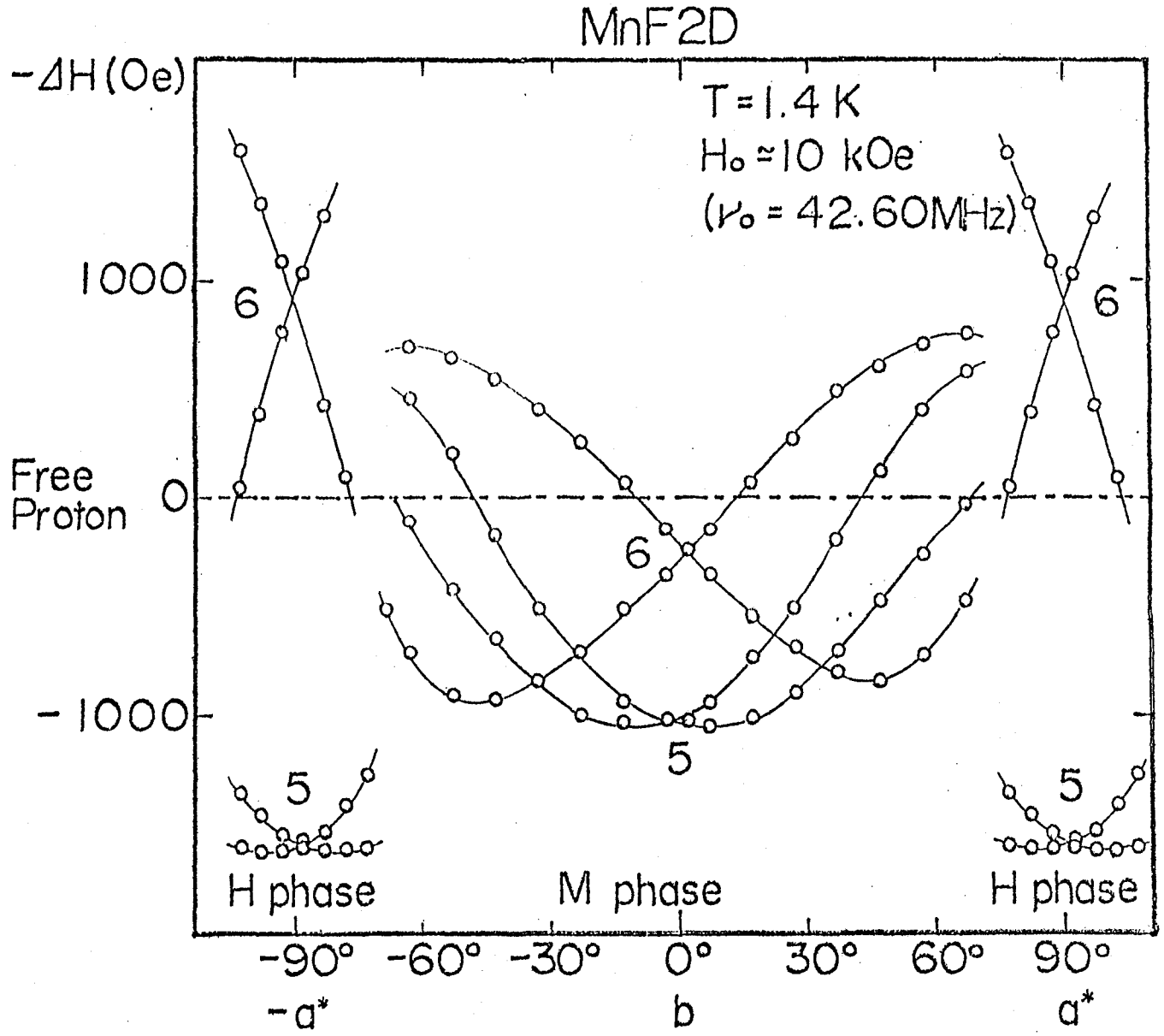

Fig.IV.A-19. Angular dependence pattern at T = 1.4 K under the field of 10 kOe.

in M phase. The frequency dependence of resonance fields at 1.4 K under the field applied along b-axis is shown in Fig.IV:A-20. Solid line corresponds to the shift of free proton, and dotted lines to the shift of proton No.5 and No.6 by the paramagnetic B ions. The discrepancy between experimental result and dotted lines is considered by the staggered moment of A subsystem. The magnitude and direction of antiferromagnetic moment L_A of A subsystem, which is calculated as the best fit, is shown in Fig.IV.A-21. The magnitude decreases gradually and the direction of antiferromagnetic moment rotates from d-axis (which inclines 30° to a*-axis from c-axis) towards a*-axis with increasing field. The direction of antiferromagnetic moment in M phase(-a*-axis) is opposite to that in Z phase (+a*-axis). The mechanism of M-Z phase transition is discussed in next section.

§IV.A-4. Mechanism of M-Z phase transition

The origin of M-Z phase transition which is like a reversal of antiferromagnetic axis is certainly the existence of "paramagnetic" B ions. Whether M or Z phase is realized is determined by the rivalry of Dzyaroshinsky-Moriya (D-M) interaction in A site and Zeeman energy which contains the staggered field in A site by the canting of B site ions.

We consider D-M interaction $-2z\vec{d}\cdot(\vec{S}_{A1} \times \vec{S}_{A2})$ as well as exchange interaction $2z|J_{AA}|\vec{S}_{A1}\cdot\vec{S}_{A2}$ and Zeeman energy. As the field in this Zeeman energy, it should be considered besides the external field itself the exchange field at A site which is caused by the saturated B site through the exchange interaction between A and B site (J_{AB}).

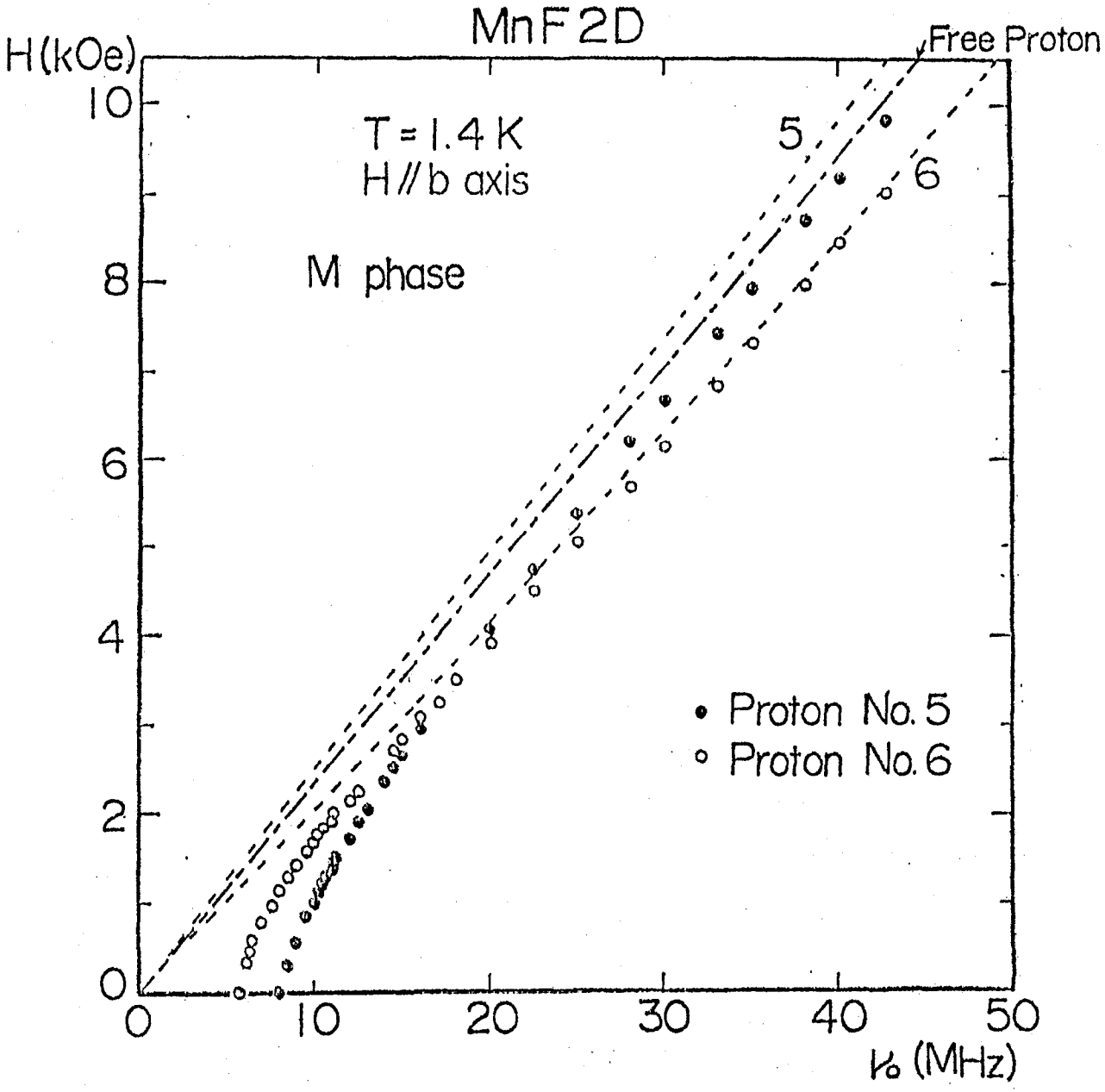

Fig.IV.A-20. Field dependence of resonance fields at 1.4 K under the field applied along the b-axis.

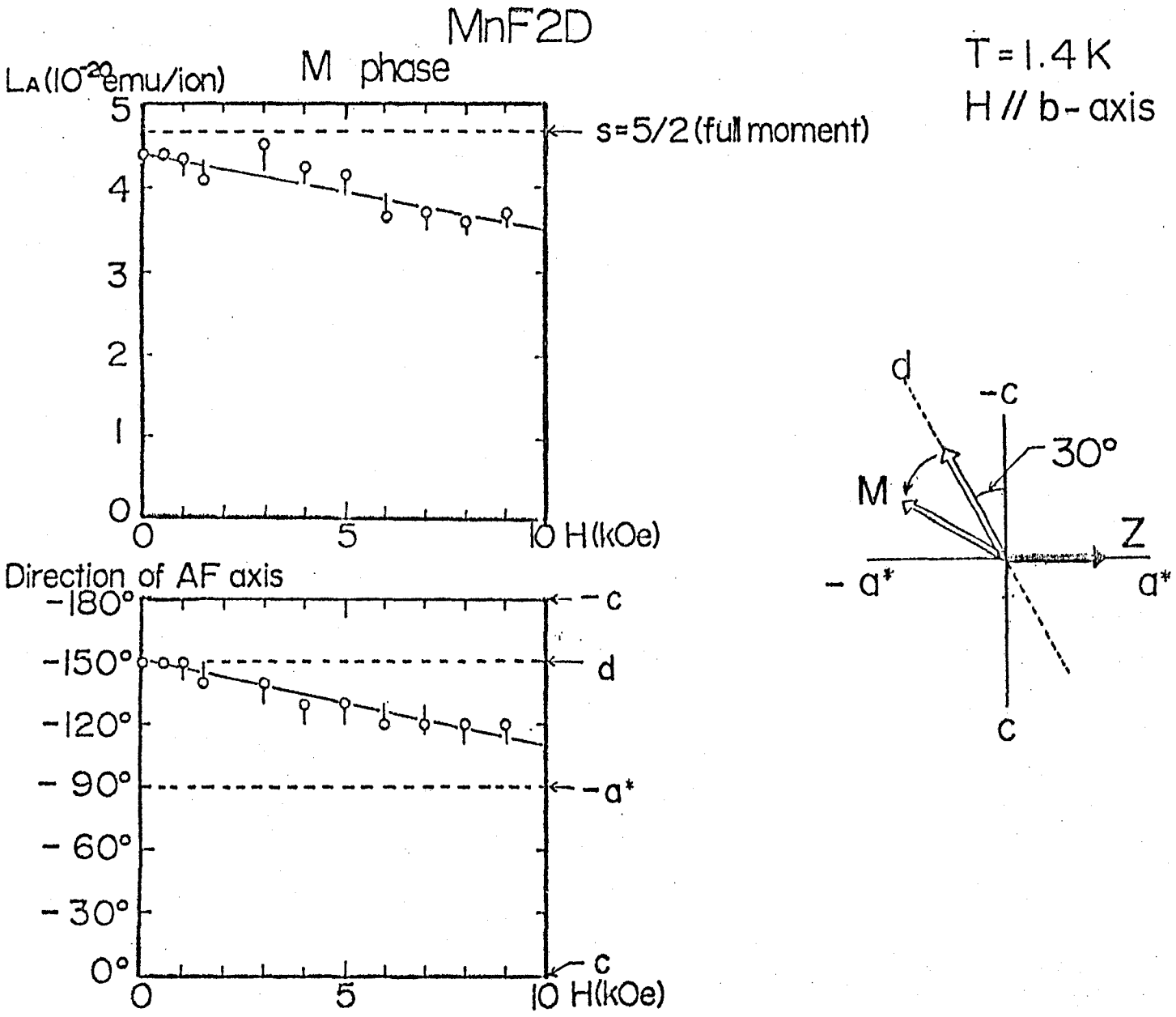

Fig.IV.A-21. Field dependence of the magnitude and the direction of antiferromagnetic moment L of A-subsystem under the field applied along the b-axis.

B site is "paramagnetic" and turns to the external field above 1.4 kOe (exchange field between A and B site) but should slightly cants because of the inequivalency of $\tilde{g}$ tensor. Accordingly the exchange field at A site acted by B site has staggered component which is perpendicular to the external field. It is sure that the direction of antiferromagnetic axis in M phase turns into -a*-axis in the vicinity of M-Z phase transition field. Schema is shown in Fig. IV.A-22, where $H_A^{//}$ is the parallel component of exchange field H_A which acts to A site from B site and opposite to the external field, and $H_A^{\perp}$ is the perpendicular component and the staggered field. We assume that B_1 moment inclines to a*-axis. Owing to this staggered component of H_A, the moment of A_1 site is possible to turn to -a* direction. In the lower external field, the canting of A site is opposite to the external field because the D-M interaction is most effective, assuming that $\vec{d}$ vector is along near c-axis. (cf. Fig.IV.A-22(a)). With increasing field Zeeman energy of external field becomes larger than D-M interaction energy, and the direction of canting changes towards the external field (cf. Fig. IV.A-22(b)). This change occurs continuously with the field. With more increasing field, the gain of Zeeman energy of the external field and D-M interaction becomes larger than that of Zeeman energy of the staggered field caused by B site. As the result A_1 and A_2 site changes each other suddenly (cf. Fig.IV.A-22(c)). This is the mechanism of phase transition from M to Z phase. If we assume that the D-M interaction is one handredth of intra-layer exchange interaction and the canting angle of B site caused by the inequivalency of $\tilde{g}$ tensor is 4°, we get the M-Z transition field as 20 kOe, which

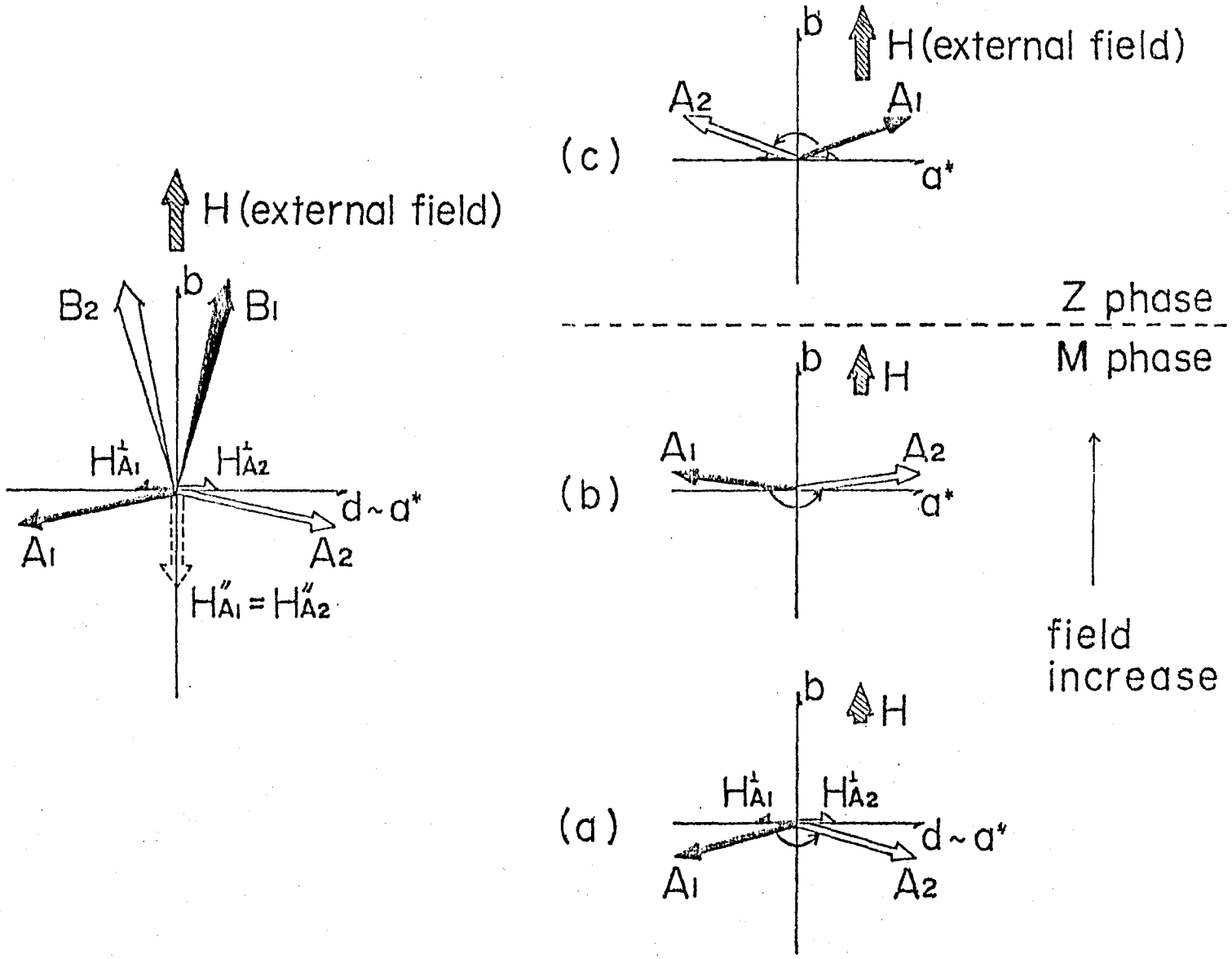

Fig.IV.A-22. Schematic illustration of the phase transition between M and Z phases.

agrees with the experimental result.

IV.B. Two-dimensional XY behaviours induced by the magnetic field

§IV.B-1. Introduction

Since the theoretical prediction of a possibility of field induced crossover of spin symmetry in low-dimensional antiferromagnets,[1,15] several experimental and theoretical investigations have been carried out for real quasi-one-dimensional (1d) systems.[2-4] We will extend the study on this spin symmetry crossover to a two-dimensional (2d) system in this chapter, by making use of experimental results on $Mn(HCOO)_2 \cdot 2H_2O$[16] in Chap.IV.A.

A phenomenological explanation of this crossover may be given as follows. We originally consider a nearly isotropic Heisenberg (or XY) antiferromagnet with the Hamiltonian such as

$$\mathcal{H} = -2J\sum_{ij} \underline{S}_i \underline{S}_j - g\mu_B H \sum_i S_i^z - \mathcal{H}_k, \qquad (4.7)$$

where J is the exchange constant between the nearest neighbour spins S_i and S_j, g is the g-factor of the spin, H is the external field applied along the z-axis, and $\mathcal{H}_k$ stands for the small anisotropic term which may be assumed here $\mathcal{H}_k = K\sum_i (S_i^z)^2$ for instance ($0 < K \ll |J|$). For an appropriate field H ($\ll |J|/g\mu_B$), a spin-flopped state is realized and the free energy of the system will decrease as $-\chi_\perp H^2/2$, where $\chi_\perp$ is the perpendicular susceptibility. In such a state, the spins are almost on the XY plane. At the limit $K \to 0$, the application of an infinitesimally small H will lead the system to the spin-flopped state. Under the circumstances, the thermal average of the z-components of the spin $\langle S_i^z \rangle$ and hence $\langle S_i^z S_j^z \rangle$ become much

smaller than those of the transverse components such as $\langle S_i^x \rangle$ and $\langle S_i^x S_j^x \rangle$; $\langle S_i^z \rangle / \langle S_i^\alpha \rangle \to 0$ and $\langle S_i^z S_j^z \rangle / \langle S_i^\alpha S_j^\alpha \rangle \to 0$ ($\alpha = x, y$). Therefore, the Hamiltonian (4.7) may be reduced effectively to an XY system at low temperatures.[1)]

The increase of $T_N(H)$ has been studied experimentally and theoretically in quasi-1d compounds.[2-4)] These results are phenomenologically explained as follows. In quasi-1d systems, the 3d transition temperature T_N is related with the spin correlation length ${}^n\xi_{1d}(T)$ along the chain as,

$$k_B T_N \simeq C_n S^2 |J'| \cdot {}^n\xi_{1d}(T_N), \tag{4.8}$$

where C_n is a coefficient which depends on the spin dimensionality n and on the lattice, and J' is the inter-chain interaction.[1)] The spin symmetry crossover mentioned above acconpanies an elongation of ${}^n\xi_{1d}(T)$, which is known to be ${}^3\xi_{1d}(T) < {}^2\xi_{1d}(T) < {}^1\xi_{1d}(T)$ for a given value of $k_B T/|J|$ ($\ll 1$), where J is the intra-chain exchange constant (n = 3, 2 and 1 correspond to the Heisenberg, XY and Ising systems, respectively). This implies the crossover from the Heisenberg (or XY) to the XY (or Ising) systems brings about the enhancement of $T_N(H)$ as can be expected by eq.(4.8).

The next three conditions are necessary for inducing the spin symmetry crossover; isotropic exchange interactions, small anisotropy energy (K) in the crystal ($|K/J| \ll 1$), and high degree of discrete dimensionality ($|J'/J| \ll 1$, where J' and J are inter- and intra= chain (or layer) interactions, respectively.).

In real 2d compounds, there has not been any experimental evidence of the spin symmetry crossover except our experimental

results on a 2d isotropic Heisenberg antiferromagnet MnF2H[16] in Chap.IV.A. Two experimental facts have been found there, which might be attributed to the field induced crossover of the spin symmetry: One is the anomalous increase of the Néel temperature $T_N(H)$ and the other is the remarkable variation of the magnetic heat capacity in the field. The aim of this chapter is to give physical explanations to those experimental facts and to reveal the 2d XY behaviours induced by the application of external field. The discussion of the crossover phenomena in a 2d system will be given for the first time in §IV.B-2 and §IV.B-3, concerning with $T_N(H)$ of MnF2H and its magnetic heat capacity, respectively. Especially in §IV.B-3, the absolute values of the heat capacity of this field induced 2d XY system will be compared with the theoretical prediction for the plane rotator model to extract a 2d XY behaviour including the critical temperature region.[17,18]

§IV.B-2. Field-induced increase of the Néel temperature $T_N(H)$ in the 2d antiferromagnet MnF2H

In the usual antiferromagnets, it is usual that the Néel temperature $T_N(H)$ decreases with increasing field H. Generally $T_N(H)$ is expressed as

$$T_N(H) = T_N(0)\{1 - a(H/H_c)^2\}^b, \qquad (4.9)$$

where a and b are the constants which depend on models assumed, and H_c is the critical field defined as $H_c = 4z|J|/g\mu_B$ (z; number of the nearest neighbour spins).[17] In the low-dimensional systems, however, this is not always the case and $T_N(H)$ can be enhanced as

has been discussed in §IV.B-1. Nevertheless, the increase of $T_N(H)$ in a "2d" antiferromagnet has not been reported except our recent work on MnF2H[16] (See Chap.IV.A). In this section, we will give a qualitative explanation to this newly observed increase of $T_N(H)$.

The Mn^{2+} spins in the 2d magnetic system in MnF2H are supposed to be quite isotropic from the ESR experiment; the ratio of the longitudinal component of the g-factor to the transverse one is estimated $g_{//}/g_{\perp} \leq 1.005$.[18] The anisotropy field in the crystal is much less than the critical field $H_c = 105$ kOe.[16] Moreover, the two-dimensionality of the system is of the order of $|J'/J| \approx 10^{-3}$.[11] These properties may satisfy the conditions for inducing the spin symmetry crossover as mentioned in §IV.B-1.

T-H phase diagrams for this 2d system in MnF2H determined from the measurements of heat capacity (C_p) and susceptibility (χ') are already shown in Fig.IV.A-6,7 and 11. The field is applied to the a*-(spin hard) axis and to the b-(spin easy) axis(Fig.IV.A-4). It should be remarked that, with increasing field along the a*-axis, $T_N(H)$ initially increases and reaches $T_N(H) = 1.10T_N(0)$ around H = 35 kOe. Then it turns to decrease down to T = 0 K at the estimated critical field $H_c = 105$ kOe. When the field is increased along the b-axis, $T_N(H)$ shifts down to the critical point at ($T_b = 3.62$ K, $H_b = 3.8$ kOe) just as a usual antiferromagnet to whose easy axis the field H is applied. However, once the value of H crosses over H_b and the spins are flopped from the b-axis onto the a*-c plane, $T_N(H)$ begins to increase and trace almost on the same boundary curve as that for H//a*-axis.[16] These facts imply that, in the process of increasing of $T_N(H)$, the thermal fluctuations of spins

along the field direction (z-axis) are suppressed by the field and that the spin-spin correlations are effectively changing from the Heisenberg type to the XY type by the reason mentioned in §IV.B-1. In much higher field than 35 kOe the Zeeman term $g\mu_B H\langle S_i^z\rangle$ may become non-negligible, and hence the $\langle S_i^z S_j^z\rangle$ components are resumed.

From the analogous consideration to the case of quasi-1d system, we can explain the increase of $T_N(H)$ of this quasi-2d isotropic system as follows. Assuming the susceptibility of isolated layers $\chi_{2d}(T)$ is known and $2z|J'|$ is the interaction between the weakly coupled layers, we can express the susceptibility $\chi_{3d}(T)$ of the system as,[19]

$$\chi_{3d}(T) = \frac{\chi_{2d}(T)}{1 - \chi_{2d}(T)\cdot 2z|J'|/g\mu_B} . \tag{4.10}$$

Then, the 3d-transition temperature T_N will appear when

$$\chi_{2d}^{\alpha}(T_N, H^{\beta})\cdot 2z|J'|/g\mu_B = 1, \tag{4.11}$$

just as in the case of quasi-1d systems (α; x, y, z and β; x, y, z).[2-4,15] The calculation of $\chi_{2d}^{\alpha}(T,H^{\beta})$ is difficult to carry out even for the classical isotropic system. Our present data does suggest that the behaviour of $\chi_{2d}^{\alpha}(T,H^{\beta})$ is essentially resemble to that of $\chi_{1d}^{\alpha}(T,H^{\beta})$ in respect of the field dependence. Then, the increase of $T_N(H)$ can be explained also in terms of the elongated spin correlation length $\xi_{2d}(T)$ in the isolated layer, in the analogous way to the case of quasi-1d systems.[1] This implies that the area $(\xi_{2d}(T))^2$ in which spins correlate together will be enlarged by applying the external field.

§IV.B-3. The 2d XY like behaviour reflected on the magnetic heat capacity in the field (and Discussion)

A new type of phase transition or ordered phase has been expected for the 2d XY system as well as for the 2d Heisenberg system. It is rigorously proved that there can be no spontaneous magnetization at a finite temperature for the isotropic Heisenberg and XY models.[20] The magnetic susceptibility, however, is pointed out to have a possibility to diverge at a finite temperature in these models.[21,22] The heat capacity for a 2d XY system is notoriously difficult to evaluate and is not clear up to now. The calculation based on the Monte Carlo simulation for the plane rotator model with $n \times n$ lattice sites ($n \leq 100$) is only one milestone that gives a overall aspect of magnetic heat capacity at present.[23,24]

Under the circumstances, we will focus here on the behaviour of magnetic heat capacity in the process of spin symmetry crossover from the Heisenberg to the XY type, by making use of our recent experimental results on MnF2H.[16] In zero field, the 2d magnetic system of this compound orders antiferromagnetically at T_N =3.69 K, exhibiting a small but sharp heat capacity peak as in Fig.IV.B-1. The absolute values of the magnetic heat capacity C_A can be well reproduced by the theoretical values evaluated from the high temperature series expansion (HTE) for the 2d isotropic Heisenberg system with $|J|/k_B$ = 0.34 K and S = 5/2,[25] down to the vicinity of T_N as drawn with a solid line in Fig.IV.B-1.[26] The small peak at T_N may be considered to be due to the dimensional crossover from the 2d system to the 3d system. As the external field is increased along the a*-axis, the roundness of shoulder of the heat capacity

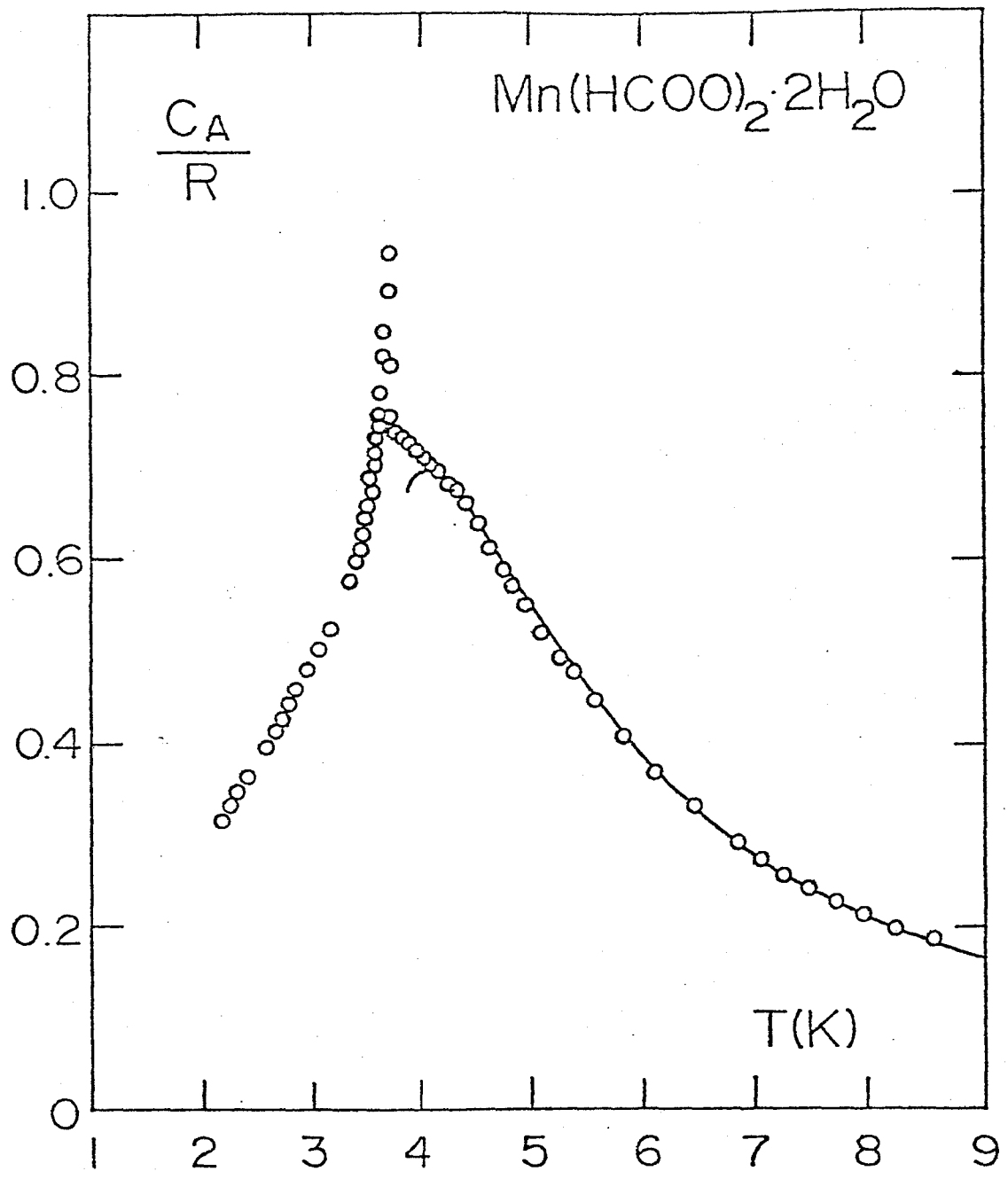

Fig.IV.B-1. Magnetic heat capacity of the 2d isotropic system in $Mn(HCOO)_2 \cdot 2H_2O$ in zero field. The solid curve is the theoretical results evaluated from the HTE method for the 2d isotropic Heisenberg system.[32)]

just above T_N begins to disappear and C_A grows to give a symmetrical behaviour, as in Fig.IV.A-12, which can not be reproduced by the HTE for the Heisenberg model any more. As has been discussed in §IV.B-2, the 2d spin system is supposed to be in an XY state when H = 20 kOe. Therefore we have tried to compare the absolute values of C_A with the theoretical results for a 2d XY (plane rotator) model just mentioned above.[23,24] The temperature axis is normalized in Fig.IV.B-2 so that the experimental heat capacity peak appears at $k_BT/J^{XY} = 1.02$, at which the theoretical results give the corresponding peak.[24] The parameter J^{XY} is taken as in

$$\mathcal{H} = -J^{XY}\Sigma \cos(\phi_i-\phi_j), \qquad (4.12)$$

where $(\phi_i-\phi_j)$ is the angle between the nearest neighbouring i-th and j-th rotators.* It is remarkable that the absolute values of C_A coincide with theoretical ones in the temperature range $k_BT/J^{XY} > 1.1$.** One of the important indication of the simulation is that the heat capacity exhibits a peak at $k_BT/J^{XY} = 1.02$.[24] In the vicinity of $k_BT/J^{XY} = 1.0$, our data exhibit a symmetrical behaviour and are apparently lager than the theoretical estimations. It should be remembered here that the 3d XY system gives a logarithmical divergence of the heat capacity at the critical point.[25] Therefore,

---

*) When H = 20 kOe, the experimental heat capacity peak appears at $T_N(H) = 3.90$ K. If we reduce $J^{XY} = 2|J|S(S+1)$ for the present system, $|J|/k_B = 0.22$ K is derived as an "effective" interaction in the field.

**) The present system is antiferromagnetic ($J < 0$). However, the results of the simulation ($J^{XY} > 0$) can be available to compare with the present data of the heat capacity.[25]

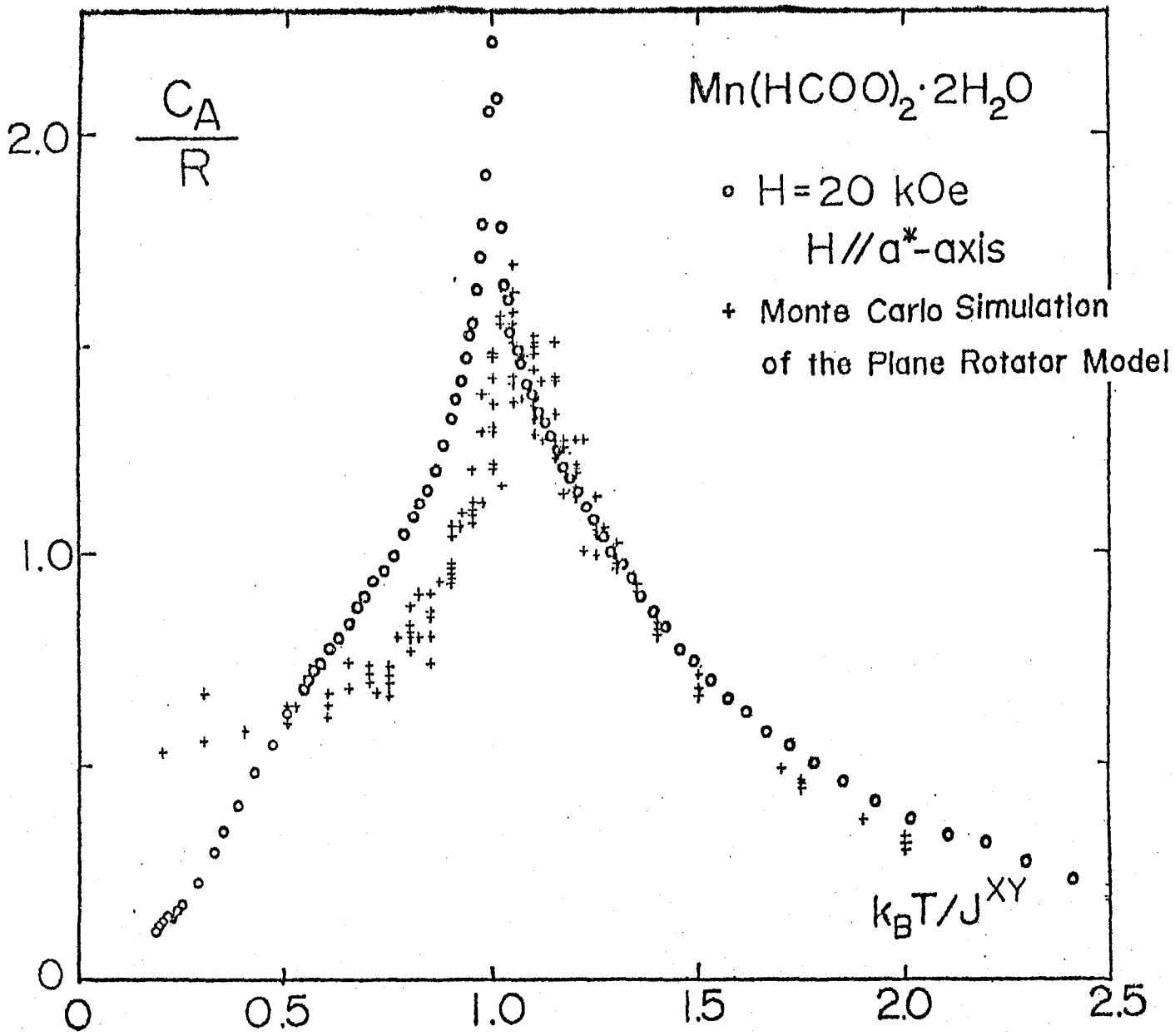

Fig.IV.B-2. Magnetic heat capacity of the 2d system in $Mn(HCOO)_2 \cdot 2H_2O$ in the field (H = 20 kOe) applied along the a*-axis, which is compared with the theoretical results evaluated from the Monte Carlo method for the 2d rotator model.

it may be possible for this 2d system to undergo a dimensional crossover from the 2d XY system to the 3d XY system as the temperature comes down to approach the critical point, giving larger values of heat capacity than those obtained from the simulations. In the temperature range $k_BT/J^{XY} < 1$, the experimental results do not agree with the theoretical ones. Especially at low temperatures, the theoretical values seem to converge at a constant value which may be inherent to the rotator model. It would be also unreasonable to treat Mn^{2+} spins as rotators down to the lowest temperatures.

When the field H = 20 kOe is applied along the b-(easy) axis, we can expect the XY behaviour as well, because of the same reason as discussed in §IV.B-2. The absolute values of C_A are shown in Fig.IV.B-3, which are nearly the same as those for H//a*-axis except the values in the vicinity of the critical region and the sharp peak at $k_BT/J^{XY} = 0.7$ which is not interesting at present.[16] In this direction of the field, the spins can not be free from the canting interaction which induces an additional staggered field H_{st} ($\propto H \cdot |D/J|$; D is an estimation of the canting interaction).[27] This staggered field gives an effect to make the appearance of roundness of the heat capacity around $T_N(H)$ just as the roundness of the heat capacity of a ferromagnet around its critical temperature region in the external field.[4]

Standing on the same theoretical treatment by the Monte Carlo method, we may expect a divergence of the staggered susceptibility at a temperature below $k_BT/J^{XY} = 1.02$.[24] The temperature dependence of the induced staggered moment under the field H = 10 kOe along the b-(easy) axis is proportional to the staggered susceptibility

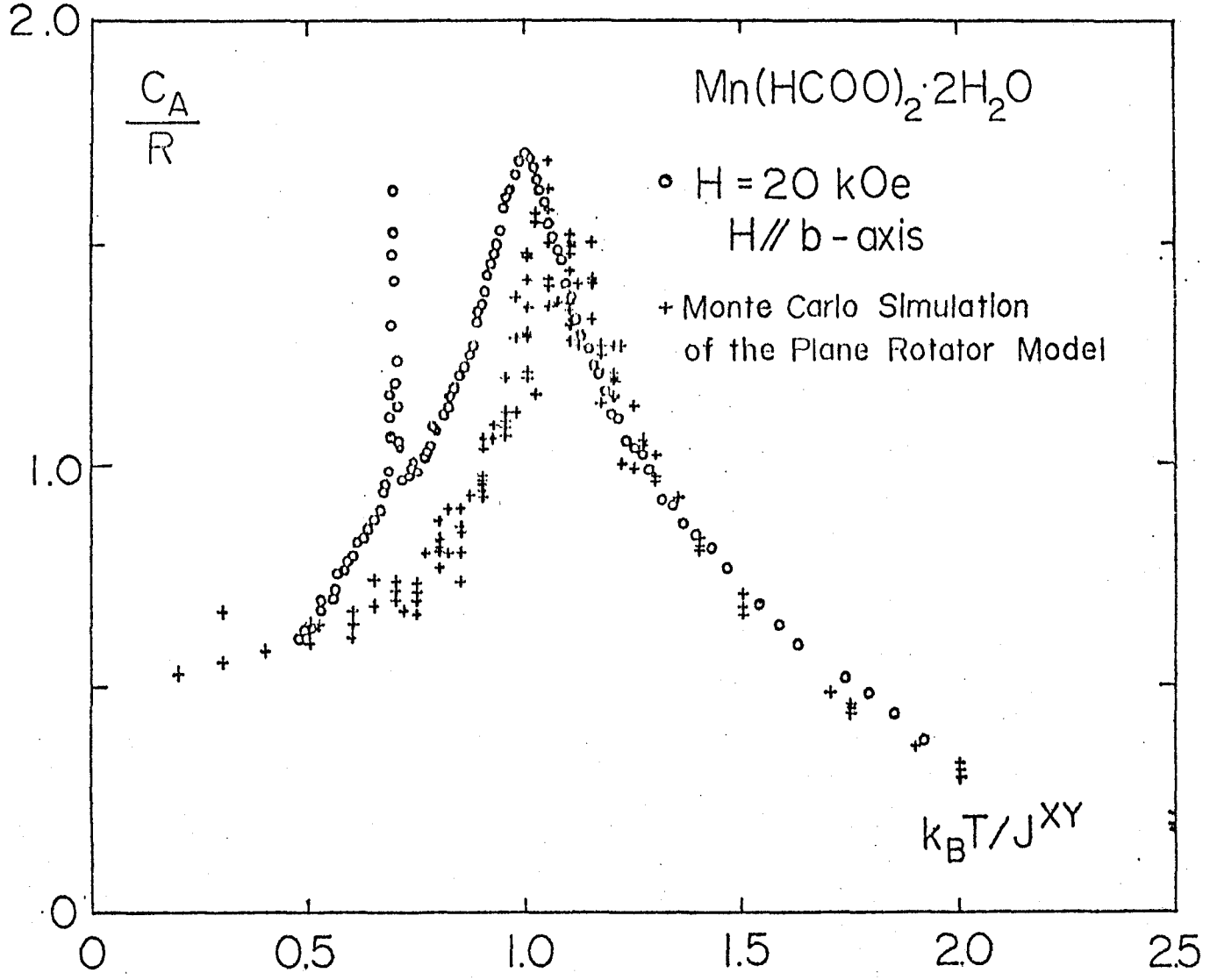

Fig.IV.B-3. Magnetic heat capacity of the 2d system in $Mn(HCOO)_2 \cdot 2H_2O$ in the field (H = 20 kOe) applied along the b-axis, which is compared with the same theoretical values as in Fig.IV.B-2.

except the vicinity of $T_N(H)$ in Fig.IV.A-15. This result may be compared with the theory of Kosterlitz and Thouless.[22].

According to Kosterlitz,[28] the susceptibility χ is divergent towards T_{KT} with the formula

$$\chi(T) \simeq A\exp(2.625 \cdot t^{-1/2}) \qquad (4.13)$$

where $t \equiv (T - T_{KT})/T_{KT}$. Some simulation results suggest that T_{KT} almost certainly lies between $k_BT/J^{XY} = 0.85$ and 0.95.[29,30,31] We tried to compare our experimental result with above equation putting $T_{KT} = T_N(H) = 3.74$ K. This is shown in the $\ln\chi$ vs $t^{-1/2}$ plot in Fig.IV.B-4 by the open triangles. Apparently, fitting is very poor. Much better fitting over a wide range of temperature (3.79 ∿ 4.2 K) is obtained if putting $T_{KT} = 3.5$ K. If the maximum temperature of heat capacity is at $k_BT/J^{XY} = 1.02$ ($T_N(H) = 3.74$ K), this fact indicates that the susceptibility diverges at $k_BT/J^{XY} = 0.95$, which may not be inconsistent with the theoretical prediction.

The 2d XY magnetic systems are rarely exist. The compound K_2CuF_4 is a 2d Heisenberg 'ferromagnet' with a small XY character (1 %). Nevertheless, it can derive a 2d XY behaviour in the susceptibility which is subject to the Kosterlitz-Thouless prediction,[32] though the experimental correction for the intrinsic quantity seems to be difficult. Taking these facts into account, we can say our present system may be a typical 2d 'antiferromagnetic' XY system for which the characteristic increase of $T_N(H)$ and magnetic heat capacity have been newly studied.

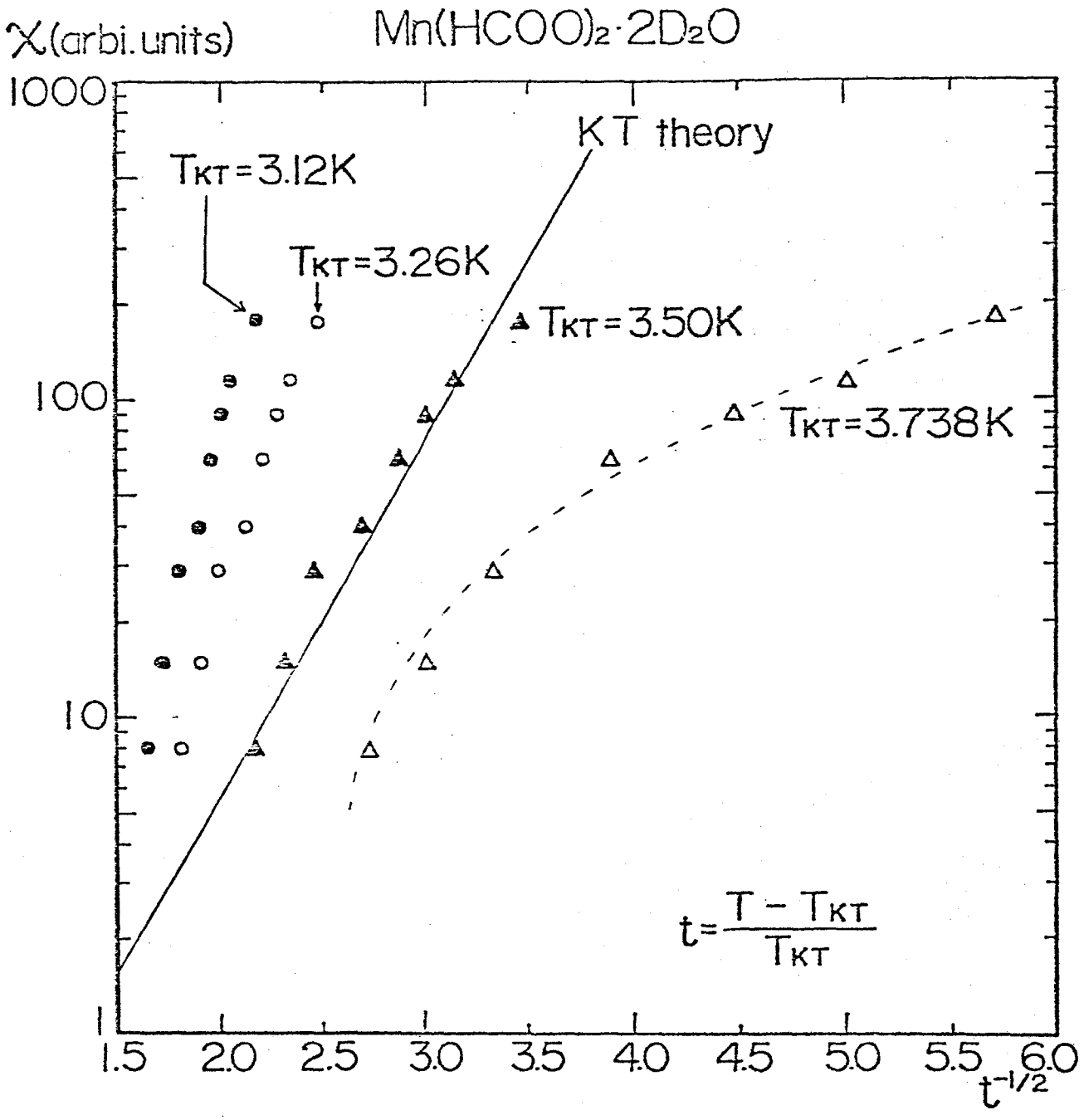

Fig.IV.B-4. $\ln\chi$ vs $t^{-1/2}$ plot, --Δ-- is for $T_{KT} = T_N(H) = 3.74$ K. under H = 10 kOe. —▲— is for $T_{KT} = 3.50$ K and the theoretical curve of Kosterlitz and Thouless.

References (IV)

1) J. Villan and J. M. Loveluck: J. Phys. (France) 38 (1977) L-77.
2) W. J. M. de Jonge, J. P. A. M. Hijmans, F. Boersma, J. C. Schouten and K. Kopinga: Phys. Rev. B17 (1978) 2922.
3) K. Takeda, T. Koike, T. Tonegawa and I. Harada: J. Phys. Soc. Jpn. 48 (1980) 1115.
4) K. Takeda, T. Koike, I. Harada and T. Tonegawa: J. Phys. Soc. Jpn. 51 (1982) 85.
5) K. Yamagata and H. Abe: J. Phys. Soc. Jpn. 20 (1965) 906.
6) M. Matsuura, Y. Ajiro and T. Haseda: J. Phys. Soc. Jpn. 26 (1969) 665.
7) J. Jr. Skalyo, G. Shirane and S. A. Friedberg: Phys. Rev. 188 (1969) 1037.
8) M. Matsuura, H. W. J. Blote and W. J. Huiskamp: Physica 50 (1970) 444.
9) K. Takeda and K. Kawasaki: J. Phys. Soc. Jpn. 31 (1971) 1026.
10) P. D. Pierce and S. A. Friedberg: Phys. Rev. 165 (1968) 680.
11) K. Takeda, T. Haseda and M. Matsuura: Physica 52 (1971) 225.
12) Y. Ajiro: J. Phys. Soc. Jpn. 27 (1969) 829.
13) J. W. Schutter, J. W. Metselaar and D. de Klerk: Physica 61 (1972) 250.
14) K. Yamagata: J. Phys. Soc. Jpn. 22 (1967) 587.
15) T. Oguchi and M. Blume: J. Phys. Soc. Jpn. 50 (1981) 254.
16) K. Takeda and K. Koyama: J. Phys. Soc. Jpn. 52 (1983) 648.
17) See, for example, K. W. Mess, E. Lagendijk, D. A. Curtis and W. J. Huiskamp: Physica 34 (1967) 126.
18) H. Morigaki and H. Abe: J. Phys. Soc. Jpn. 23 (1967) 462.

19) Y. Imly: Phys. Rev. B13 (1976) 3018.

20) N. D. Mermin and H. Wagner: Phys. Rev. Lett. 17 (1966) 1133.

21) H. E. Stanley and T. A. Kaplan: Phys Rev. Lett. 17 (1966) 913.

22) J. M. Kosterlitz and D. J. Thouless: J. Phys. C6 (1973) 1181.

23) S. Miyashita, H. Nishimori, A. Kuroda and M. Suzuki: Prog. Theor. Phys. 60 (1978) 1669.

24) J. Tobochnik and G. V. Chester: Phys. Rev. B20 (1979) 3761.

25) See, for example, D. D. Betts: in Phase Transition and Critical Phenomena, Vol. 3, ed. C. Domb and M. S. Green (Academic Press. N.Y.).

26) Y. Yamamoto, M. Matsuura and T. Haseda: J. Phys. Soc. Jpn. 43 (1977) 1550.

27) M. Matsuura and Y. Ajiro: J. Phys. Soc. Jpn. 41 (1976) 44.

28) J. M. Kosterlitz: J. Phys. C7 (1974) 1046.

29) J. Villain: J. Phys. (Paris) 36 (1975) 581.

30) W. J. Shugard, J. D. Weeks and G. H. Gilmer: Phys. Rev. Lett. 41 (1978) 1399.

31) W. L. McMillan: unpublished.

32) K. Yamaji and J. Kondo: J. Phys. Soc. Jpn. 35 (1973) 1181.

Chapter V. Ordering of $Mn_{1-x}Zn_x(HCOO)_2 \cdot 2H_2O$ and $Mn_{1-x}Zn_x(HCOO)_2 \cdot 2D_2O$ - Randomly diluted 2d Heisenberg system -

§V-1. Introduction

As the one example of the ordering of two-dimensional (2d) Heisenberg system with a small perturbation, the random dilution effect by the non-magnetic ions is investigated. In random system, the physical properties which can not be appeared in regular system would be expected to be closed up. As the example of random diluted system, $Mn_{1-x}Zn_x(HCOO)_2 \cdot 2H_2O$ and $Mn_{1-x}Zn_x(HCOO)_2 \cdot 2D_2O$ would be examined in this chapter.

Recently many experimental and theoretical works have been made on various random systems like spin glasses [1-5], mixtures of ferro- and antiferromagnets[6-8] and so on. A general character of random system is the spacial inhomogenety of cooperativity such as the magnitude and/or the direction of local field, the connectivity to the neighbours and so on, which results in a successive character of ordering process from the initial local to the final unified long range order.[9-11]

An interesting system is a random diluted quasi 2d magnet, in which a furcation of a phase transition into successive ones may occur on account of the special lattice structure from the viewpoint of cooperativity.[11]

Actually in $Mn_{1-x}Zn_x(HCOO)_2 \cdot 2H_2O$ (MnZnF2H), a divergent singularity of susceptibility at T_N in $Mn(HCOO)_2 \cdot 2H_2O$ (MnF2H)[12] has been found to furcate systematically with x into two successive ones at T_{p1} and T_{p2}.[13] NMR experiment in this chapter shows that

the phase below T_{p2} is an ordered state with the same configuration as the pure system below T_N. Here, we report a new finding of another anomaly of susceptibility at a temperature T_0 near and above T_{p1} using a SQUID magnetometer. And this anomaly at T_0 is confirmed by the measurement of heat capacity. Then we investigate neutron diffraction to get the information for spin correlations.

§V-2. Experimental results and analysis

V-2.1 Susceptibility and spontaneous magnetization

The susceptibility and spontaneous magnetization were measured accuracy using a SQUID magnetometer in the same way as MnF2H in §III-2.3. Figure V-1(a) is an example (x = 0.011) of the temperature dependence of χ_b in a negligibly weak external field H_0 ($\lesssim$ 3 mOe) along the b-axis. The peak height at T_0 of susceptibility is much weaker than those at T_{p1} and T_{p2}, which is the reason why the first anomaly has not long been detected by a conventional Hartshorn bridge method. Figure V-1(b) and (c) are the temperature dependences of χ_c and spontaneous magnetization M_c^s along the c-axis measured simultaneously. The spontaneous magnetization is obtained by a so called "field cooling method" which is usually applied to ferromagnets. This method is already mentioned in §III-2.3. It is noticed that M_c^s decreases in three steps as temperature increases corresponding to the three anomalies of susceptibility, and also that M_c^s disappears around T_0 and not at T_{p1} although the magnitude is extremely small above T_{p1}. As seen in the figure, the anomalies of χ_c at T_{p1} and T_{p2} are much weaker than those of χ_b showing a strong anisotropy. While the anomaly of χ_c at T_0 is not much

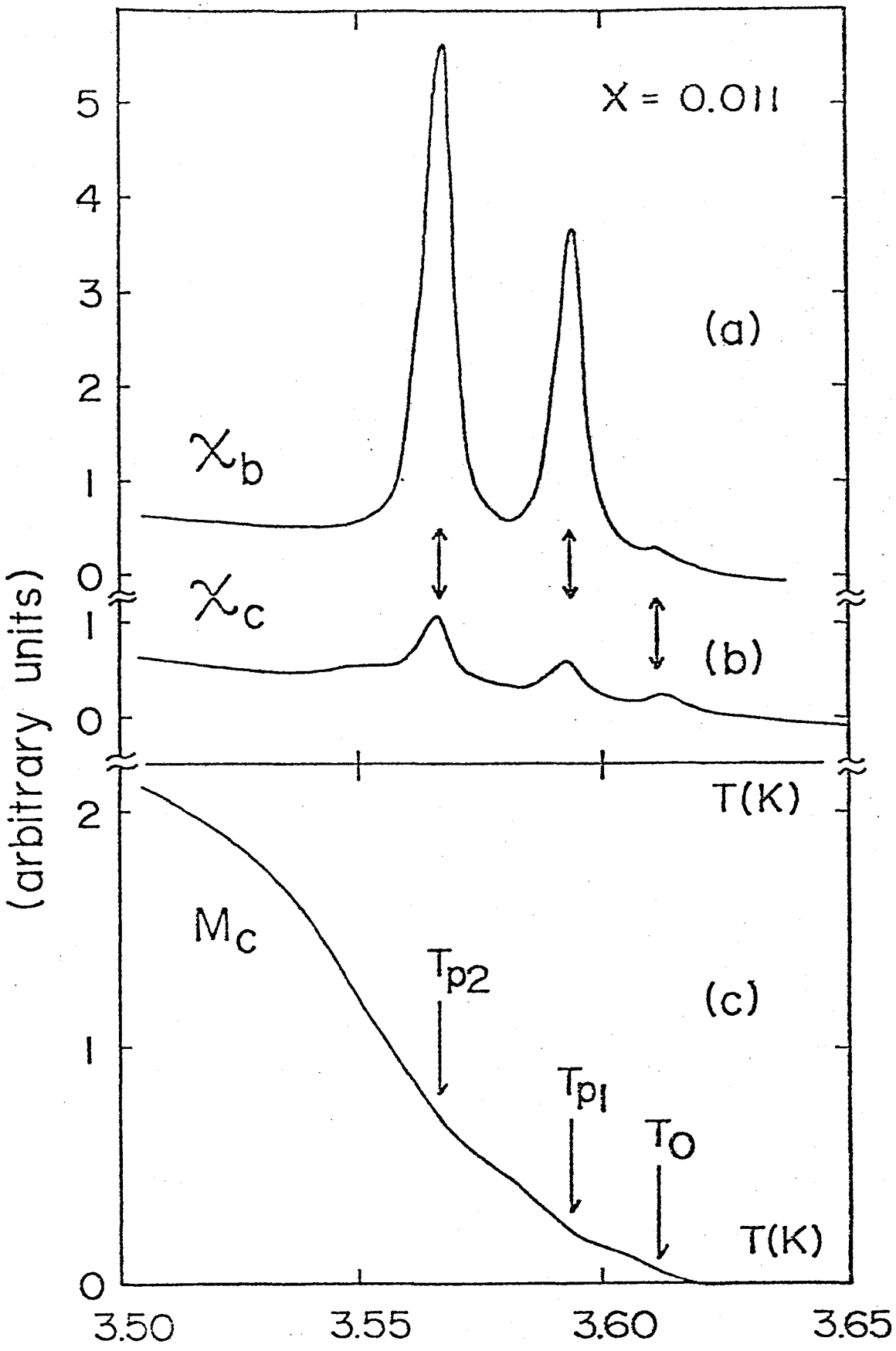

Fig.V-1. Temperature dependences of the susceptibilities (a) χ_b, (b) χ_c and (c) spontaneous magnetization M_c^s of $Mn_{1-x}Zn_x(HCOO)_2 \cdot 2H_2O$, x = 0.011. The cooling field H_c for M_c^s is 120 mOe.

different from that of χ_b. The temperature T_0 is found to change systematically with concentration x and tends to T_N for $x \to 0$ as shown in Fig.V-2. For the concentration $x > 0.05$, the anomaly of susceptibility at T_0 is broad out, although the anomalies at T_{p1} and T_{p2} are still sharp enough.

From these facts, T_0 should be taken as the transition temperature from the paramagnetic into an ordered state. Then, the very weak susceptibility anomaly at T_0 suggests that the correlation is not extended infinitely at T_0 but limitted in a finite area.

V-2.2 Heat capacity

Heat capacity for the single crystal of $Mn_{1-x}Zn_xF2H$ were measured. FigureV-3 is an example of temperature dependence of heat capacity for the case of $x = 0.011$. There are three anomalies, of which temperatures agree with those of susceptibility peaks. This experimental results convince the fact that three anomaly temperatures correspond to the three phase transition points. For the concentration $x \geq 0.10$, the double peak of susceptibility at T_{p1} and T_{p2} are still sharp enough but heat capacity has only double humps. The substances of these three phases and the mechanisms of this successive transitions will be examined by proton NMR and neutron diffraction in V-2.3 and in V-2.4, respectively.

V-2.3 Proton NMR

The NMR signals were observed for the proton No.5 and No.6 in the diluted salt below T_{p2}. An example of the line profile at 2.0 K

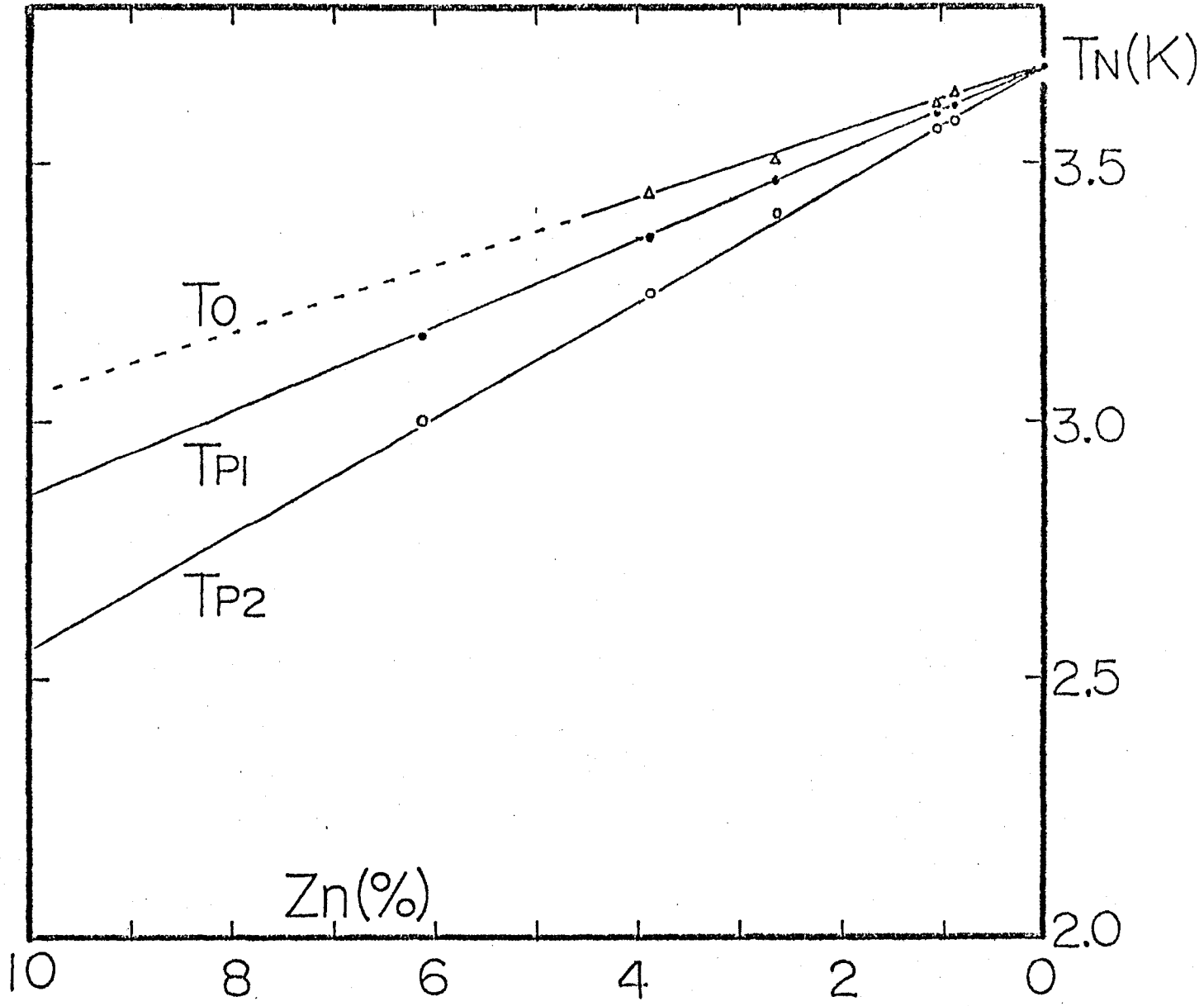

Fig.V-2. Dependences of T_0, T_{p1} and T_{p2} of $Mn_{1-x}Zn_xF2H$ on concentration x.

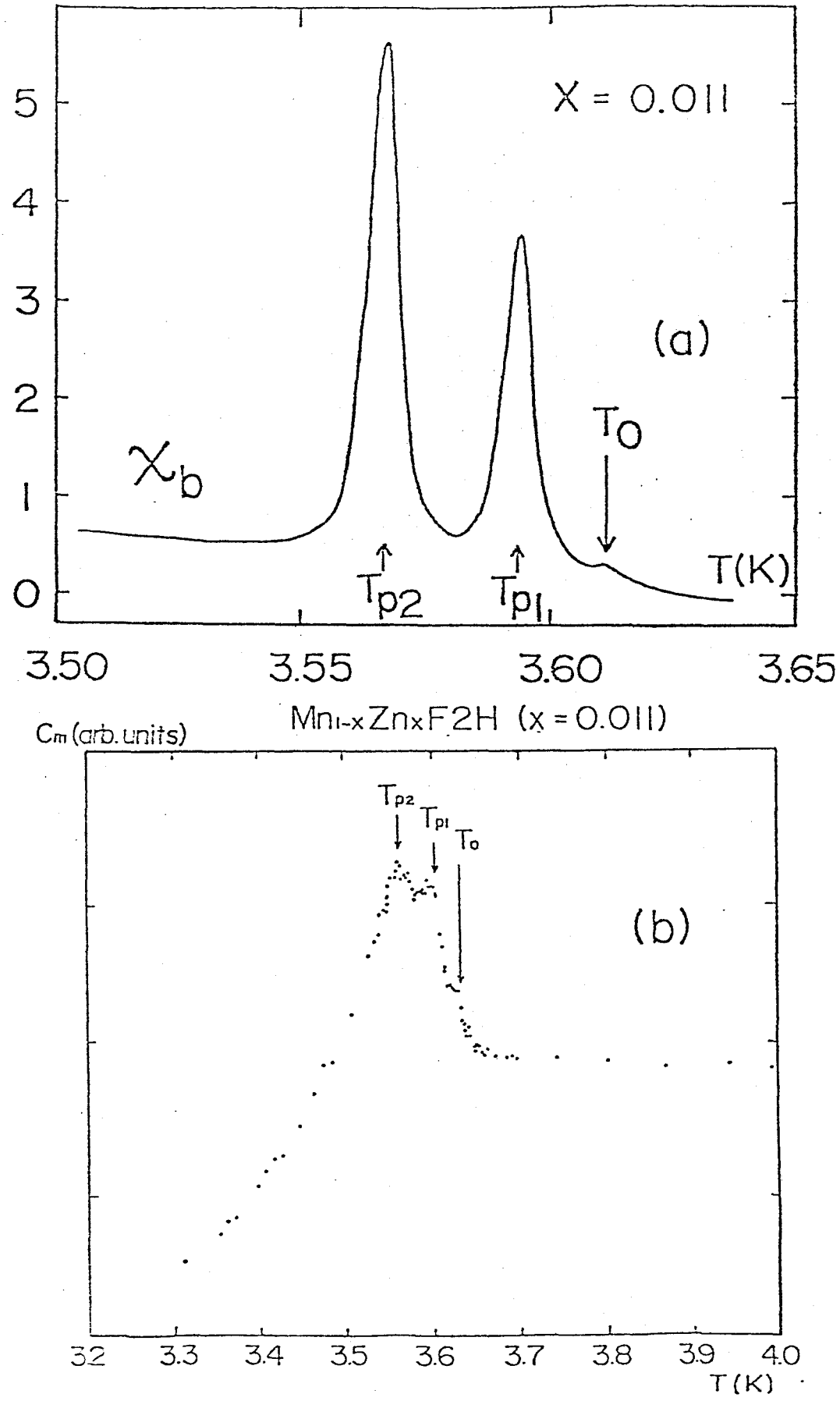

Fig.V-3. Temperature dependence of (b) heat capacity for the case of x = 0.011, with comparison of that of (a) susceptibility for the same concentration x.

in the external field of 50 Oe is shown in Fig.V-4(a) and compared with that for the pure salt (b). For both protons No.5 and No.6, the line width for the diluted salt is much broader than that for the pure salt. The signal intensity for the dilute salt is much weaker than that for the pure salt. Both the width and the intensity for the dilute salt depend strongly on the external static field H_0. The former increases and the latter decreases as increasing H_0. Such characteristics of line profiles are due to the inhomogeneous broadening, which indicates a static distribution of local field at proton site in the dilute salt.

The signal intensities for both protons No.5 and No.6 depend also on temperature. These decreases as temperature increases and especially rapidly near T_{p2}. While, any rapid increase of line width is not apparently noticed towards T_{p2}.

To check the difference or the equality of the dipole sum tensor at proton sites of No.5 and No.6 by the deuteration, the angular dependence pattern in ac-plane at T = 8.0 K > T_N or T_0 was examined for both dilute and pure salts under the external field of 4.7 kOe. The pattern for the dilute salt is shown in Fig.V-5(a) and compared with that for the pure salt in (b). There is almost no discrepancy between them. This fact indicates that the dipole sum tensor for the dilute salt is nearly equal to that for the pure salt.

To identify the spin structure in the state below T_{p2}, the patterns or the dependences of NMR frequencies on the external field direction against the crystal axis of protons No.5 and No.6 are examined at T = 2.0 K and H_0 = 50 Oe. The results are collected

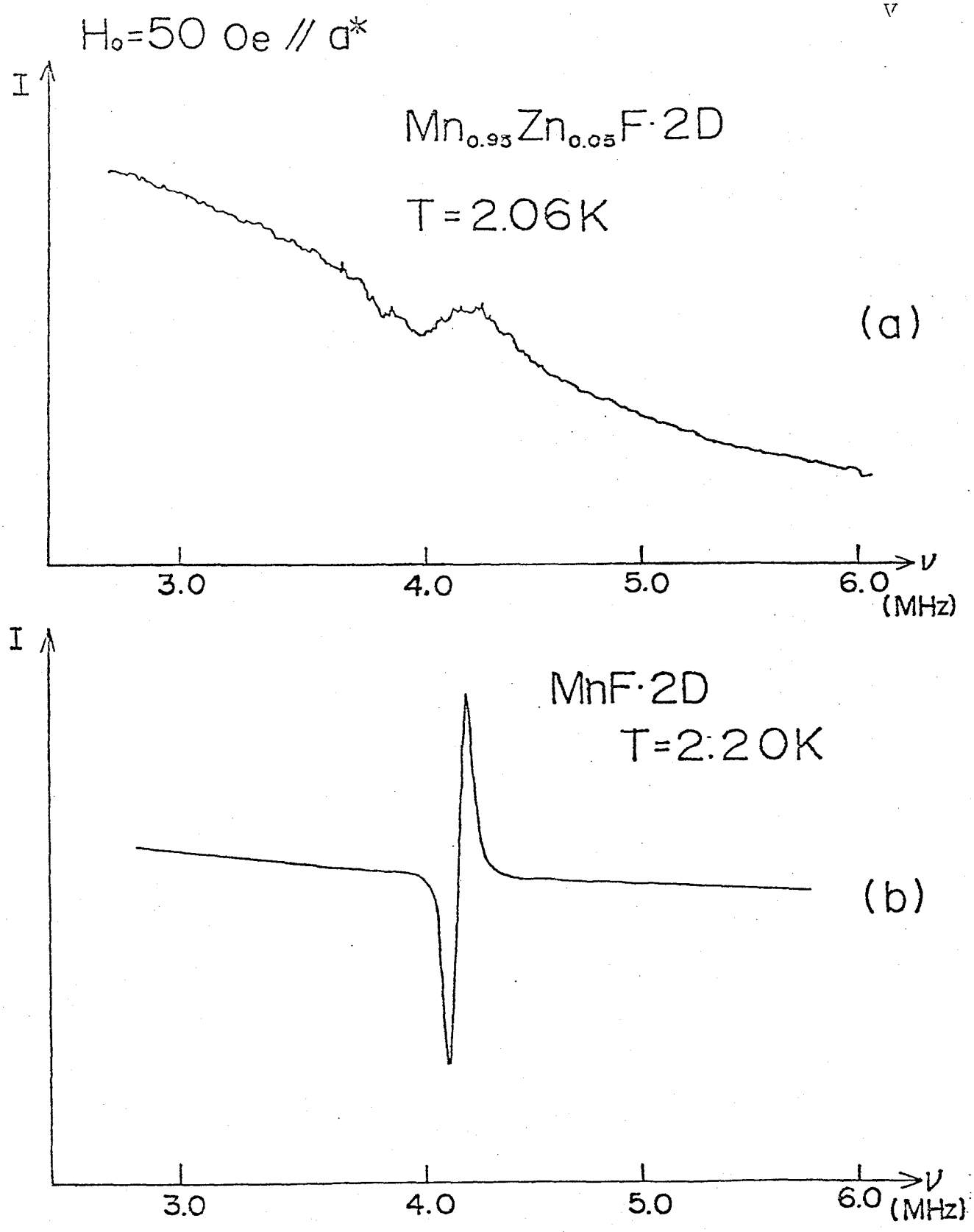

Fig.V-4. (a) Line profile of NMR signals for the proton No.5 of $Mn_{1-x}Zn_xF2D$ (x = 0.04) at 2.0 K in the external field of 50 Oe. (b) That for the pure salt under the same condition.

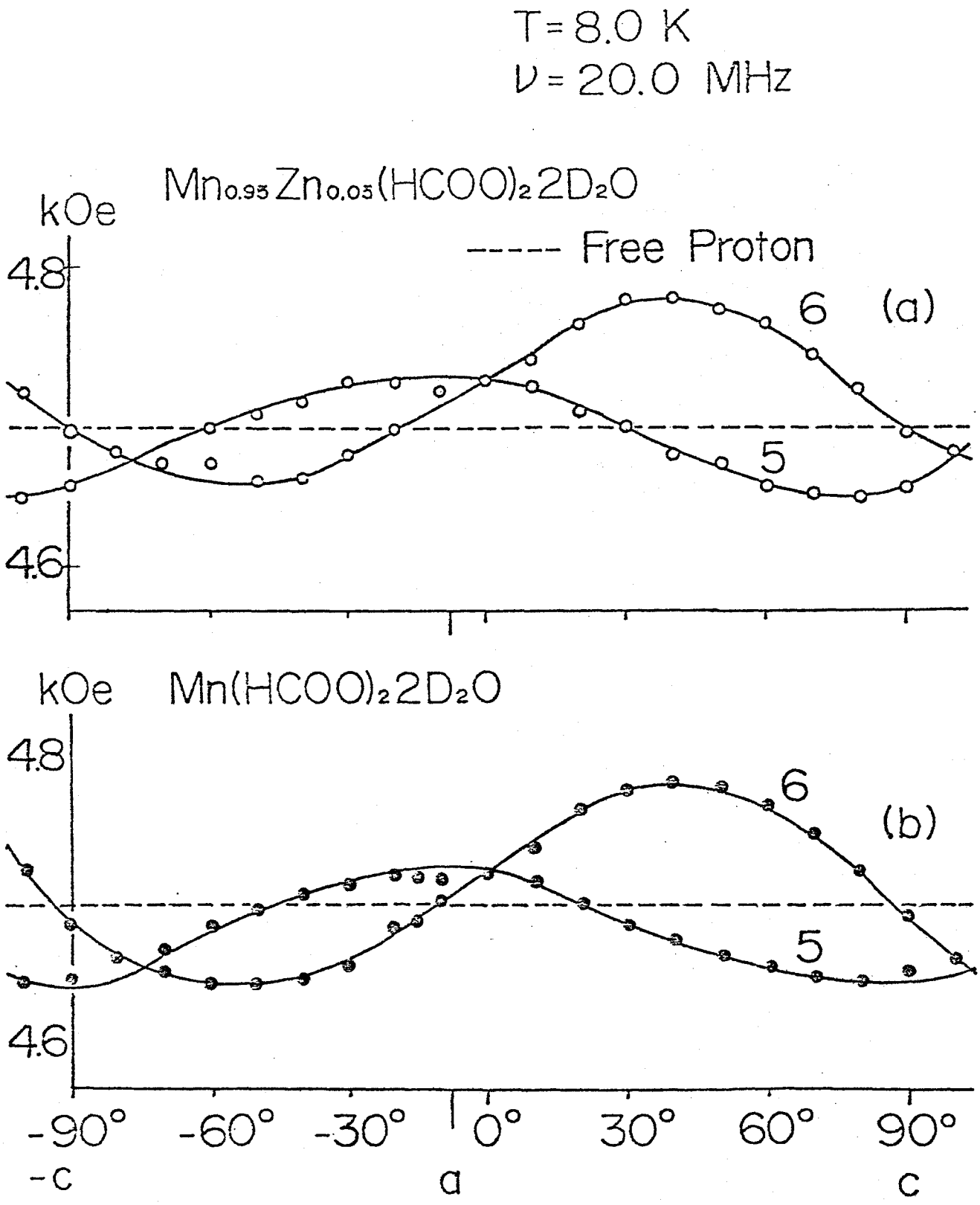

Fig.V-5. Angular dependence pattern in ac-plane at T = 8.0 K > T_N under the field of H_0 = 4.7 kOe for (a) dilute salt (x = 0.04) and (b) pure salt.

in upper side of Fig.V-6(a) and (b) and compared with those for the pure salt in lower side of the same figure, respectively. No essential difference is found between the patterns for the dilute and the pure salts, from which the spin structures for these salts are concluded to be quite the same as each other at least in the skelton. While, as for the spin structure in the state between T_{p1} and T_{p2}, no imformation is avairable from proton NMR even in the skelton, because no NMR signal can be detected at all in this temperature region.

To look after the growing feature of spontaneous local moment of both A and B ions, respectively, the temperature dependences of the resonance frequencies of proton No.5 and No.6 at zero field were examined. The results are collected in Fig.V-7(b). The susceptibility of the very sample is shown in Fig.V-7(a) for a comparison. In regular system, each local ionic moment is taken usually proportional to the sublattice magnetization to which each ion belongs. In random system, such a relation would not be applicable in general. However, in the present case, the spin structure for the dilute salt is the same as that for the pure salt in the skelton. So, we expect the proportionality relation between the local moment and the sublattice magnetization and use it in the same analysis in Chap.III (§III-2.2).

As the results, the resonance frequencies of proton No.5 and No.6; ω_5 and ω_6 are expressed just the same as the case of pure salt as a function of only the magnitudes of $|L_A|$ and $|L_B|$ as

$$\omega_i = |L_A| \cdot F_i(\eta), \quad (i = 5,6) \qquad (5.1) \equiv (3.11)$$

where η is the ratio $|L_A|/|L_B|$ and F_i is a function of only η.

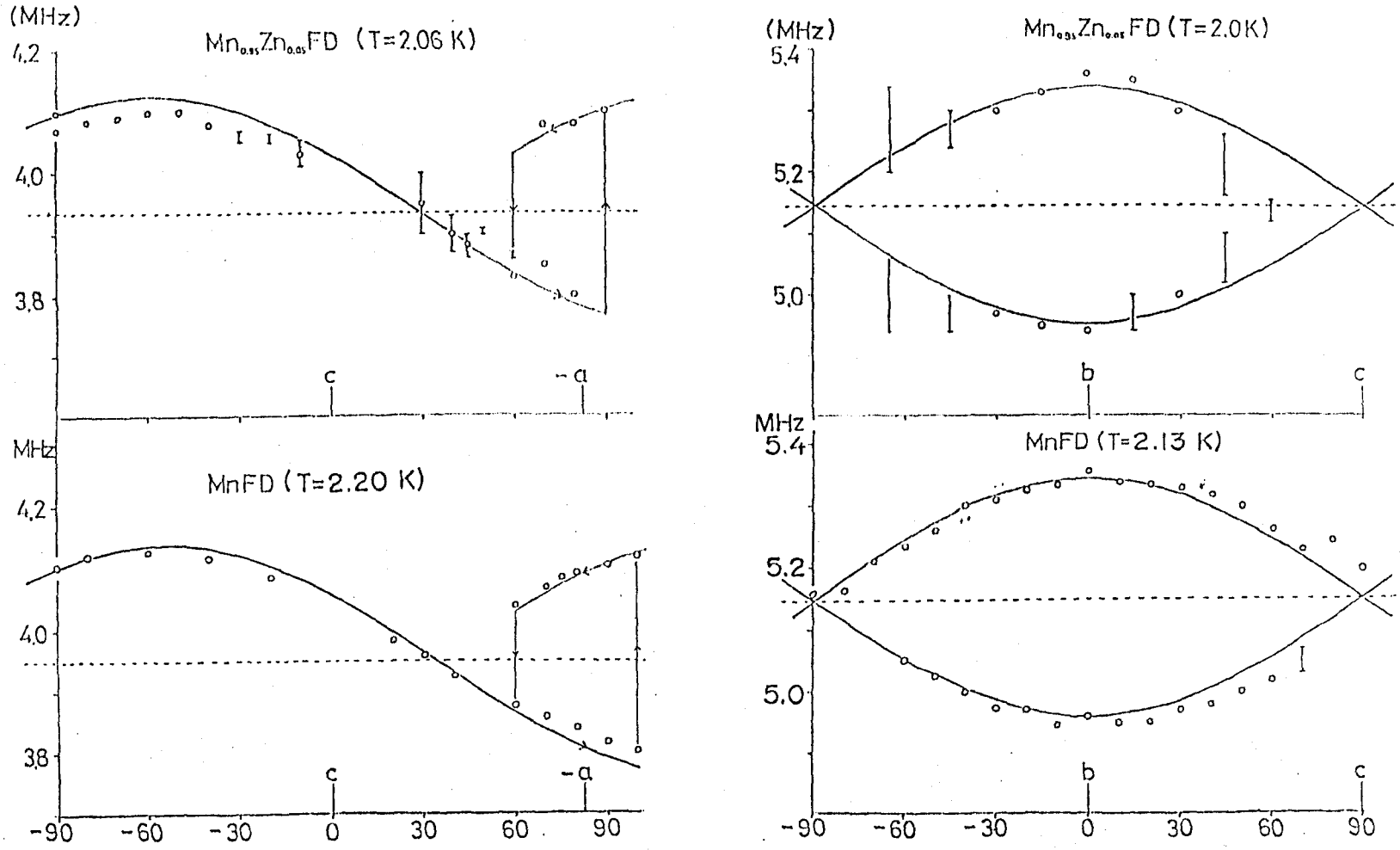

(a) ac-plane

(b) bc-plane

Fig.V-6. Angular dependence patterns in (a) ac-plane and (b) bc-plane at T = 2.0 K and H_0 = 50 Oe: upper side is for the dilute salt (x = 0,04) and lower side is for the pure salt.

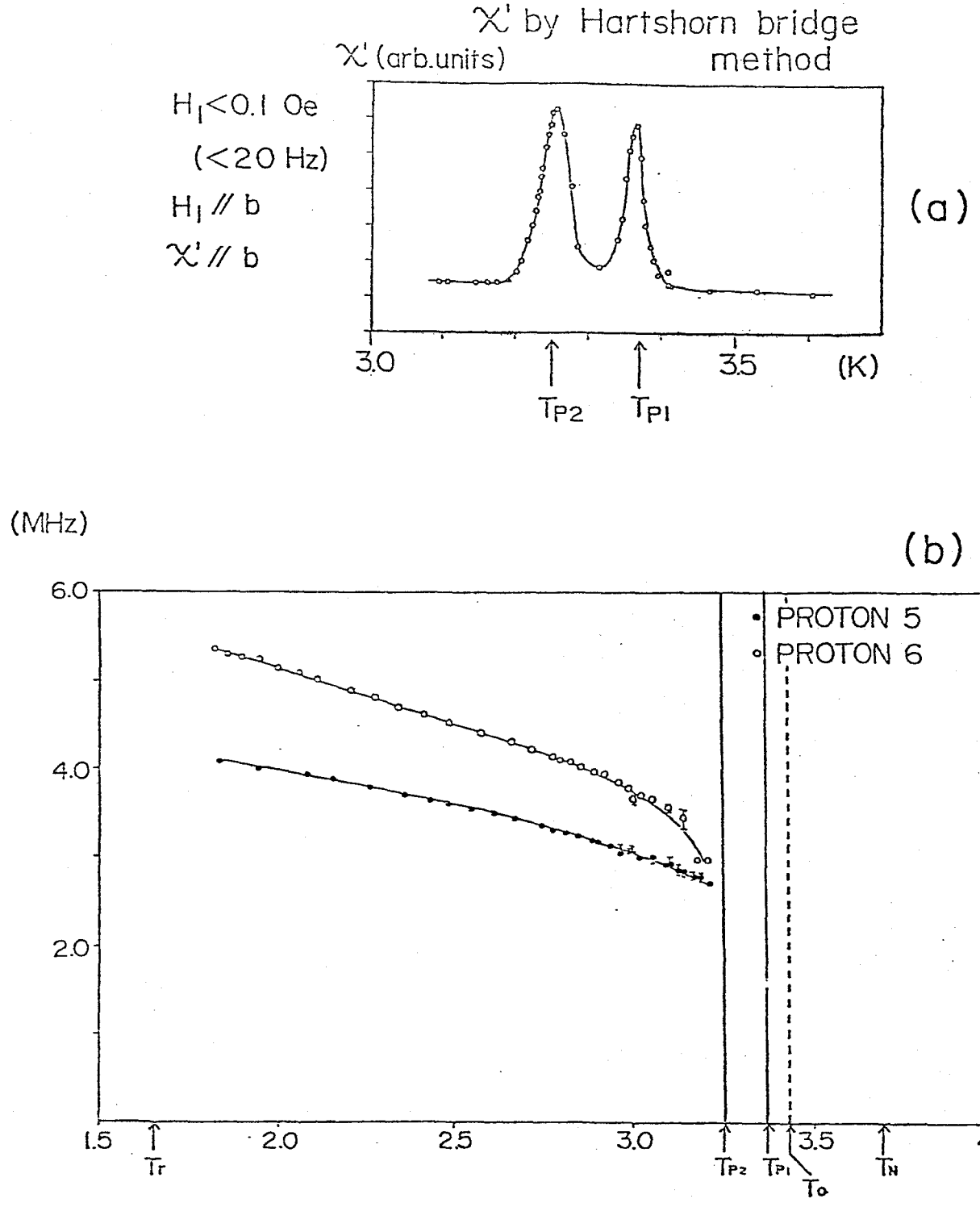

Fig.V-7. (a) Temperature dependence of the susceptibility (x = 0.0

(b) Temperature dependence of the resonance frequencies of proton No.5 and No.6 at zero field (x = 0.04).

Thus, we get $|L_A|$ and η by applying eq.(5.1) to the experimental data in fig.V-7(b). The obtained temperature dependences of $|L_A|$ and η are collected in Fig.V-8(b) and V-9(b) and compared with those for the pure salt in Fig.V-8(a) and V-9(a), respectively. The temperature dependences of $|L_A|$ for the dilute and the pure salts are almost the same, if the critical temperature for the former is taken as T_{p1} as seen in the figure or as T_0. The behaviours of η for these salts are also similar to each other except very near T_{p2} and show a Curie-Weiss's law. As temperature approaches to T_{p2}, however, η for the dilute salt increases rapidly indicating a divergent character.

V-2.4 Neutron diffraction

The development of intra-plane spin correlation in the anti-ferromagnetically coupled (100) planes is directly confirmed by a Bragg ridge along the (100) direction. The line profiles for the cross section of the ridge at various temperatures are summarlized in Fig.V-10. The temperature dependence of the peak intensity I_r of the ridge is shown in Fig.V-11(b). The intensity I_r reaches the maximum around T_0 and almost constant between T_0 and T_{p1}. It decreases monotonously below T_{p1} and no anomaly is noticed around T_{p2}. The temperature dependence of the line width of the Bragg ridge was roughly examined and is shown in Fig.V-12(b). The line width is narrowest around T_0. The half intensity width is however, larger than those for nuclear Bragg reflection or for the (001) magnetic Bragg point reflection far below T_{p2} which is shown as the resolution width in Fig.V-12(b), directly indicating that the

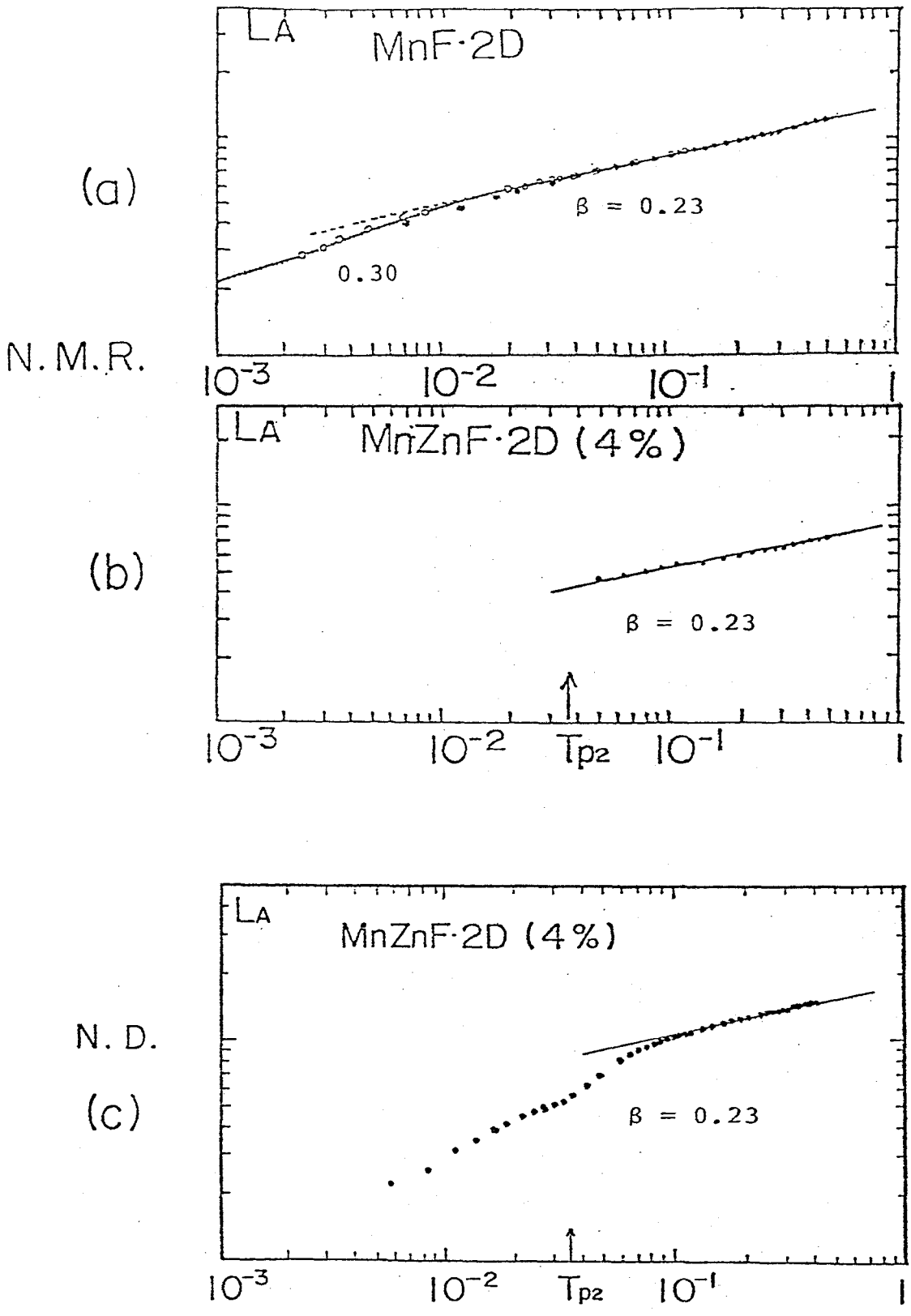

Fig.V-8. Temperature dependence of $|L_A|$ for

(a) pure salt by NMR,

(b) dilute salt: x = 0.04 by NMR, $T_{pl} \rightarrow T_c$,

(c) dilute salt: x = 0.04 by N. D. $T_{pl} \rightarrow T_c$.

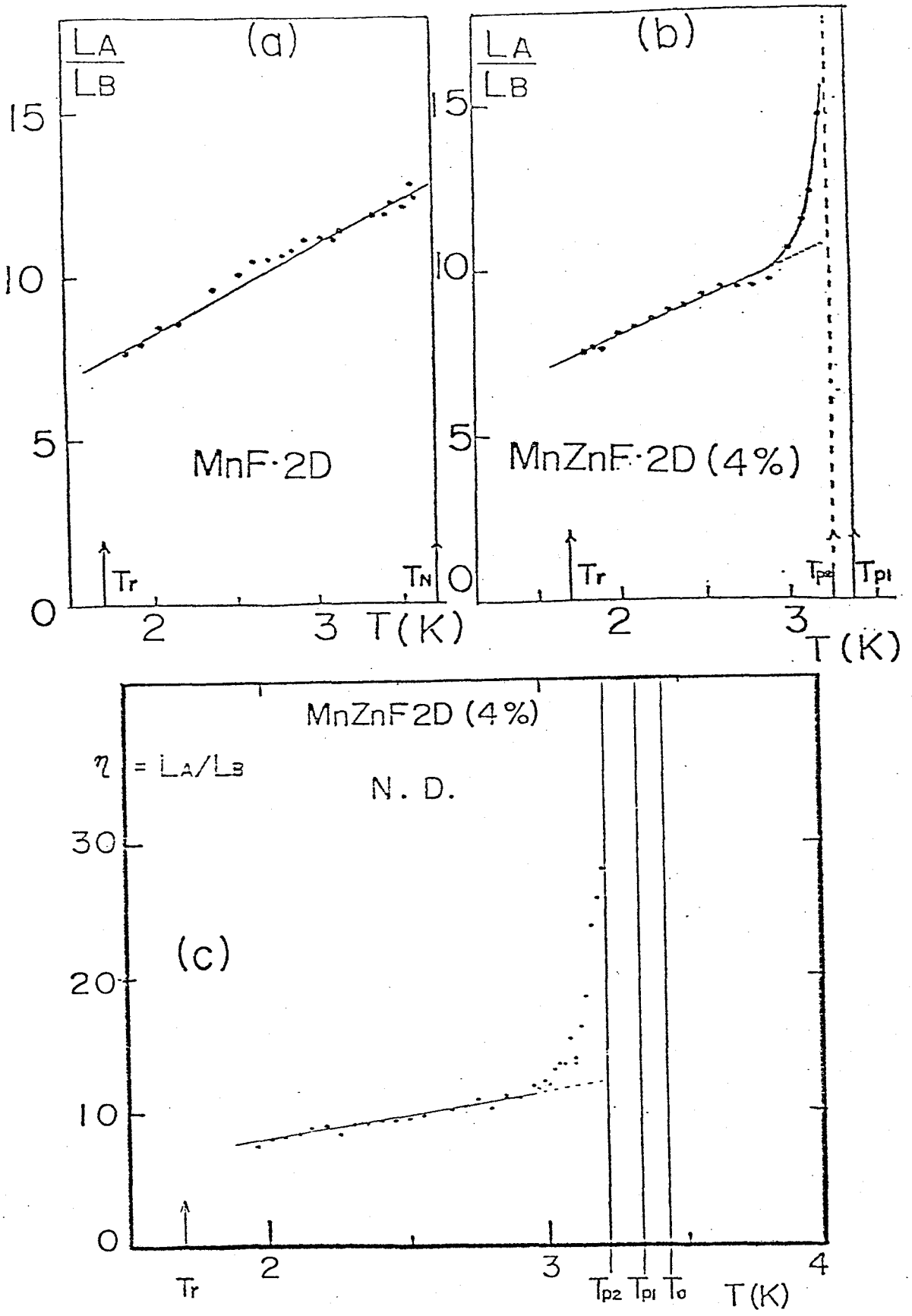

Fig.V-9. Temperature dependence of $\eta = L_A/L_B$ for

(a) pure salt by NMR,

(b) dilute salt: x = 0.04 by NMR, $T_{pl} \rightarrow T_c$

(c) dilute salt: x = 0.04 by N. D. $T_{pl} \rightarrow T_c$.

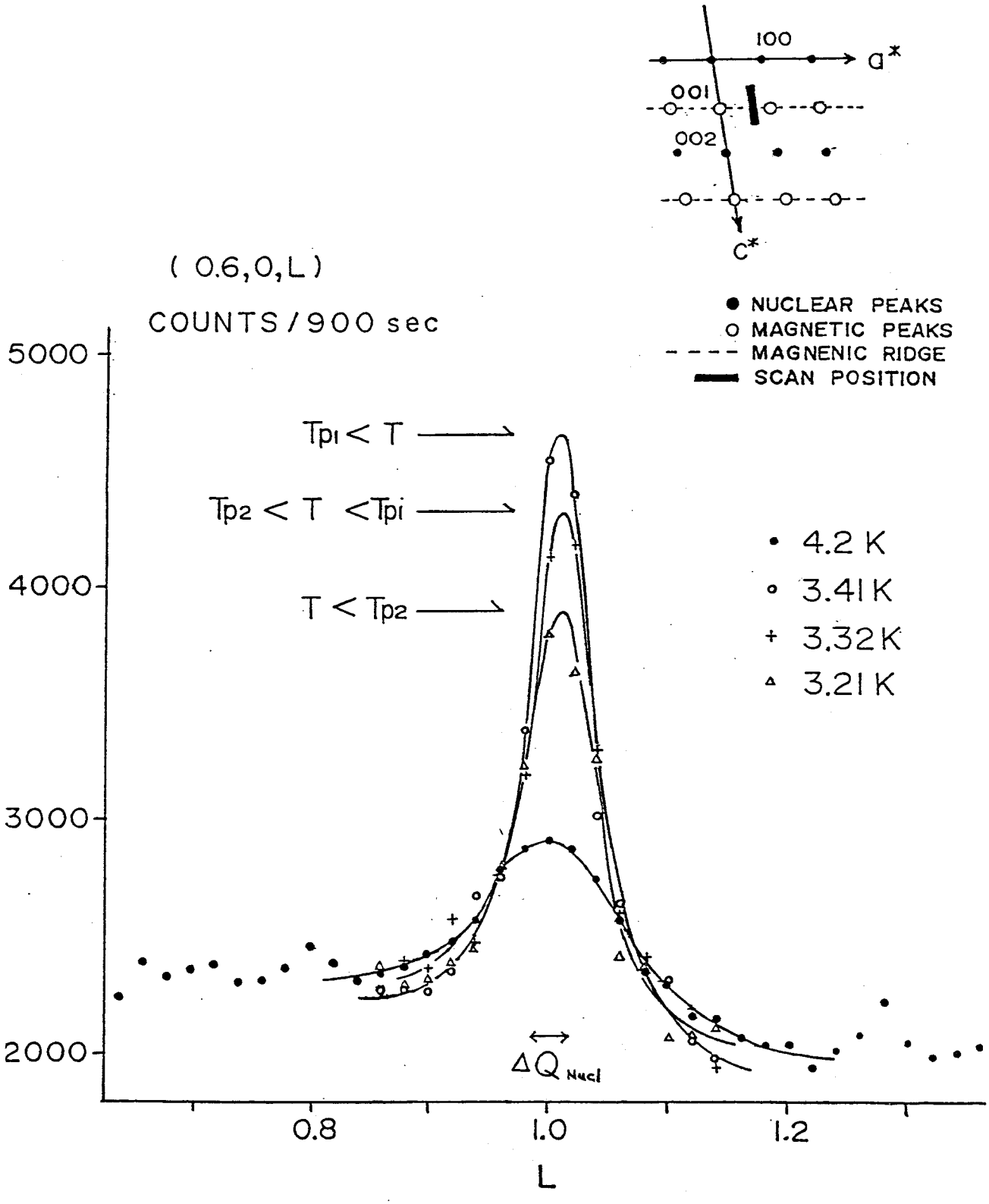

Fig.V-10. Line profiles for the cross section of the Bragg ridge for various temperatures. x = 0.04. Inset shows the scan position of the magnetic ridge.

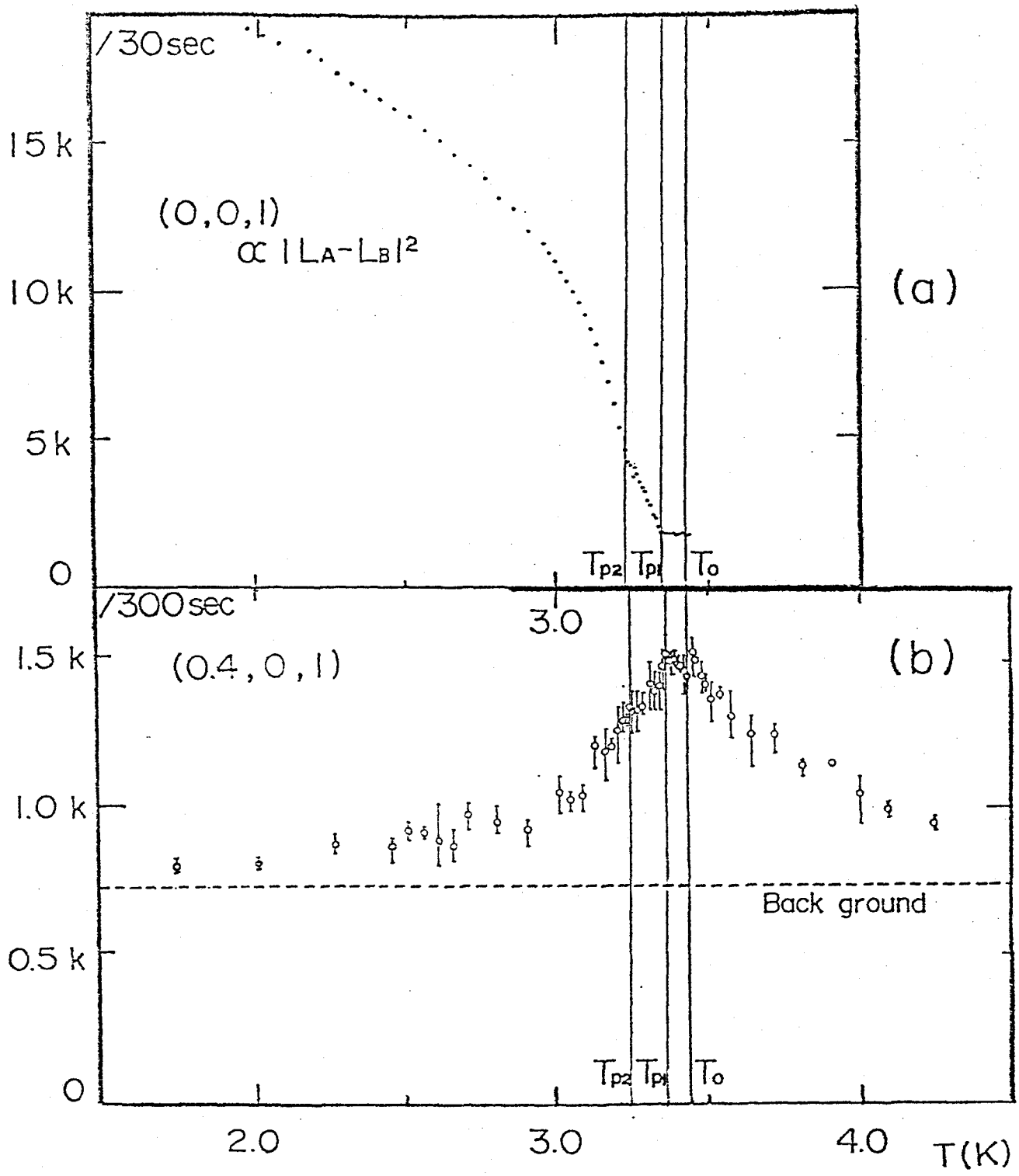

Fig.V-11. Temperature dependences of the intensity of

(a) (001) Bragg point reflection and

(b) Bragg ridge at (0.4 0 l) for dilute salt: x = 0.04.

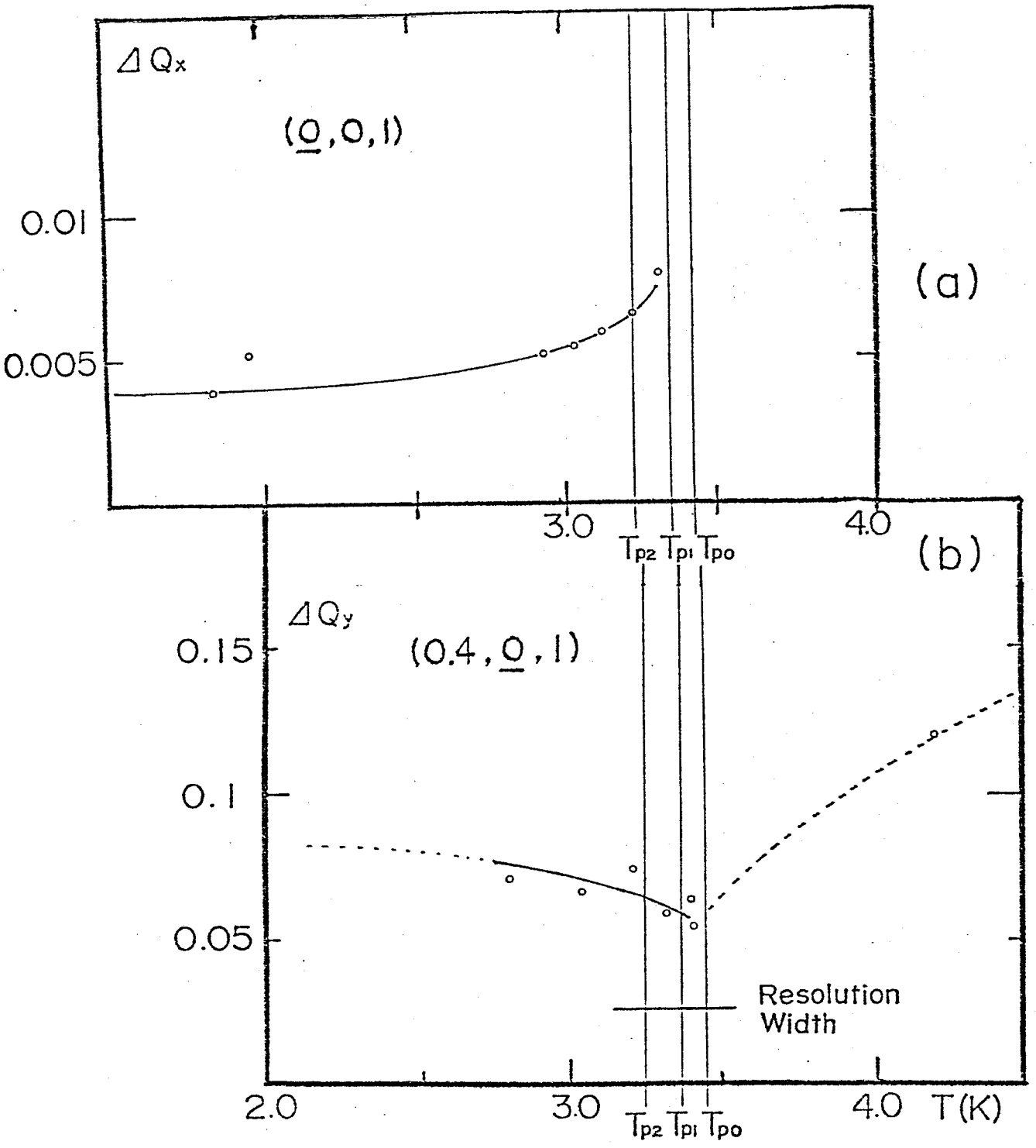

Fig.V-12. Temperature dependences of the line width of

(a) (001) Bragg point reflection and

(b) Bragg ridge for dilute salt: x = 0.04.

intra-plane correlation is not extended to infinity.

The (001) Bragg point reflection intensity I_p was observed, to see the growing feature of 3d order parameter. Figure V-11(a) is the temperature dependence of I_p. A remarkable is that I_p does not start to grow up at T_0 but at T_{p1}, which indicates that the transition at T_0 and the intermediate state between T_0 and T_{p1} are of a 2d system. While, the transition at T_{p1} is that from the 2d into a 3d ordered state. The growth rate of I_p, however, is almost linear at T_{p1} and changes appreciably around T_{p2}. The line profile for the (001) Bragg reflection was examined in detail and is shown in Fig.V-12(a). The width gets gradually narrow as temperature decreases and at 2.0 K ($T \sim 0.7 \cdot T_{p2}$) it is almost the same as that for nuclear Bragg reflection showing the perfect 3d long range order at the temperature. Any appreciable change, however, is observed around T_{p2}.

The (101) Bragg reflection intensity was also observed. It is known that the (001) intensity is proportional to $(L_A - L_B)^2$ and the (101) is to $(L_A + L_B)^2$. The proportional constants are determined from the resolution function. As the result we can get the magnitude of staggered moment of A and B site, L_A and L_B or L_A and η. The temperature dependences of L_A and η by the experiment of neutron diffraction are shown in Fig.V-8(c) and V-9(c), respectively. However, this estimation is rather unreliable above about 3 K that is below $\varepsilon \simeq 10^{-1}$ because of the gradual change of half intensity width as shown in Fig.V-12(a). The temperature dependence of η is similar to that by NMR experiment. And the critical index β of L_A is the same as that by NMR experiment except

very vicinity of the critical point T_{p2}.

The line profile of the Bragg ridge for $T_{p1} < T < T_0$ and that of Bragg point for $T_{p2} < T < T_{p1}$ are shown in Fig.V-13(a) and (b), respectively. Both of these widths are greater than the reaolution widths. As the results, both the intra-plane correlation length for $T_{p1} < T < T_0$ and the inter-plane correlation length for $T_{p2} < T < T_{p1}$ are not infinitely long. The 2d long range order for $T_{p1} < T < T_0$ and 3d l. r. o. for $T_{p2} < T < T_{p1}$ are both imperfect and the perfect 3d l. r. o. is realized far below T_{p2}.

§V-3. Discussion

As mentioned in §V-2.1, the transition at T_0 is that from the paramagnetic into an ordered state with a small but finite spontaneous magnetization. From the results in §V-2.4, the transition at T_0 and the intermediate state between T_0 and T_{p1} are concluded to be a 2d system. The measured line width for the Bragg ridge around T_0 is about twice as large as that for nuclear Bragg reflection. The correlation length is thus limited to a finite value even at T_0. The absence of inter-plane correlation between T_0 and T_{p1} is attributable to the finite correlation length in each plane at T_0 as shown by a simple free energy consideration[11] and may be one of some features of quasi 2d random system.

As mentioned in §V-2.4, the transition at T_{p1} is that from the imperfect 2d l. r. o. into a imperfect 3d ordered state. A characteristic fact is the slow (almost linear) growth rate of I_p at T_{p1}. It is essentially different from those for the pure system of $x = 0$ and other regular systems at T_N or T_c where I_p changes with

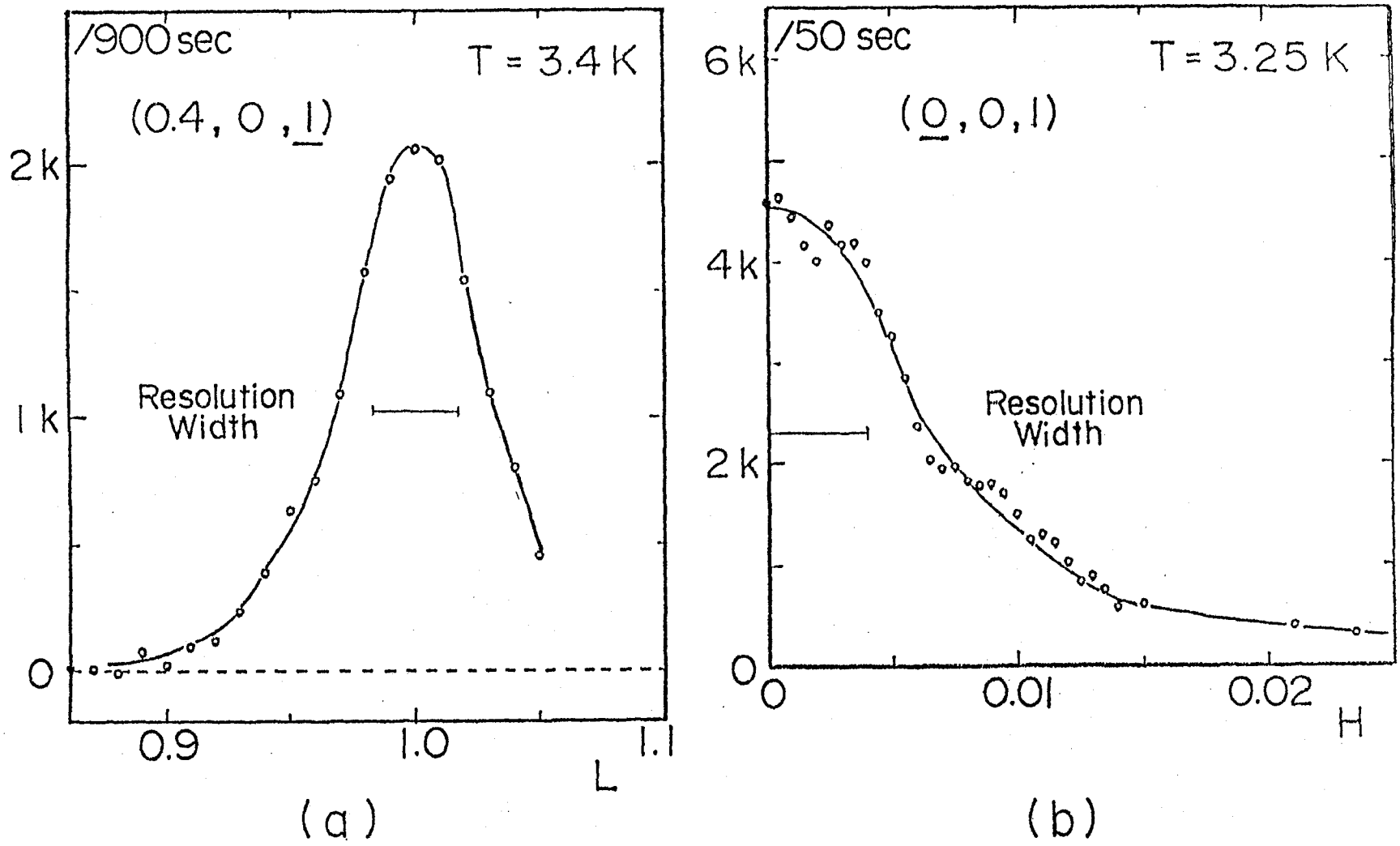

Fig.V-13. (a) Line profile of the Bragg ridge for $T_{p1} < T < T_0$.

(b) Line profile of the Bragg point for $T_{p2} < T < T_{p1}$.

temperature as $(T_c - T)^{2\beta}$ and β is the critical index of magnetization.

The transition at T_{p2} is that into another 3d ordered state which is quite the same state as in the pure system below T_N as mentioned in §V-2.3. From the descreate change of I_p at T_{p2} and strong anisotropy of susceptibility peak at T_{p2}, a spin reorientation type transition may be suspected to occur at the temperature. But no experimental evidence is obtained by searching various many reflections which can detect the probable reorientation. The possibility is therefore completely ruled out. The origin of the transition at T_{p2} is not clear at present but may be a ordering of "paramagnetic" B ions.

It may be attributable to the characteristic inter-plane structure of MnF_2H[14], in which mutually independent paramagnetic ions are sandwiched between the adjacent antiferromagnetic planes. Since the inter-plane correlation is just brought through the paramagnetic ion, the intermediary Mn^{2+} ion (B site) is a good "observer" of the inter-plane correlation.

It is certainly considered from the results of neutron diffraction that T_{p1} is the temperature of the onset of 3d long range order. Because the Bragg point intensity begins to grow below T_{p1}. As seen in §V-2.3 and 2.4, most of B ions is considered to order at T_{p2} in the internal field produced by ordered A ions. Then, what is happen at T_0 ? It is suspected that "pre-ordered phase" is realized at T_0 in this system before the occurence of the long range order at T_{p1}. We consider that this "pre-ordered phase" may appear generally in random systems.

References (V)

1) V. Cannella and J. A. Mydosh: Phys. Rev. B6 (1972) 4220.

2) S. F. Edwards and P. W. Anderson: J. Phys. F5 (1975) 965.

3) D. Sherrington and S. Kirkpatric: Phys. Rev. Lett. 35 (1975) 1792.

4) M. Suzuki: Prog. Theor. Phys. 58 (1977) 1151.

5) Y. Miyako, S. Chikazawa, T. Sato and T. Saito: J. Magn. Magn. Materials 15-18 (1980) 139.

6) M. Sakata and F. Matsubara: Prog. Theor. Phys. 55 (1976) 672.

7) S. Katsura: Prog. Theor. Phys. 55 (1976) 1049.

8) Y. Ueno and T. Oguchi: J. Phys. Soc. Jpn. 40 (1976) 1513.

9) D. E. Khmel'nitskii: Zh. Eksp. Teor. Fiz. 73 (1975) 1960.

10) S. L. Ginzburg: Zh. Eksp. Teor. Fiz. 73 (1977) 1961.

11) M. Matsuura: Physica 108B (1981) 845.

12) M. Matsuura, Y. Ajiro and T. Haseda: J. Phys. Soc. Jpn. 26 (1969) 665.

13) M. Matsuura, Y. Yamamoto, S. Ohtake, K. Koyama and T. Haseda: J. Magn. Magn. Materials 15-18 (1980) 235.

14) K. Osaki, Y. Nakai and T. Watanabe: J. Phys. Soc. Jpn 119 (1964) 717.

Appendix

—— Phase diagram for $Cu(HCOO)_2 \cdot 2H_2O \cdot 2CO(NH_2)_2$ ——

The field sweep charts of differential susceptibility ($\nu \simeq$ 10 MHz) along a*-axis are shown for the various reduced temperatures T/T_N in Fig.VI-1. These peaks correspond to the phase transition from 4 sub-lattice to 2 sub-lattice structure. Tracing down the shift of this peak on the T-H plane, we get phase boundary curve between 4 sub- and 2 sub-lattice structure as in Fig.VI-2. The peak of susceptibility becomes gradually broad as the temperature decreases. However the vertical axis is scaled in arbitrary units concerning zero point. Various charts are gathered for the guide to eye. The temperature sweep charts of susceptibility under the various external fields along the a*-axis are gathered in Fig.VI-3. The sharp peak at $T_N(0)$ = 15.5 K shifts towards lower temperature side rather sensitively with increasing field. This boundary coincides with that determined from the field sweep measurement of susceptibility.

In Fig.VI-3, we note that another broad shoulder begins to grow on the higher temperature side of the susceptibility peak. This broad maximum shifts to the higher temperatures, separating from the sharp peak, with increasing field. This broad maximum becomes broad out under the field larger than about 1 kOe. The trace of these maximum points describes a phase boundary curve between 2 sub-lattice and paramagnetic phases in Fig.VI-2 as is shown below.

In the same way as mentioned above, we can get the phase

boundary for the field applied along the c-axis. Figure VI-4(a) shows the phase boundary up to 12 kOe determined by the measurements of susceptibility. This phase diagram is similar with that for H//a*-axis. The temperature dependence of the line shift of proton NMR is shown in Fig.VI-4(b). There are two transition points. These experimental results are consistent with the fact that 4 sub-lattice structure in which spins are anti-parallel to nearly c-axis is realized below 8 K and 2 sub-lattice structure in which spins are anti-parallel to b-(L_2-)axis between 8 K and 16 K.

The field dependence of NMR line shift below the transition field (about 2 kOe) is shown in Fig.VI-5. The experimental data are shown with open circles and calculated points are with closed circles. This calculation was performed with the variables of 4 sub-lattice moment towards z-axis $M_z^{(4)}$ and 2 sub-lattice moment towards y-axis $M_y^{(2)}$. The field dependences of $M_y^{(2)}$ and $M_z^{(4)}$ are shown in Fig.VI-6(a). The change of the vector of magnetization $\vec{M}$ is shown in Fig.VI-6(b). The transversal axis indicates $M_z^{(4)}/M_f$ and longitudinal axis $M_y^{(2)}/M_f$, where M_f is the full moment of Cu^{2+} ion. Dotted line shows the circle with constant $|M| = 0.7 \cdot M_f$. It is shown that the sublattice moment becomes larger with the appearance of 2 sub-lattice moment and approaches the theoretical value.

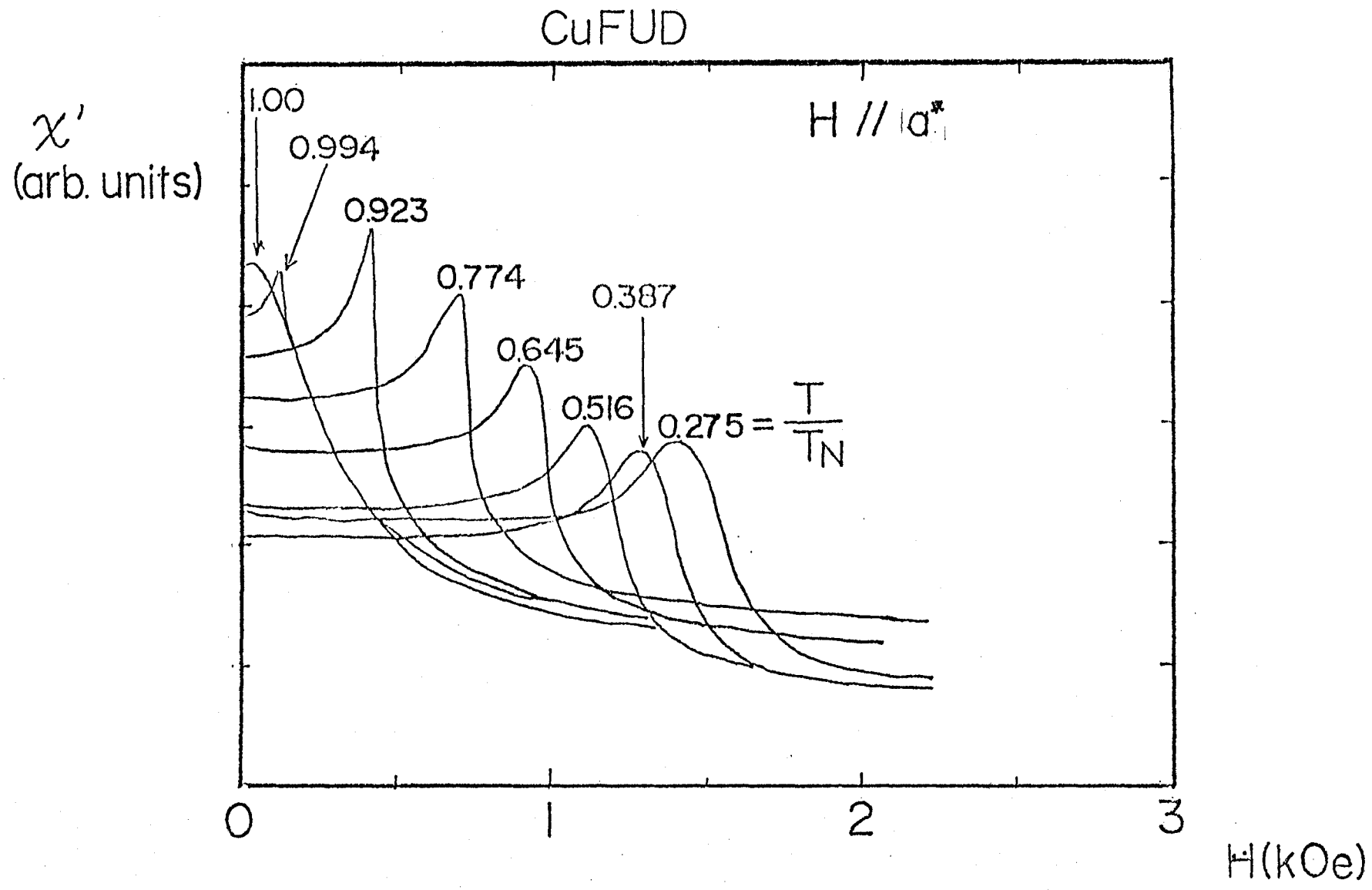

Fig. A-1. Field sweep charts of differential susceptibility along a*-axis for the various temperatures below T_N = 15.5 K. χ a* and H_0 a*-axis.

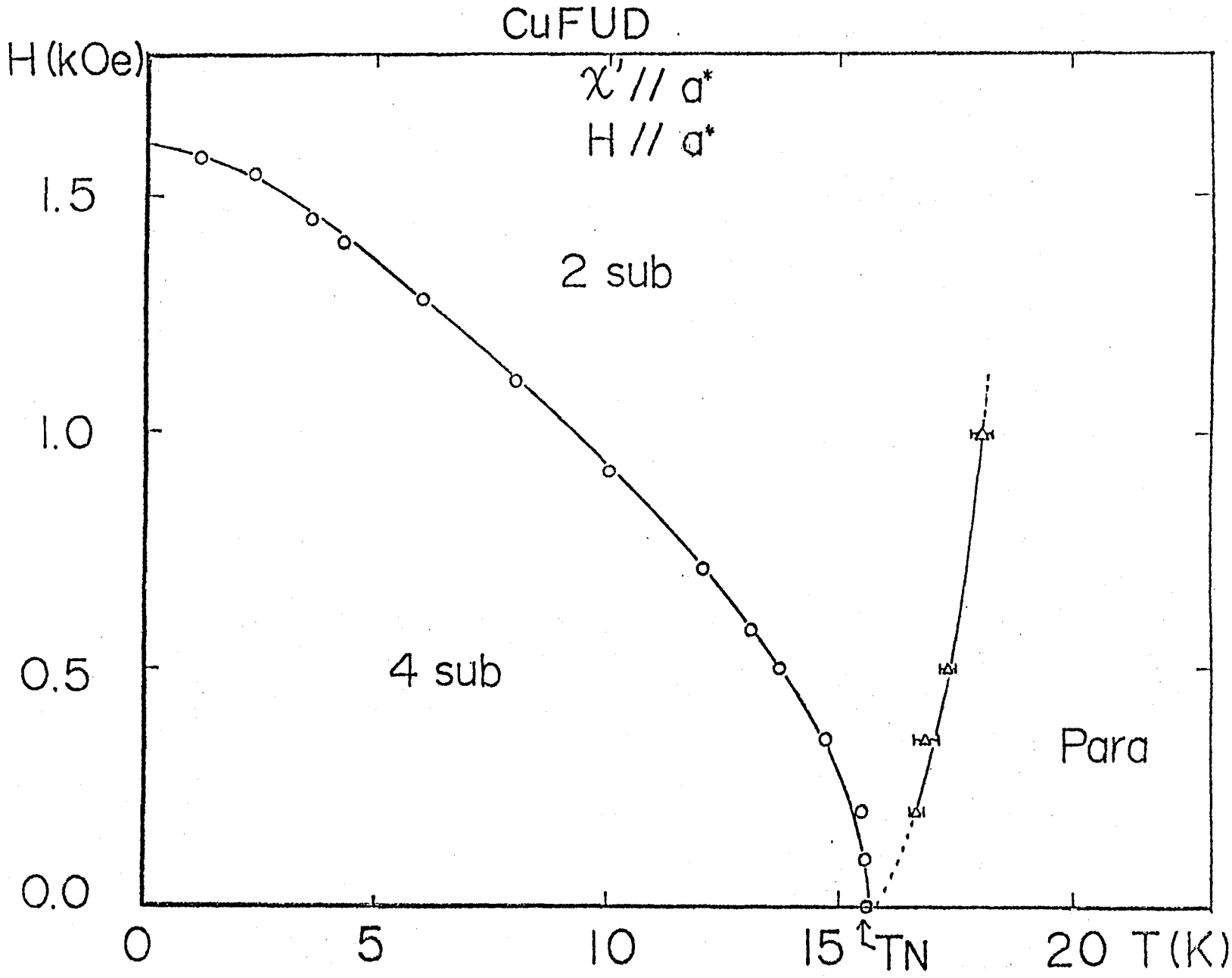

Fig. A-2. T-H (temperature-external field) phase diagram for the field along a*-axis.

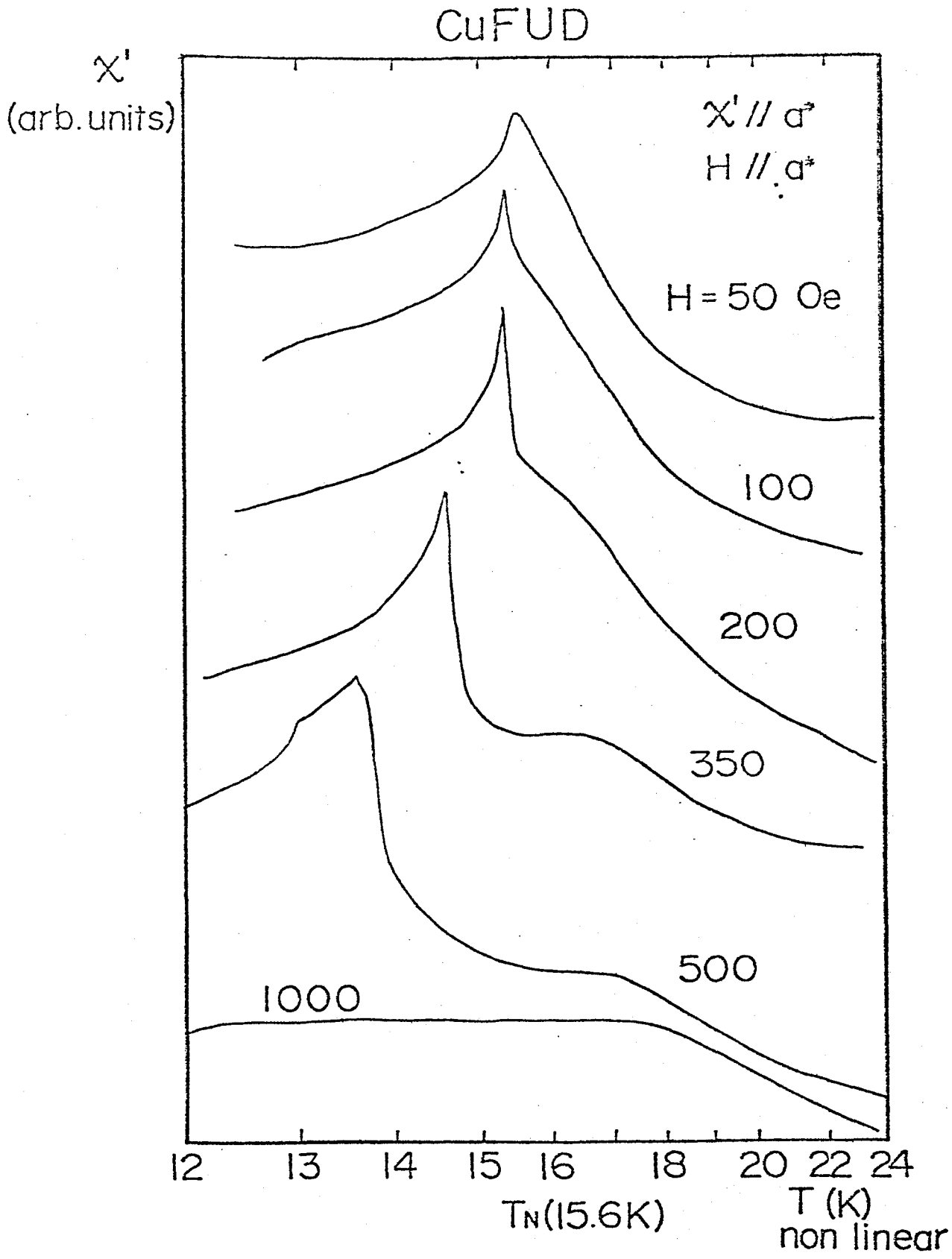

Fig. A-3. Temperature sweep charts of differential susceptibility along a*-axis under the various external fields.

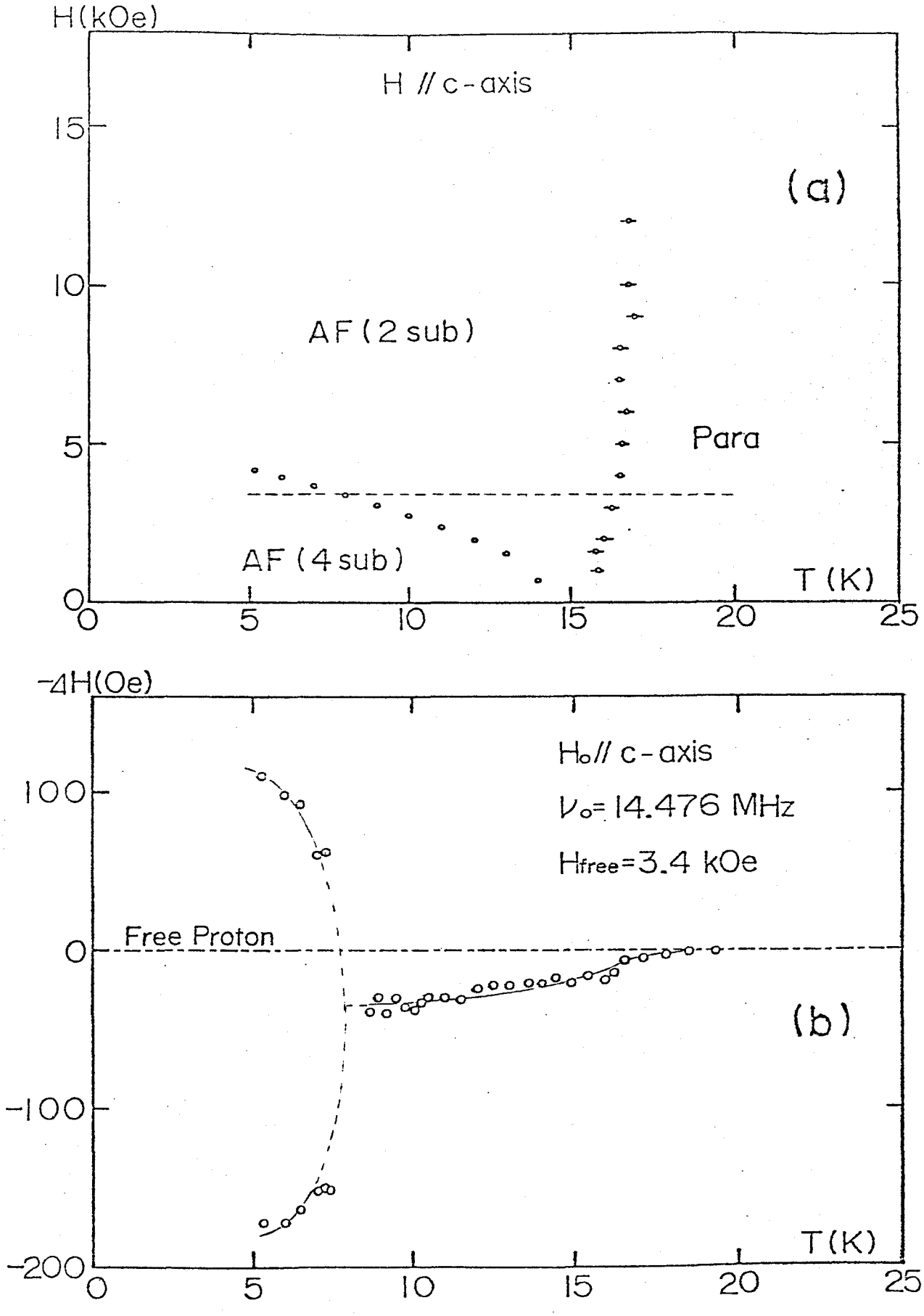

Fig. A-4. (a) T-H phase diagram for the c-axis up to 12 kOe.
(b) Temperature dependence of the line shift of proton NMR.

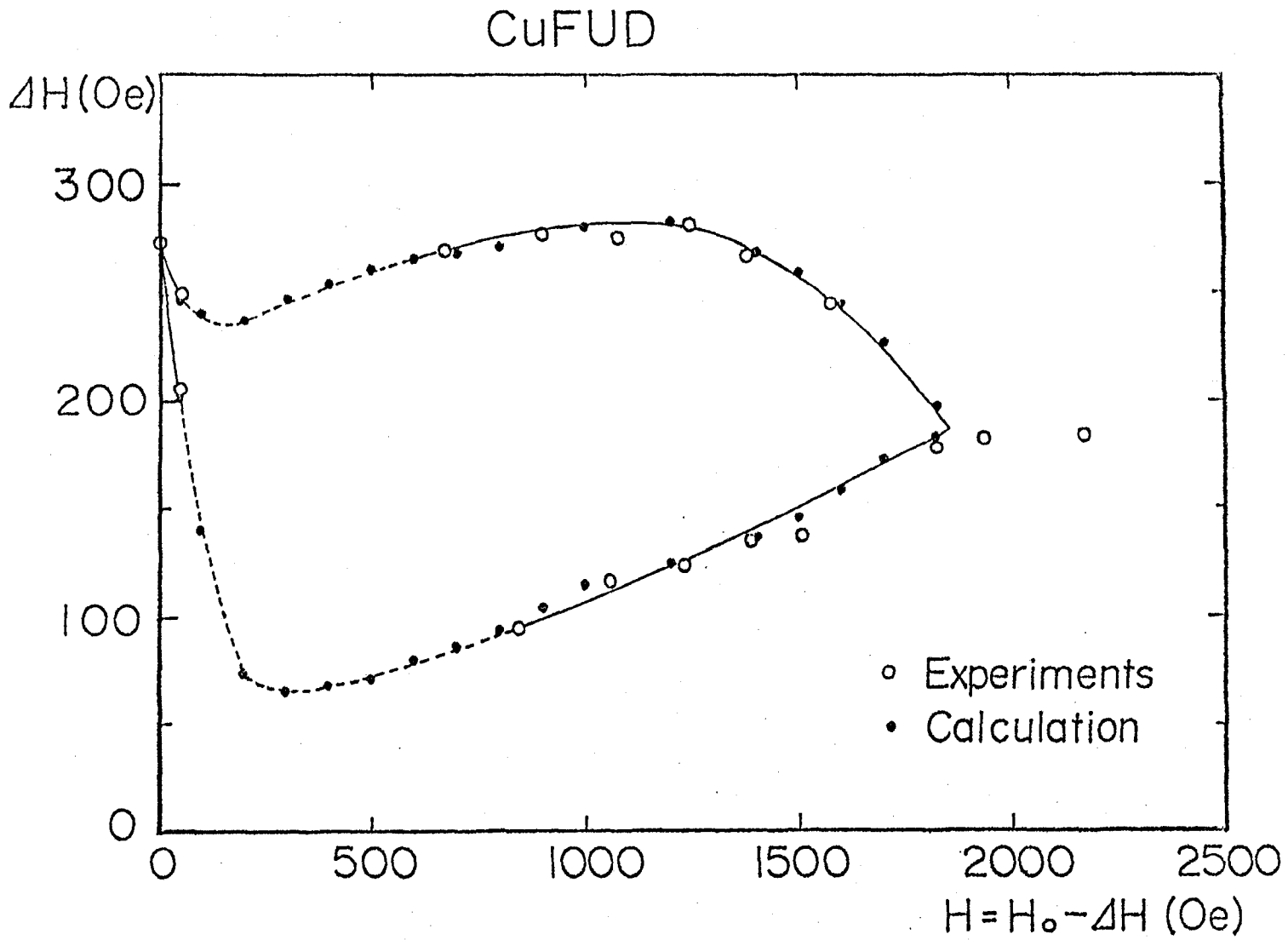

Fig. A-5. Field dependence of NMR line shift below the transition field (about 2 kOe) H a*-axis and T = 4.2 K. ∘ experimental data • calculated data.

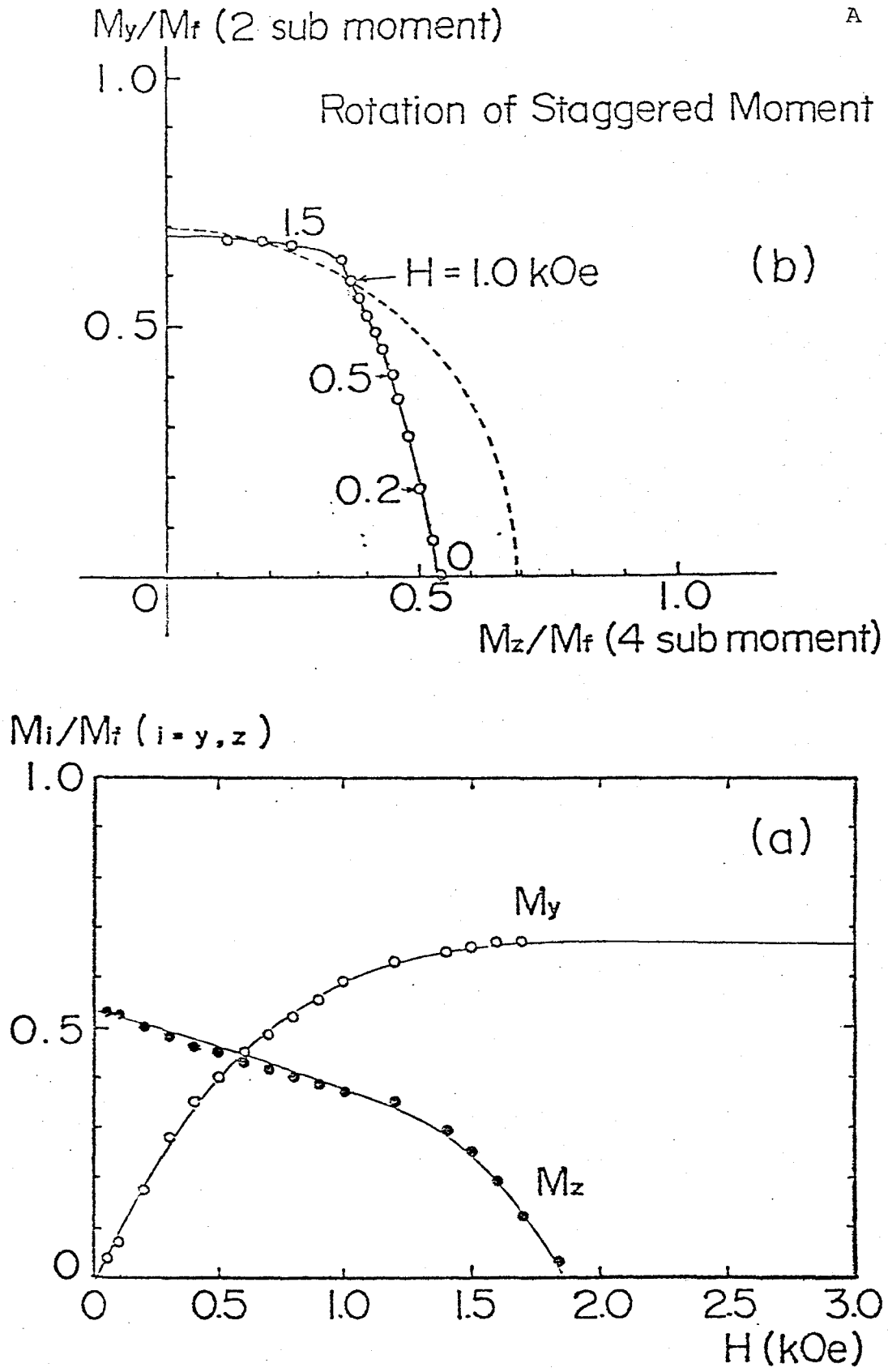

Fig. A-6. (a) Field dependences of 2 sub- ($M_y^{(2)}$) and 4 sub= lattice moment ($M_z^{(4)}$).
(b) Field dependences of amplitude and direction of the sublattice magnetization.

Acknowledgements

The author would like to express his sincere thanks to Professor T. Haseda and Professor M. Matsuura for the encouragement and stimulating discussions in the course of this study. He is indepted to Dr. K. Amaya for carrying out the experiment by operating the I.G.C. superconducting magnet up to 115 kOe in Chap.IV. His thanks are due to Dr. K. Takeda for the measurement of heat capacity in Chap.IV and Chap.V.and various discussions on the spin symmetry crossover phenomena induced by the field. Thanks are also due to Dr. S. Miyashita of the University of Tokyo who kindly gave us the results of the Monte Carlo simulation. His heartly thanks are due to the cooperation with Dr. Y. Yamamoto (now at Central Glass Co. Ltd.) in the preceding work which is indispensible to one in Chap.V. The neutron diffraction experiment in Chap.V could be made owing to the arrangement by Proffesor K. Hirakawa of Institute for Solid State Physics (ISSP), the University of Tokyo. Many kind assistances in neutron diffraction experiment by Proffesor H. Ikeda of Ochanomizu University and Mr. Y. Kawamura of ISSP, the University of Tokyo. He also thanks to Mr. H. Nobumasa for proceeding the NMR measurement in the course of this study and to Mr. Y. Murakami for his help in the measurement by a SQUID magnetometer in Chap.III and Chap.V. Thanks are due to Mr. A. Kawai for his assistance in preparation of experimental apparatus. He thanks the colleagues of Haseda laboratory for their helps throughout this work.